The LHCb calorimeter

Sergey Barsuk, LAL Orsay (IN2P3/CNRS and Paris-Sud University)

EPD seminar at IHEP, June 3, 2016

The LHCb experiment at LHC

JINST 8 (2013) P08002, INT.J.MOD.PHYS.A30 (2015) 1530022

- LHCb: precision studies of rare effects in b- and c-physics
- **Forward peaked HQ production** at the LHC, second b in acceptance once the first b is in
- Forward region 1.9 < η < 4.9, **~4% of solid angle**, but **~40% of HQ production x-section**

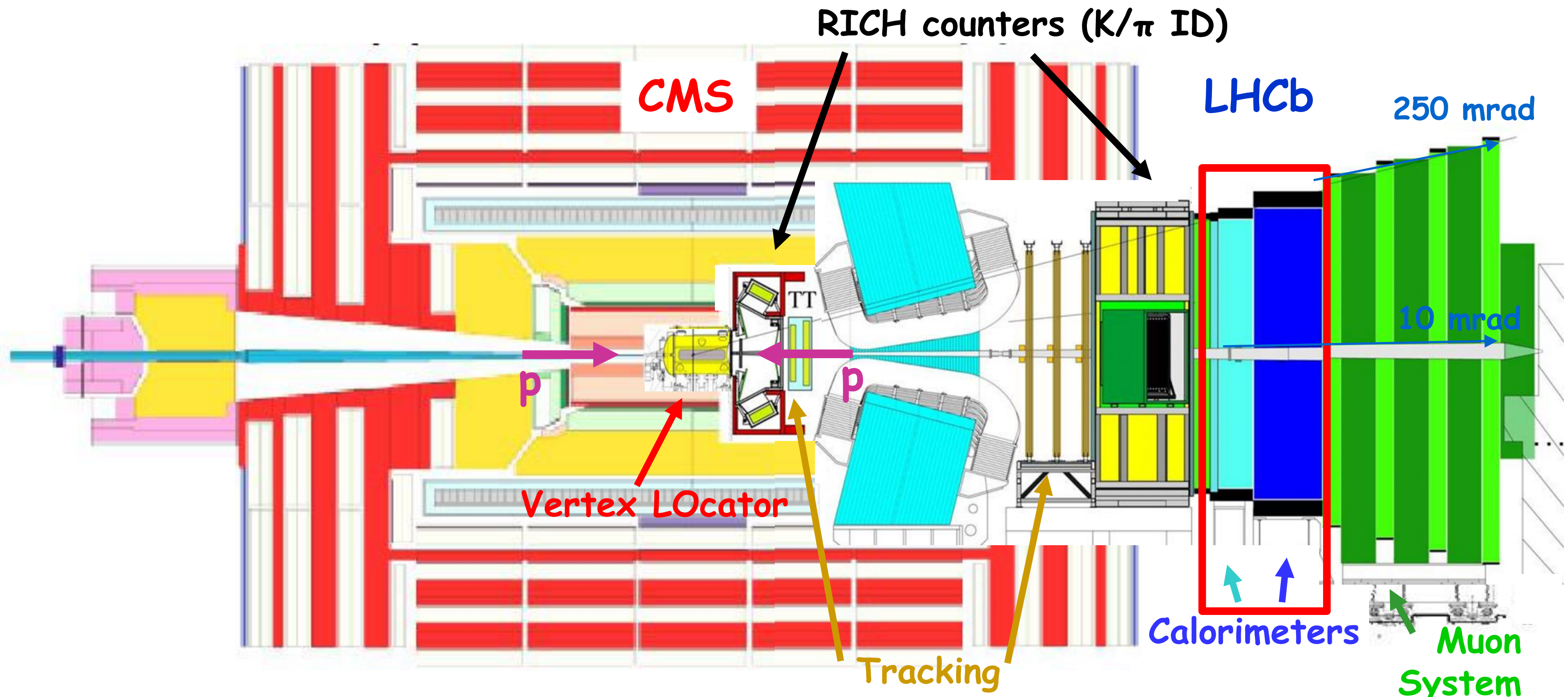

- Unique and complementary acceptance
- **Complementary production measurements** and overlap in terms of rapidity

LHCb detector – single-arm forward spectrometer 10-250 mrad (V), 10-300 mrad (H)

JINST 8 (2013) P08002, INT.J.MOD.PHYSA 30 (2015) 1530022

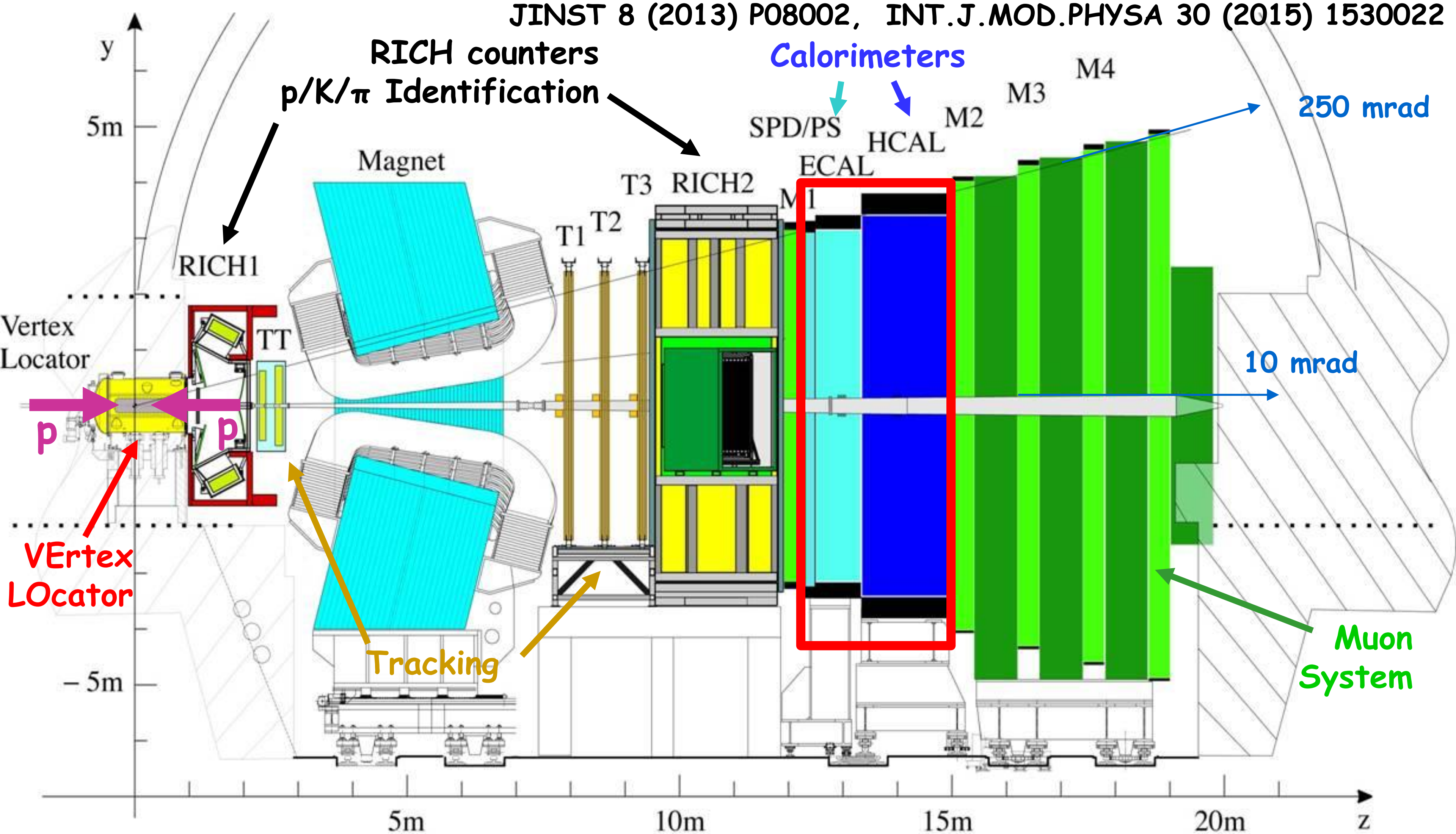

Vertex reconstruction:	Kinematics:	PID:	Trigger:
VELO	Magnet	RICHs	Muon Chambers
	Tracker	Calorimeters	Calorimeters
	Calorimeters	Muon Chambers	Tracker

LHCb operation

- LHCb collected data corresponding to ∫Ldt ~38 pb^{-1} in 2010, 1.1 fb^{-1} in 2011, 2.1 fb^{-1} in 2012

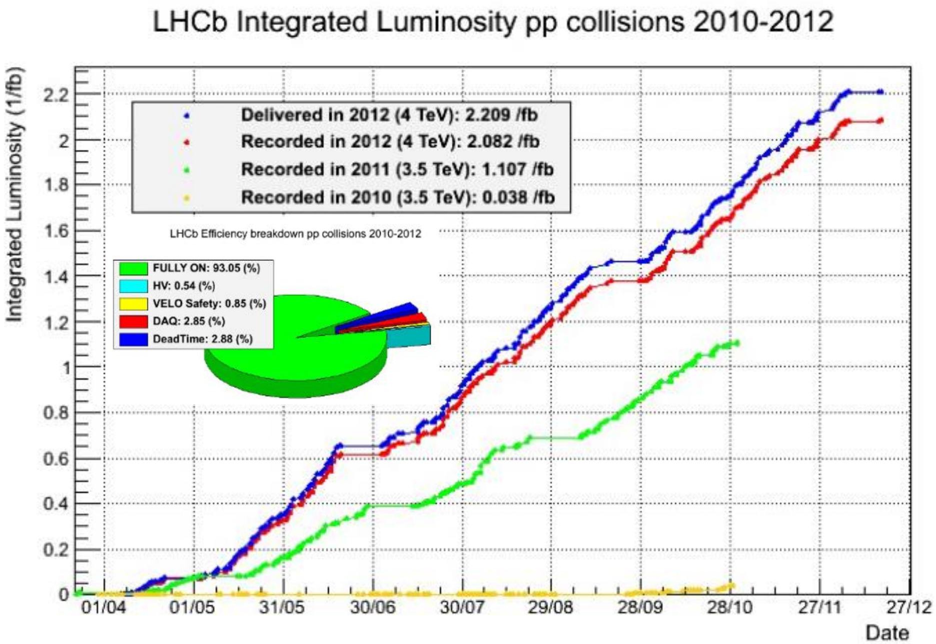

- And 0.3 fb^{-1} in Run II
- Stable LHCb operation
- Recording >1pb^{-1}/hour running at up to $L \sim 4\times10^{32}$ $cm^{-2}s^{-1}$ (higher, than nominal, 2×10^{32} $cm^{-2}s^{-1}$) in auto-leveling mode

LHCb luminosity levelling

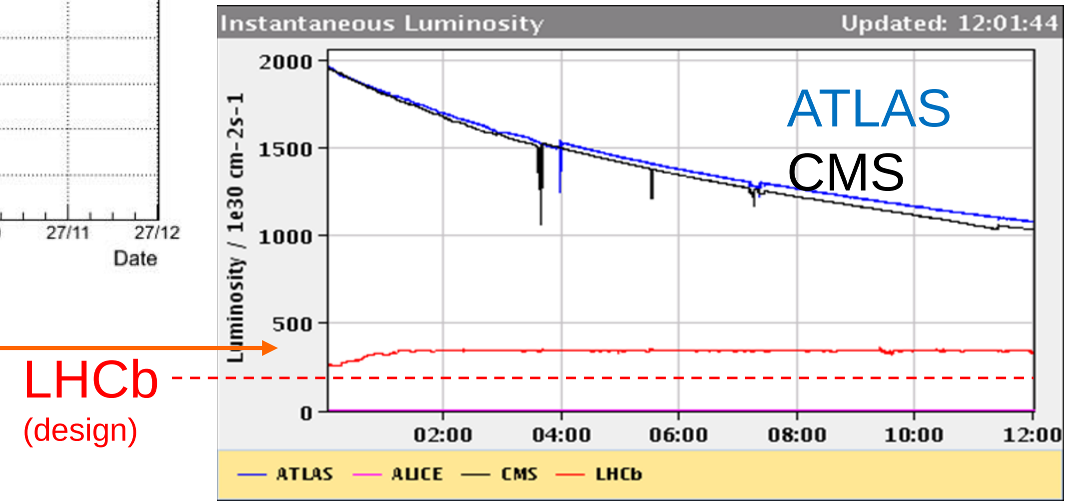

- Visual average **number of vertices** is higher, μ ~1.4, compared to nominal μ =0.4
- Higher μ → higher track multiplicity, 1 PV gives 30 tracks/rapidity range, more difficult reconstruction

→ background for D and B decay vertex reconstruction and matching

average minimum distance between 4 PVs ~12 mm, comparable to average B travel distance ~10 mm

It is often useful to have an idea of the internal structure even if it is invisible …

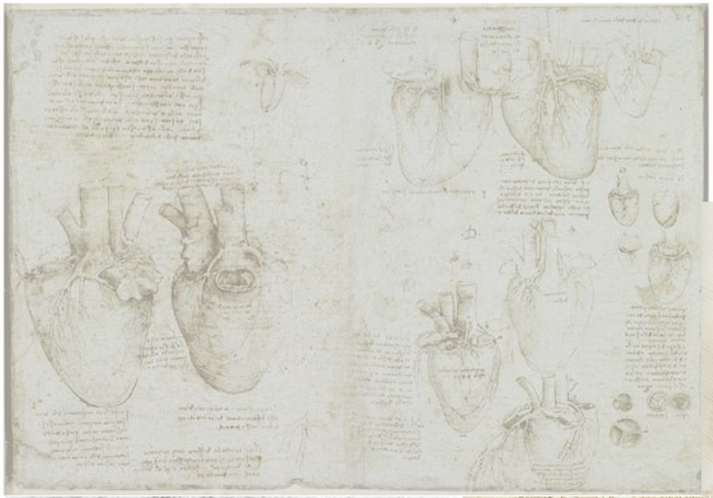

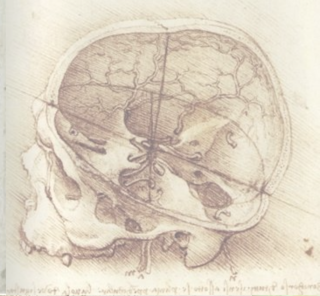

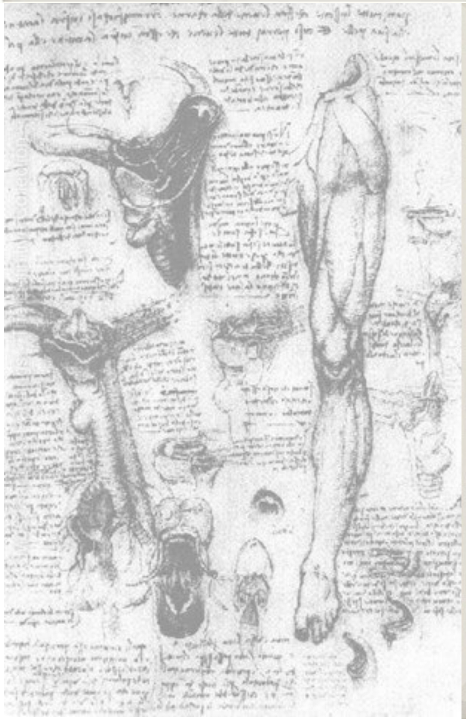

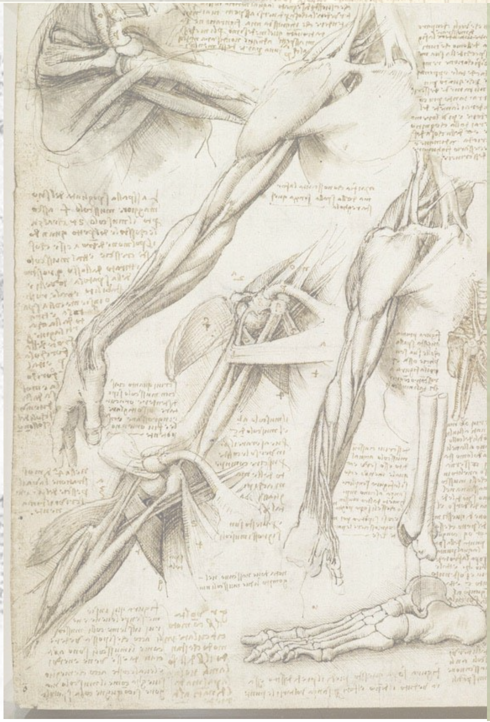

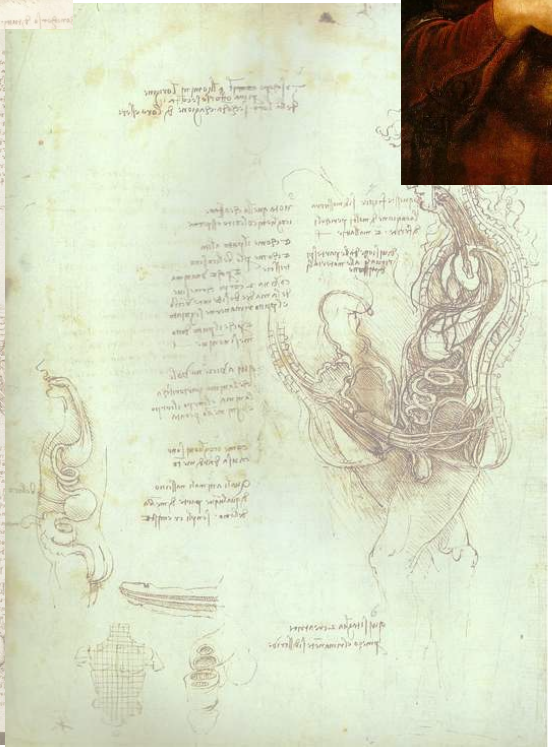

VELO: Vertex LOcator

JINST 8 (2013) P08002, JINST 9 (2014) 09007

- 88 semi-circular microstrip Si sensors
- Double-sided, R and φ layout, in each module
- 300μ thick n-on-n sensors
- Strip pitches from 40 to 120μ
- Second metal layer - routing lines

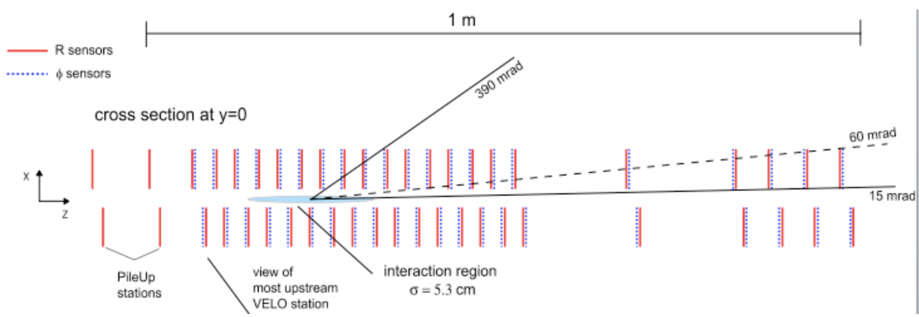

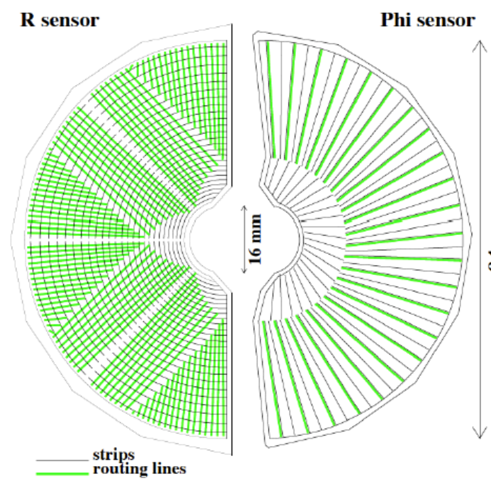

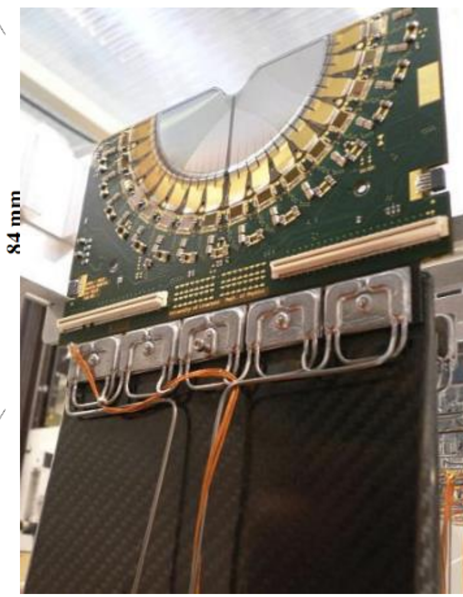

- First active strip at 8.2mm
- Moves away every fill and centers around the beam with self measured vertices
- Evaporative CO_2 cooling
- Operates in vacuum, separated from LHC by 300μ thick RF foil

VELO: precise reconstruction of tracks and vertices

- Excellent spatial resolution, down to 4μ for single tracks
- Precise impact parameter measurement,
  $\sigma_{IP} = 11.6 + 23.4/pT \;\; [\mu]$
- Precise primary vertex reconstruction,
  $\sigma_x = \sigma_x = 13\mu$, $\sigma_z = 69\mu$ for a vertex of 25 tracks

Impact parameter resolution

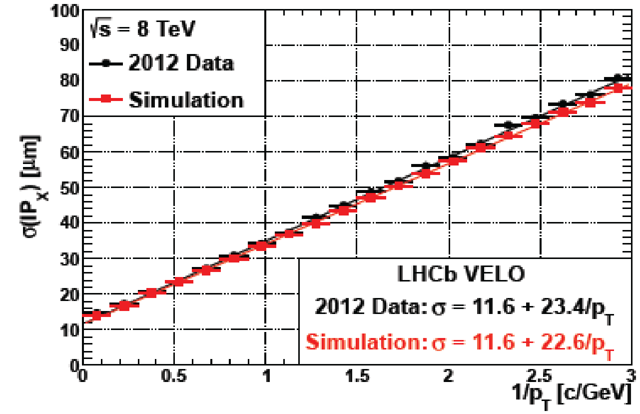

JHEP 04 (2014) 114

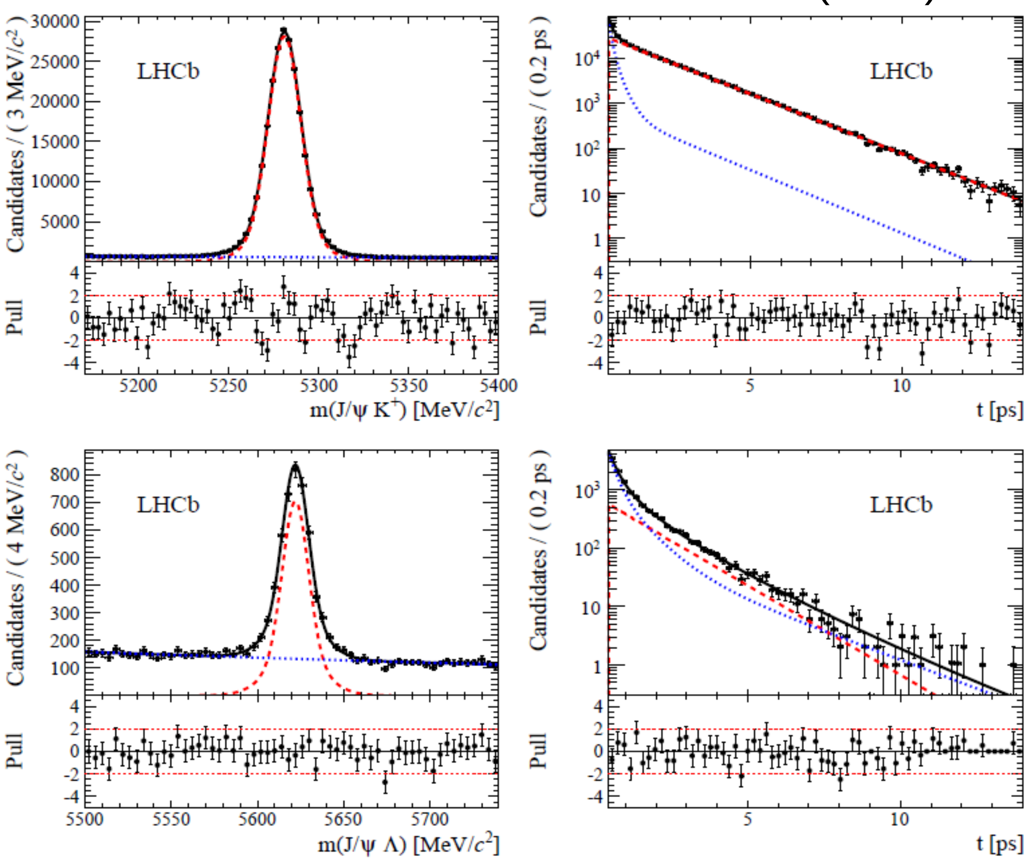

- Detector well understood, simulation describes data
- Vertex Locator (VELO) provides excellent proper time resolution

Lifetime	Value [ps]	PDG [ps]
$\tau_{B^+ \to J/\psi K^+}$	$1.637 \pm 0.004 \pm 0.003$	1.641 ± 0.008
$\tau_{B^0 \to J/\psi K^{*0}}$	$1.524 \pm 0.006 \pm 0.004$	1.519 ± 0.007
$\tau_{B^0 \to J/\psi K^0_s}$	$1.499 \pm 0.013 \pm 0.005$	1.519 ± 0.007
$\tau_{\Lambda^0_b \to J/\psi \Lambda}$	$1.415 \pm 0.027 \pm 0.006$	1.429 ± 0.024
$\tau_{B^0_s \to J/\psi \phi}$	$1.480 \pm 0.011 \pm 0.005$	1.516 ± 0.011

(F.S.: 1.429 ± 0.088)

- Vertex resolution allows to resolve fast (x~27) $B_s\overline{B}_s$ oscillations

- $B_s^0 \to D_s^- \pi^+$

$D_s^- \to \phi(K^+K^-)\pi^-$
$D_s^- \to K^{*0}(K^+\pi^-)K^-$
$D_s^- \to K^+K^-\pi^-$ nonresonant
$D_s^- \to K^-\pi^+\pi^-$
$D_s^- \to \pi^-\pi^+\pi^-$

New J. Phys. 15 (2013) 053021

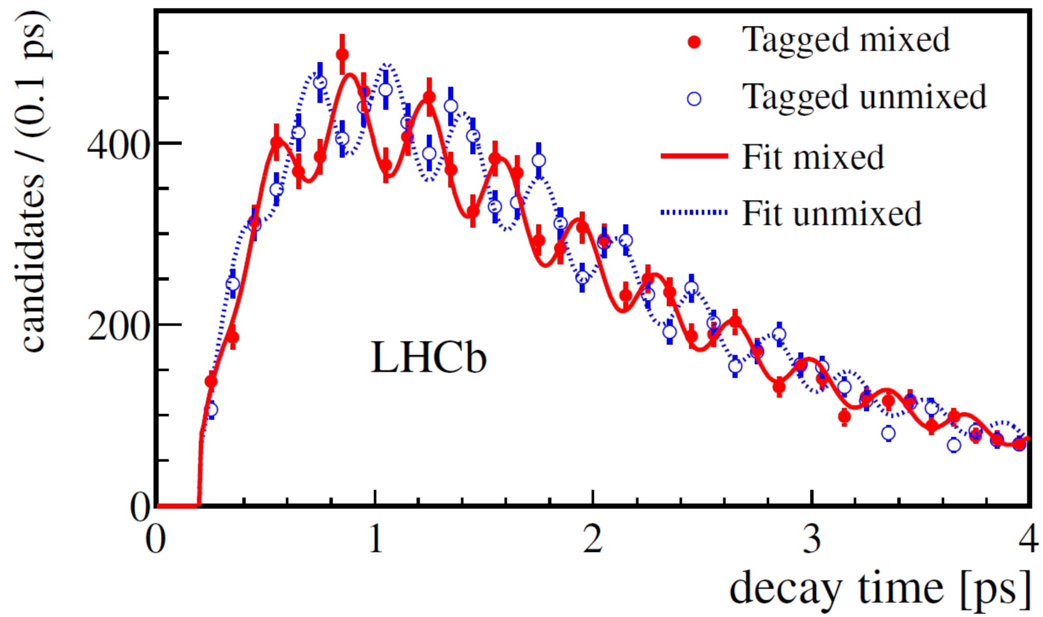

$$\Delta m_s = 17.768 \pm 0.023\,(\text{stat}) \pm 0.006\,(\text{syst})\ \text{ps}^{-1}$$

Charged hadron identification: RICH detectors

Eur.Phys.J. C73 (2013) 2431

2 Detectors, 3 Radiators

RICH 1

Acceptance 25-300 mrad

Side view

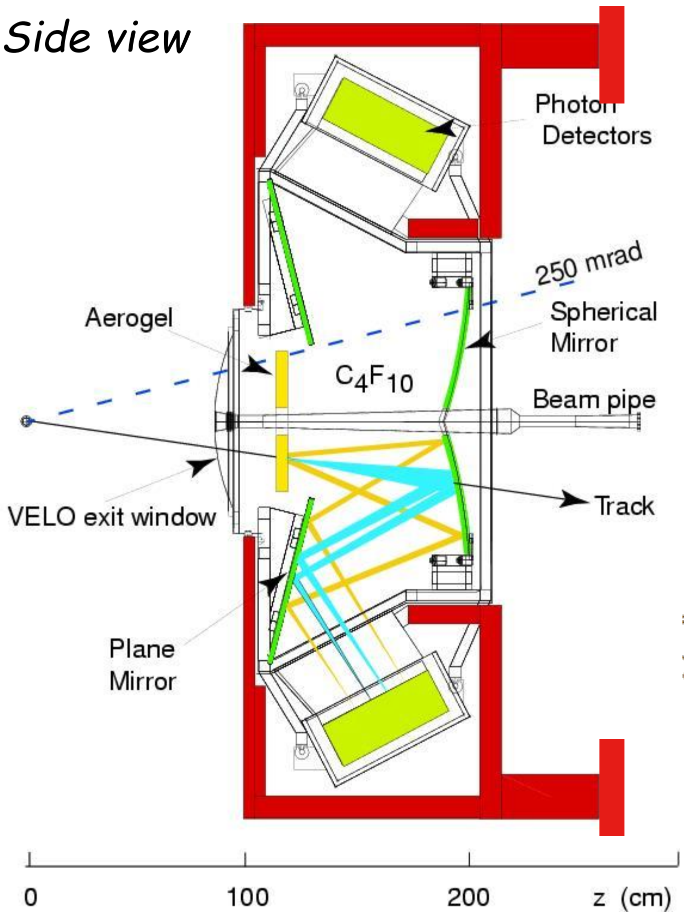

Silica Aerogel:
n=1.03
1-10 GeV/c

C_4F_{10}:
n=1.0014
Up to ~70 GeV/c

CF_4:
n=1.0005
Up to ~100 GeV/c

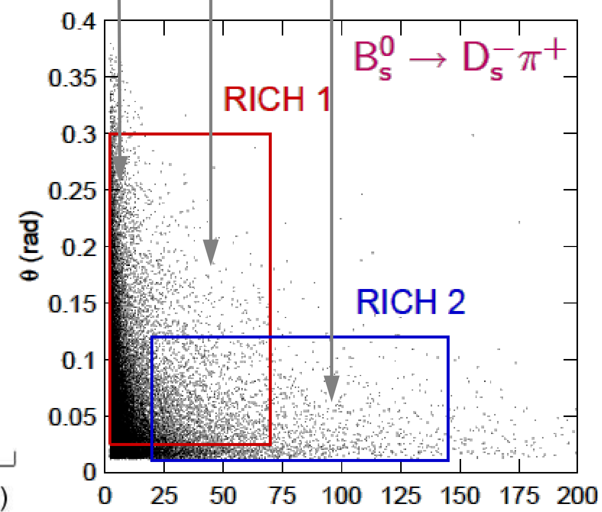

RICH 2

Acceptance 15-120 mrad

Top view

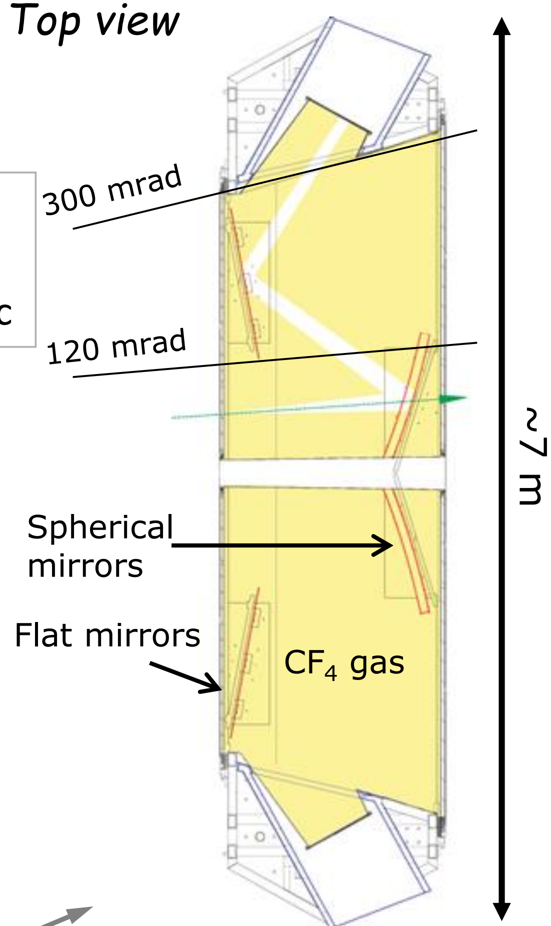

Note Scale Difference

RICH detectors

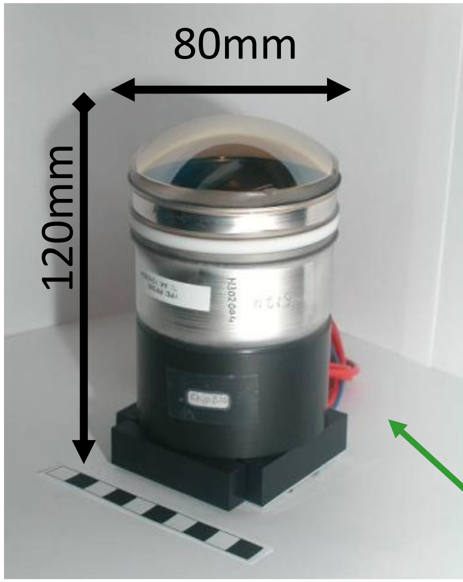

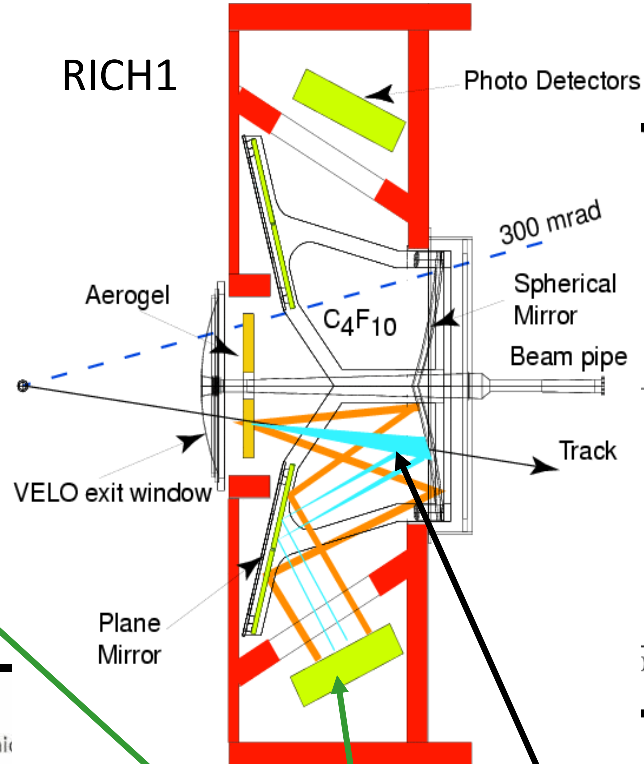

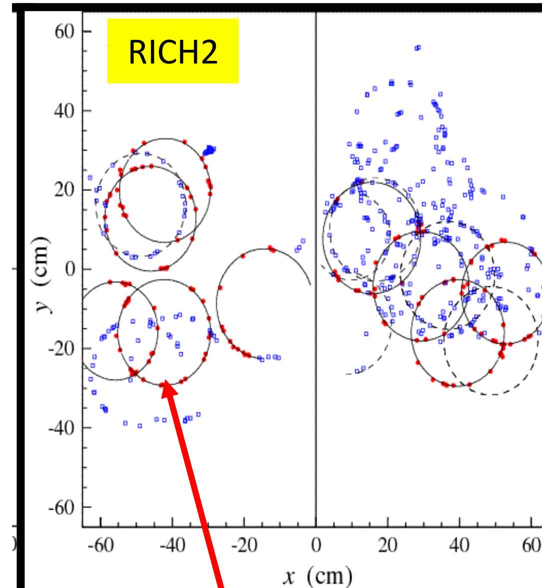

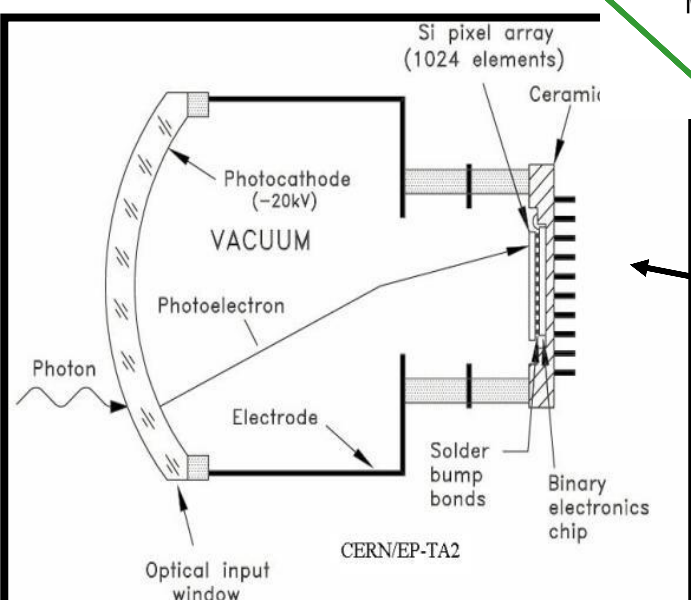

Photons from Cerenkov cone
focused onto rings
recorded by
Hybrid Photo Diodes arrays, out of acceptance.
Each containing a 1024 Si pixel array.

RICH1: **Aerogel** and **C_4F_{10}** RICH2: **CF_4**

RICH detectors

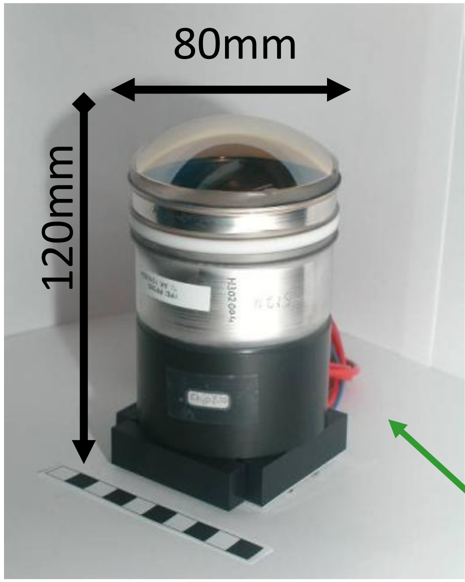

RICH1

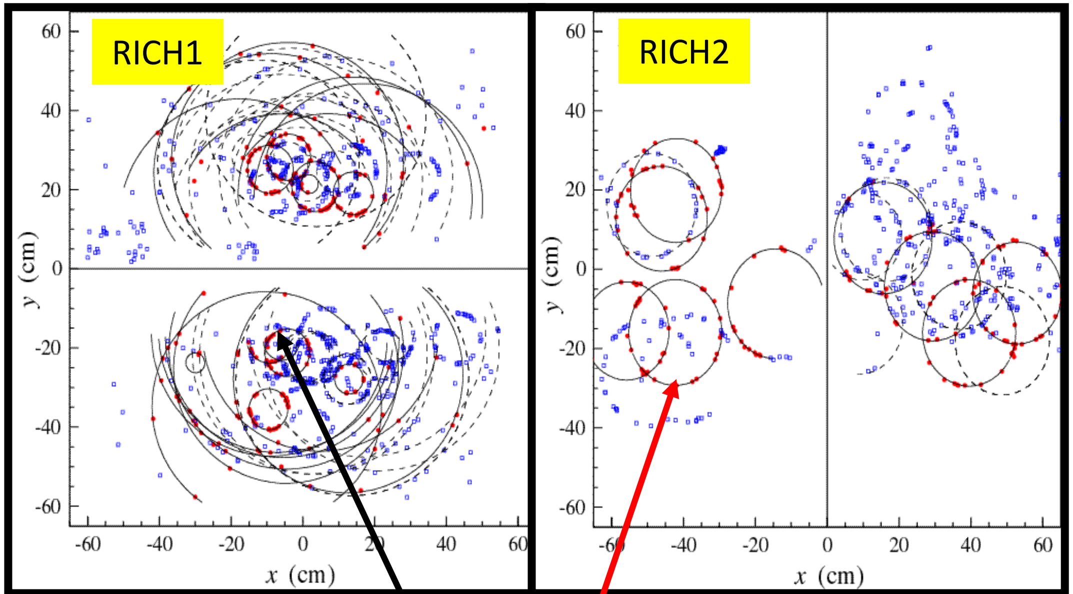

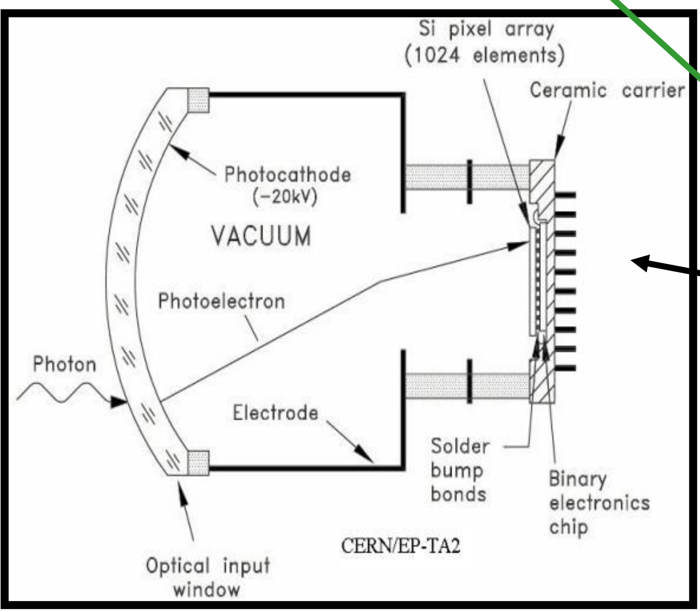

Photons from Cerenkov cone
focused onto rings
recorded by
Hybrid Photo Diodes arrays, out of acceptance.
Each containing a 1024 Si pixel array.

RICH1: **Aerogel** and $\mathbf{C_4F_{10}}$ RICH2: $\mathbf{CF_4}$

RICH1 mirrors and Aerogel

- Photodetectors are positioned in tolerable radiation zone
- Light is guided outside hot area by a system of large, precise, minimum material and radiation hard mirrors

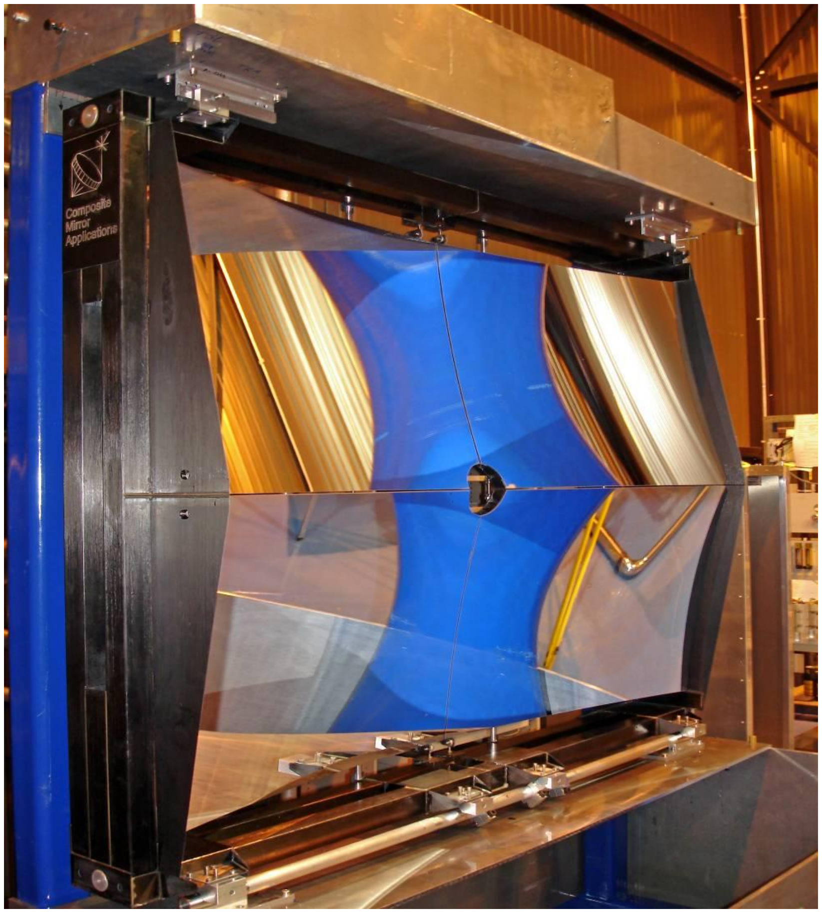

Carbon fibre mirrors for low material budget

Aerogel is inside a gas tight box flushed with CO_2 to avoid performance degradation from exposure to C_4F_{10}

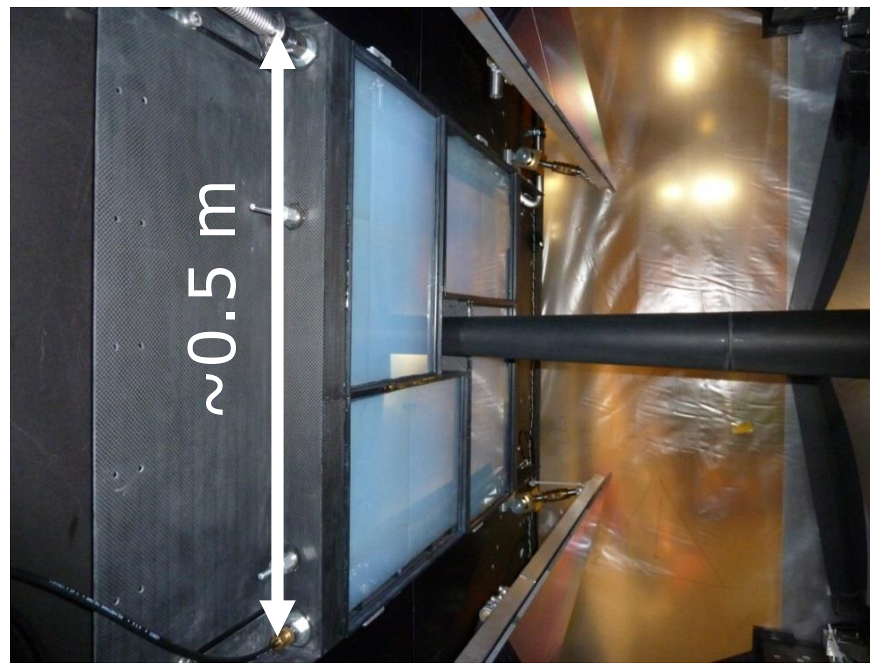

- Genuine π/K/p samples identified from kinematics only
- PID performance evaluated from data

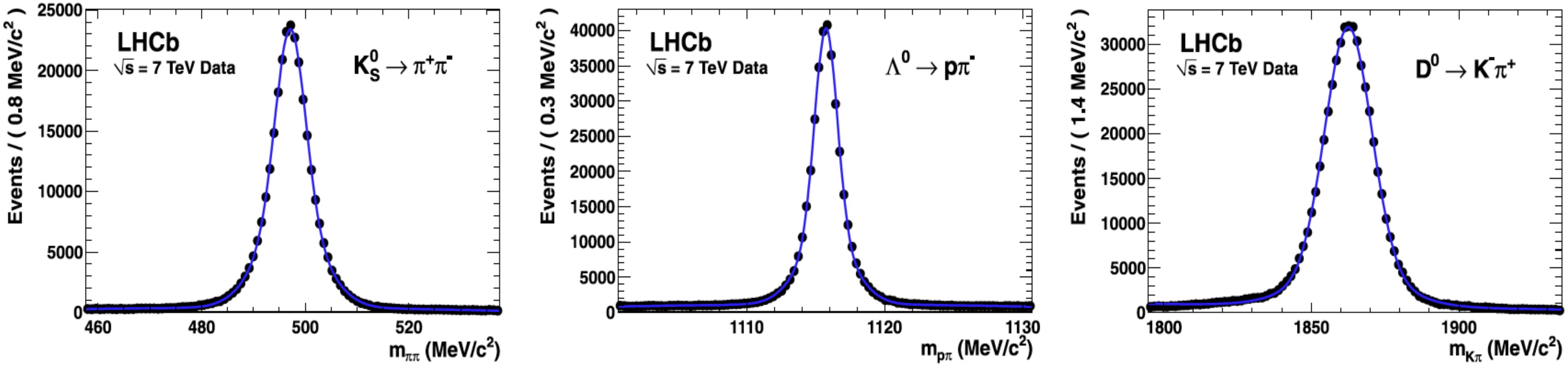

- Efficiency/rejection: reasonable agreement between data and simulation

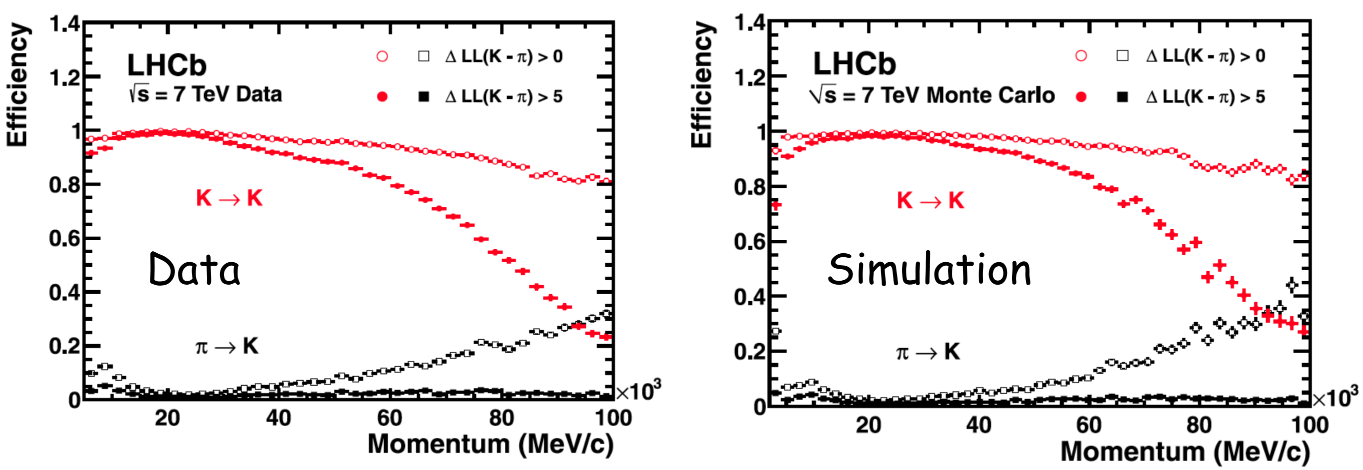

RICH: charged hadron identification performance

charmless two-body b-hadron decays

JHEP 10 (2012) 037

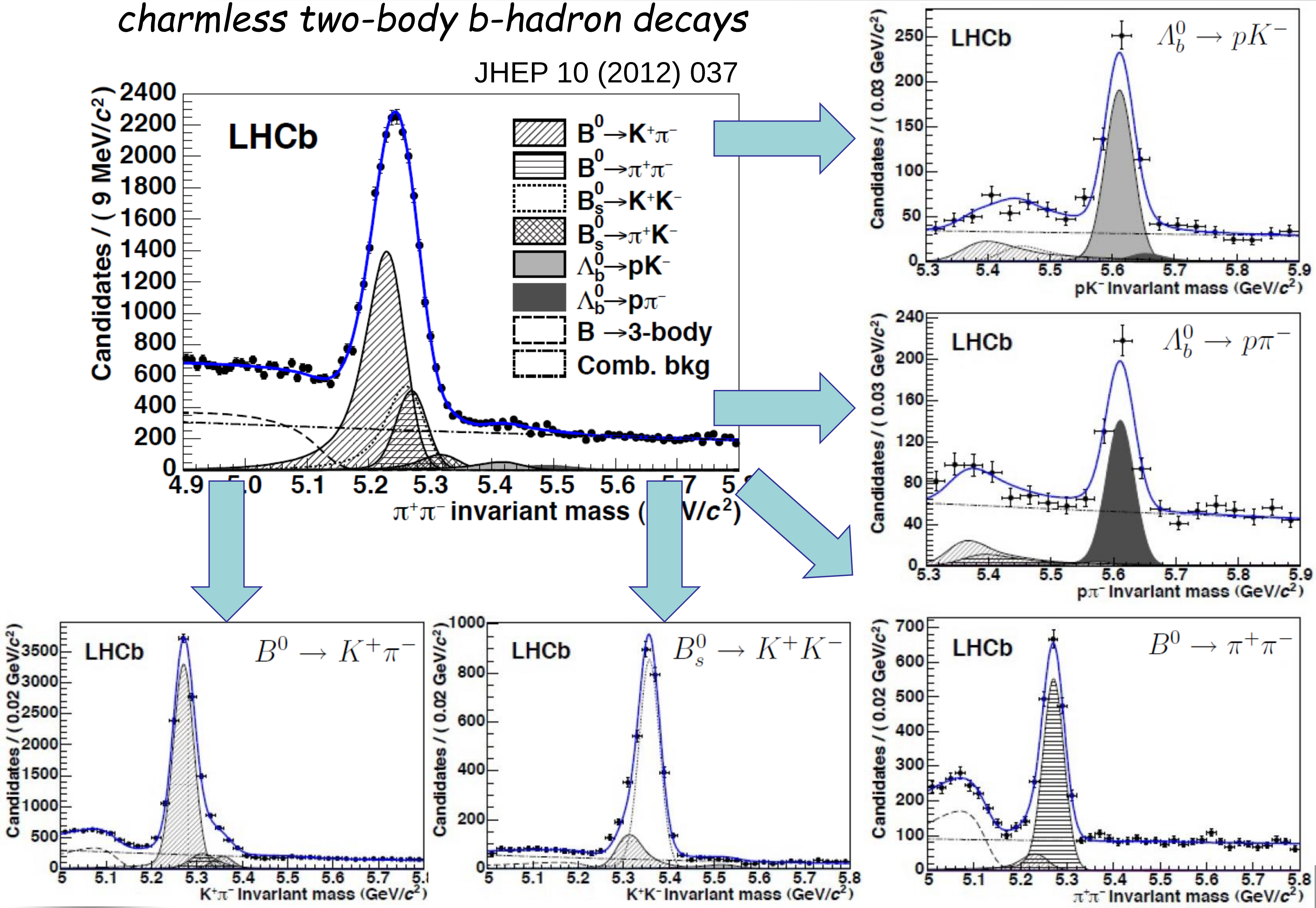

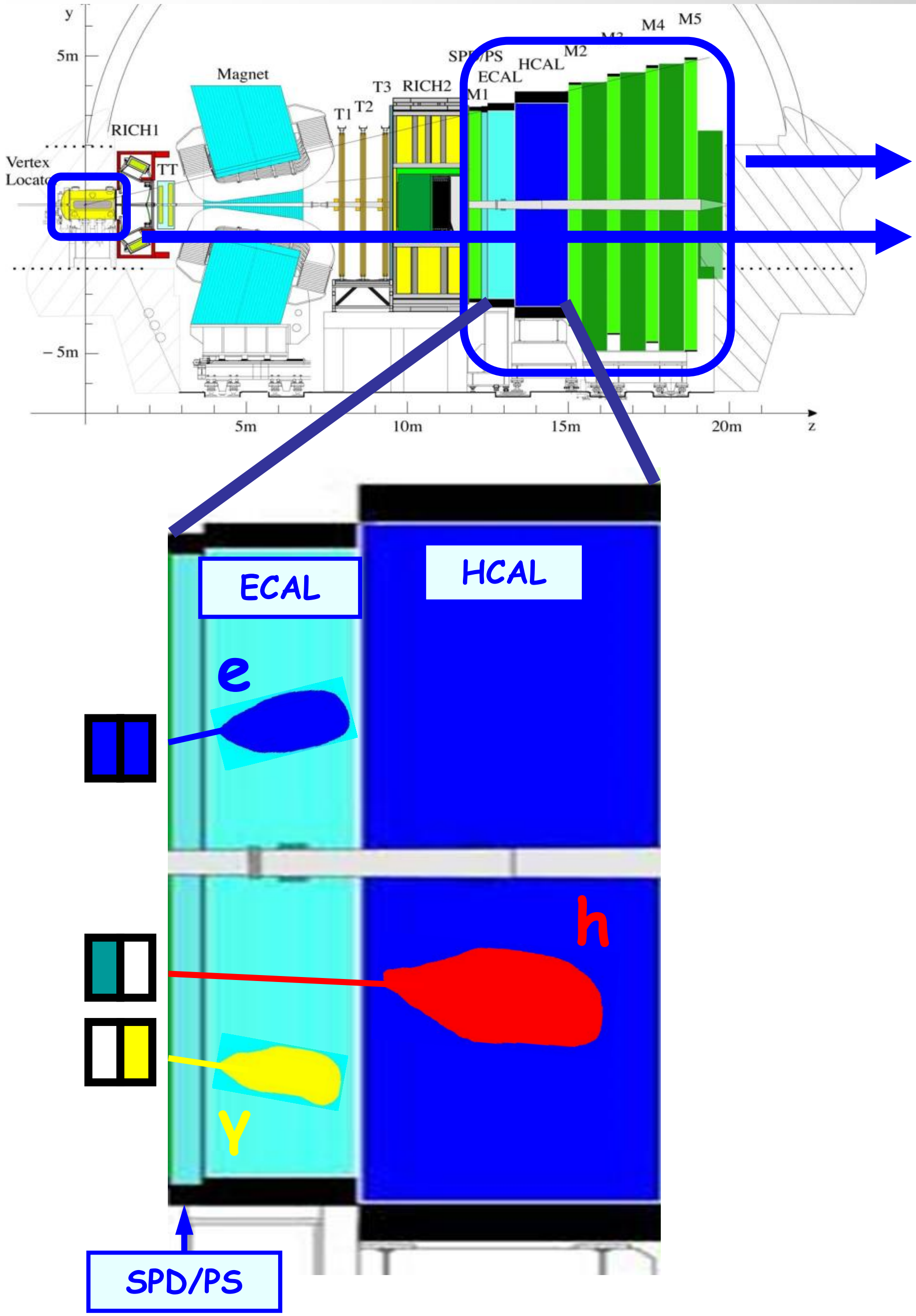

10 MHz

L0 (hardware):

high p_T h, μ, μμ, $e^{\pm}$, γ, π^0 alleys

(optionally: veto busy events)

Fully synchr. (40 MHz), 4μs latency

1 MHz

HLT (PC farm, full event)

HLT1: confirms L0 candidate with tracker and VELO

HLT2: global event reconstruction, inclusive selections

~ 5 kHz

JINST 8 (2013) P04022

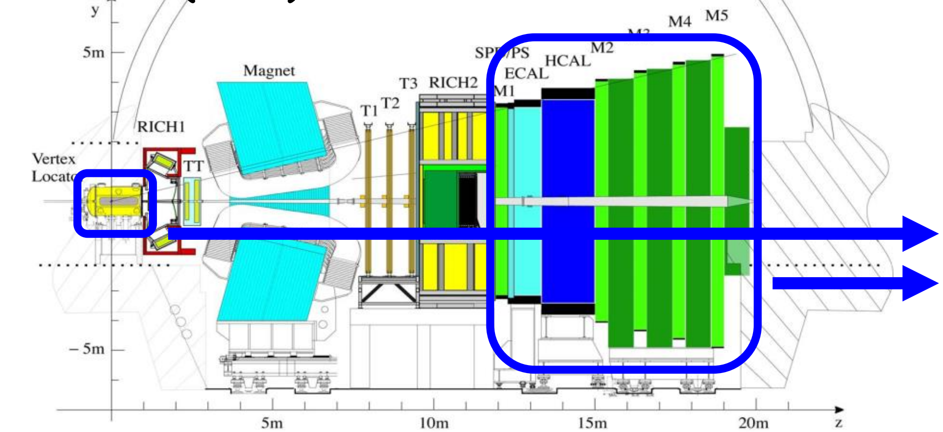

- Performant LHCb trigger: hardware **L0**, software **HLT**

- New trigger features
- **Same online and offline reconstruction and PID**
  - prompt alignment and calibration
  - completely automatic and real-time
- **Physics out of the trigger** with Turbo Stream
  - Raw info discarded, candidates directly available few hours after being recorded

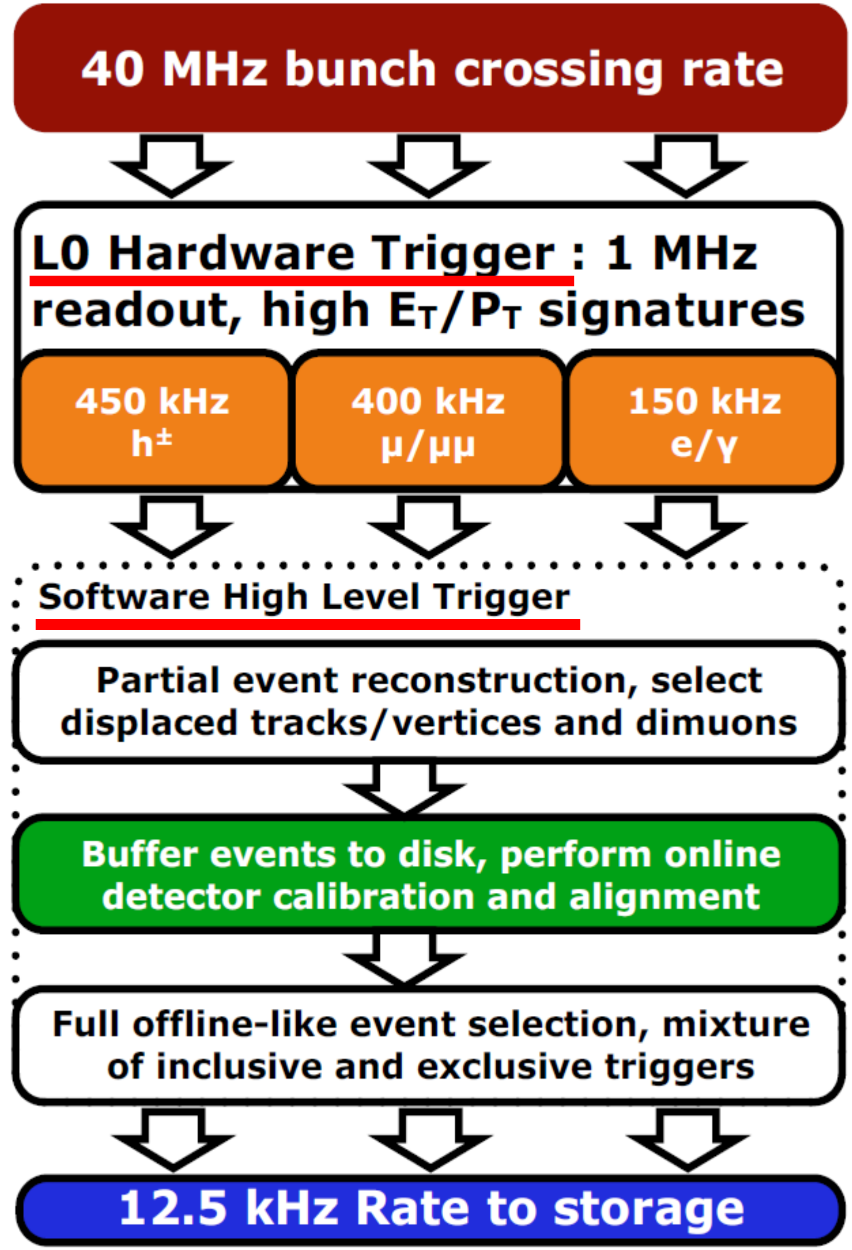

The LHCb calorimeters

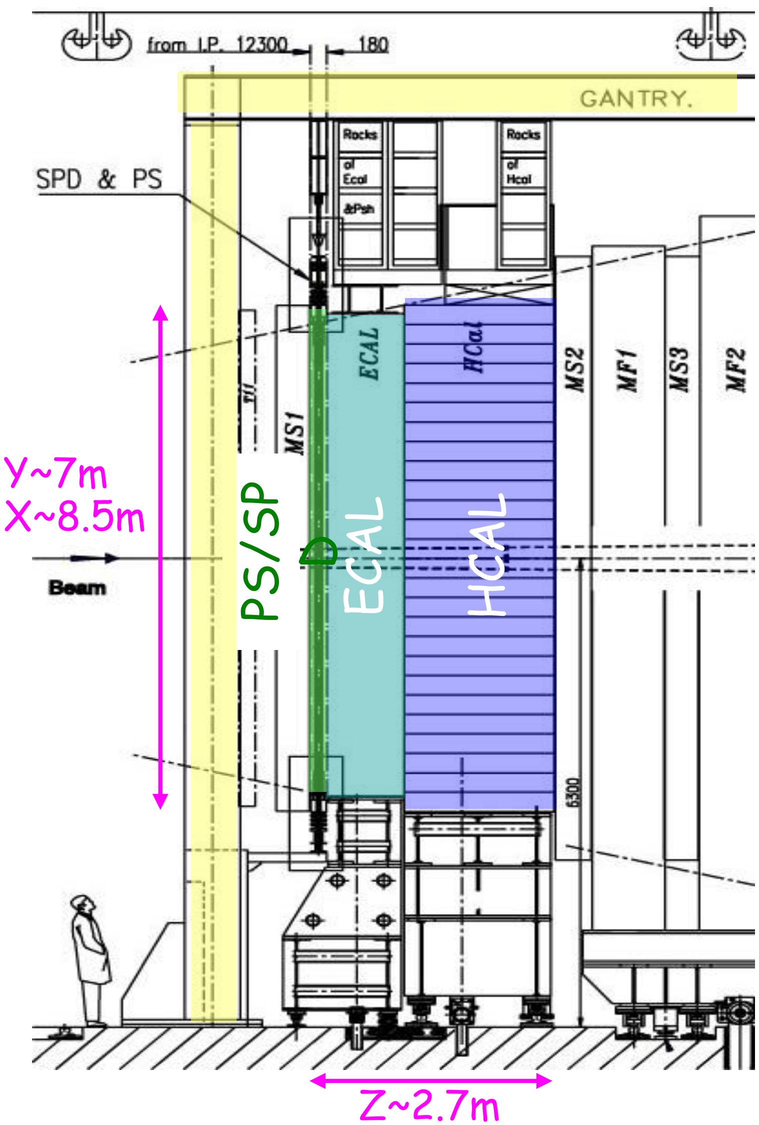

Three calorimeters PS, ECAL, HCAL
and one threshold device SPD

arranged in the pseudo-projective geometry, variable granularity

Preshower (PS) and Scintillator Pad Detector (SPD):

- PID for L0 electron and photon trigger
- electron, photon/pion separation by PS
- photon/MIP separation by SPD
- charged multiplicity veto by SPD

Electromagnetic Calorimeter (ECAL):

- E_T of electrons, photons and π^0 for L0 trigger
- reconstruction of π^0 and prompt γ offline
- particle ID

Hadron Calorimeter (HCAL):

- E_T of hadrons for L0 trigger
- particle ID

L0 trigger ➔ Calorimeters R-O every 25ns

Three calorimeters PS, ECAL, HCAL and one threshold device SPD

arranged in the pseudo-projective geometry, variable granularity

Common principles:

- determination of the shower energy
  - scintillator tiles, Polystyrol + 2.5% PTP + 0.01% POPOP
  - shifting wavelength with optical fibers, Kuraray Y-11(250) MSJ
- R-O with PMT (Hamamatsu R7899-20 for ECAL and HCAL; 64 ch. MAMPT for SPD/PS), HV setting with Cockcroft-Walton bases
- monitoring stability of the R-O chain
  - use LED light injected during empty bunches
  - monitor LED stability with PIN diode wherever precision needed (ECAL, HCAL)
- pp-collisions every 25 ns
  - detector response within 25 ns
  - R-O within 25 ns
  - spill-over cancellation with FEE

Scintillator Pad Detector (SPD) and PreShower (PS)

- Two layers of scintillator interspaced by 2.5 Xo lead
- Light transported via clear fibers to the MAPMT at the detector periphery

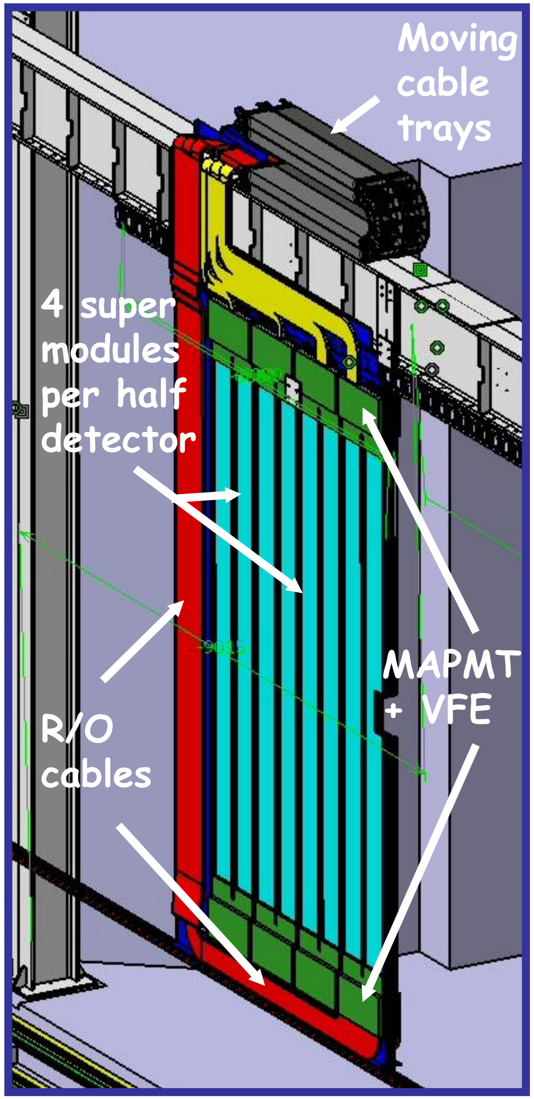

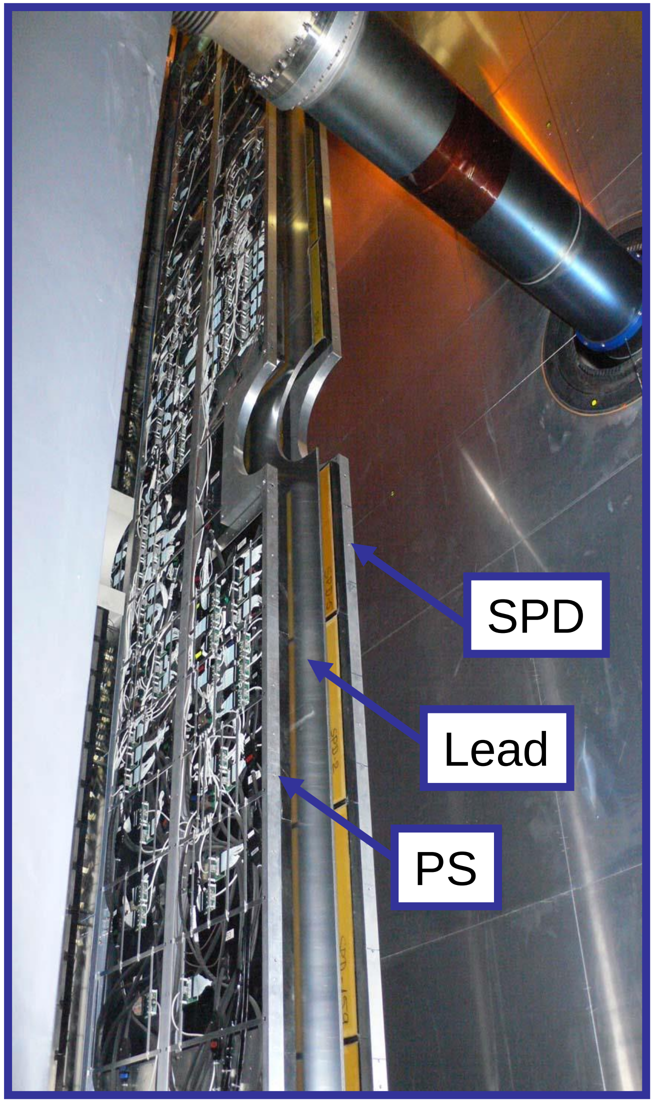

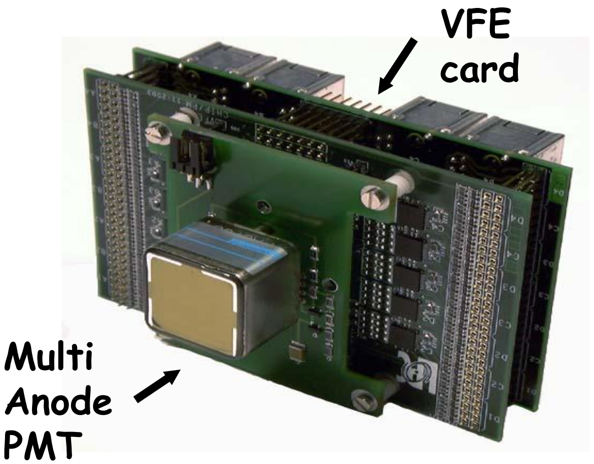

- Active area: 7.8m x 6.3 m
- Space constraint: 18cm in depth
- PS+SPD built from 16 super modules
- Segmentation matches ECAL cells
- Total of 12032 cells / R-O channels

Scintillator Pad Detector (SPD) and PreShower (PS)

PS / SPD modules

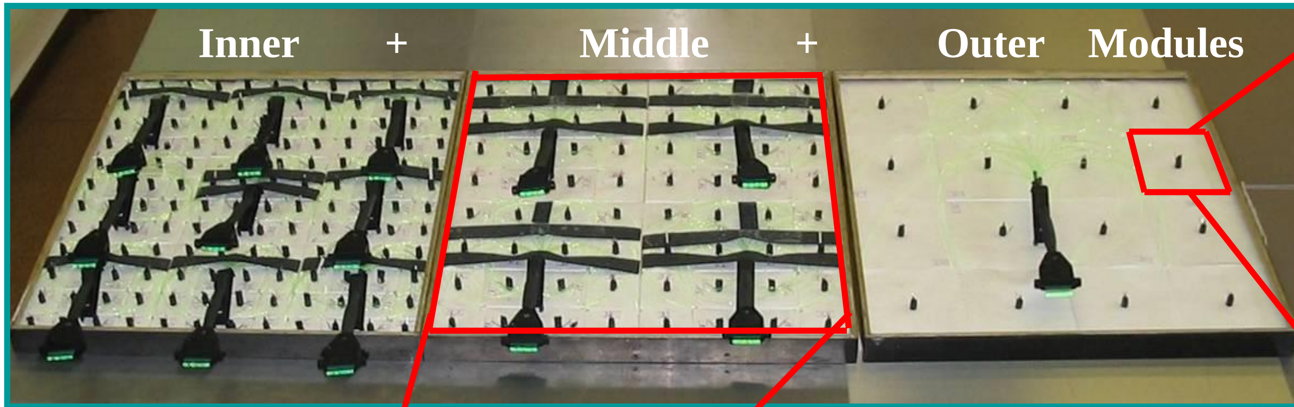

Scintillator + coiled fiber

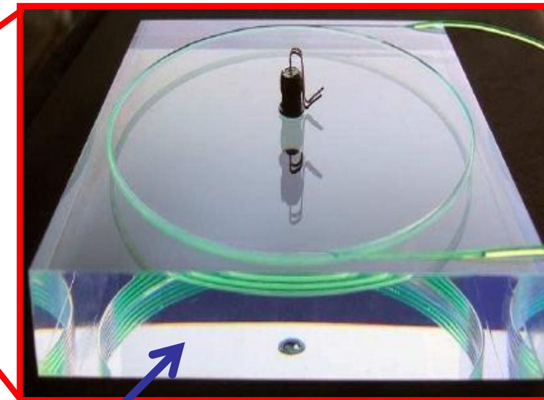

15 mm thick tile with coiled WLS fiber
+ ~3m long clear fibers and interconnects

16 super modules for PS & SPD

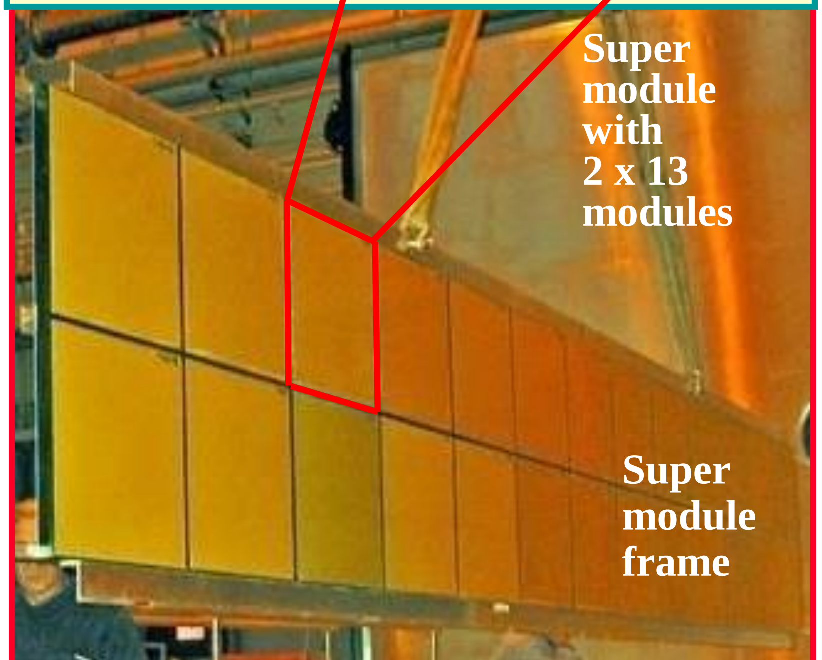

All super-modules tested with cosmics in horizontal position:

<N p.e.>/MIP varies

from **19 p.e./MIP** to **29 p.e./MIP** depending on the cell size

Hadron calorimeter (HCAL)

- Two retractable halves each consisting of 26 modules stacked on a movable platform

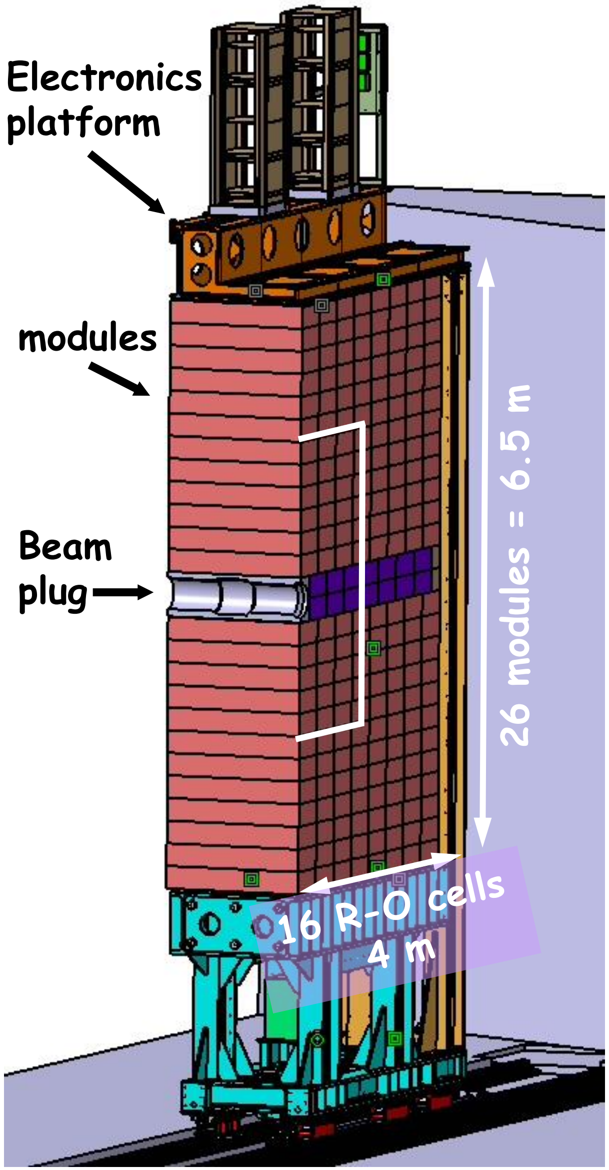

- **Tile calorimeter**
- Active area:
  8.4 x 6.8 m^2
- Instrumented depth:
  120 cm (5.6 λ_I)
- Inner zone:
  cells 131 x 131 mm^2
- Outer zone:
  cells 262 x 262 mm^2
- In total 1488 cells
- LED based monitoring system
- Built-in ^{137}Cs calibration system for *in situ* calibration
- Moderate energy resolution:

$$\frac{\sigma}{E} = \frac{(69 \pm 5)\%}{\sqrt{E}} \oplus (9 \pm 2)\%$$

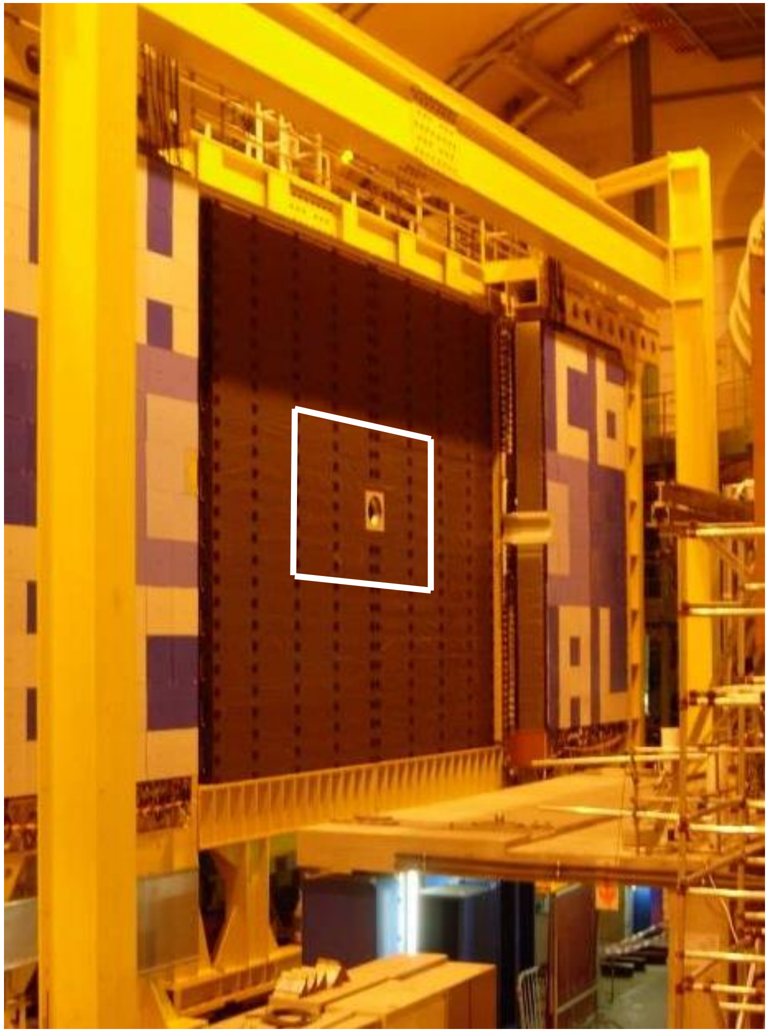

HCAL module

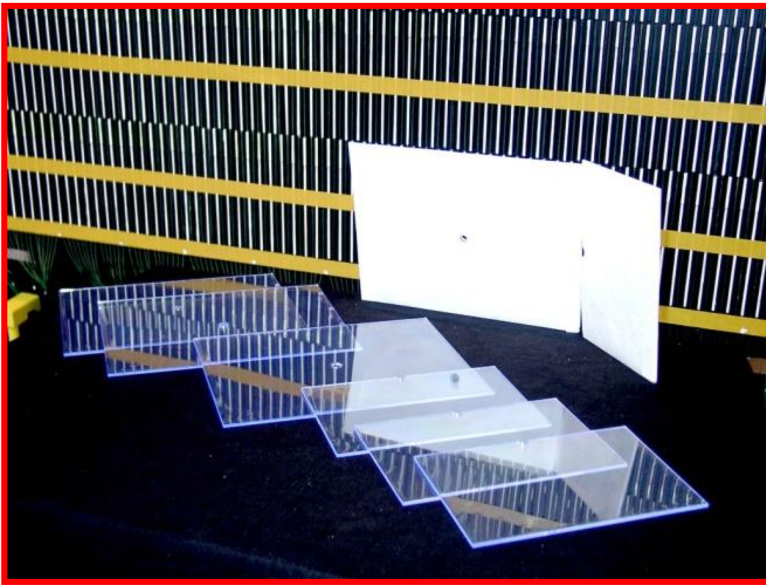

Fiber-tile contact length adjusted to compensate light attenuation difference

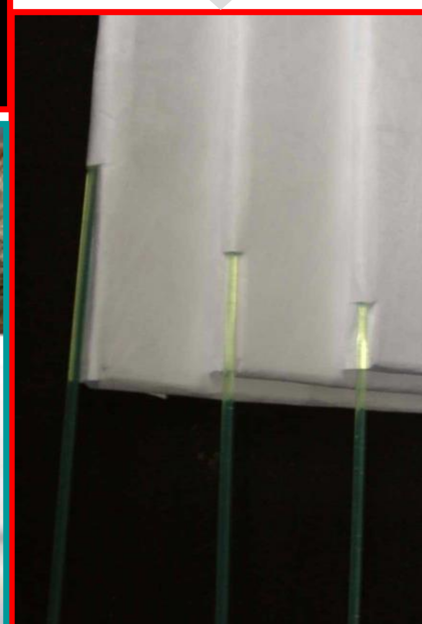

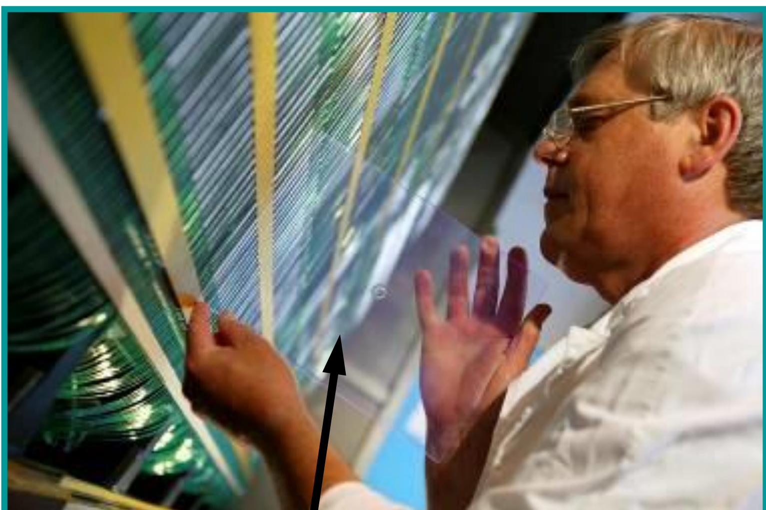

Scintillator tile
256 mm x 197 mm x 3 mm

52 modules with longitudinal tiles

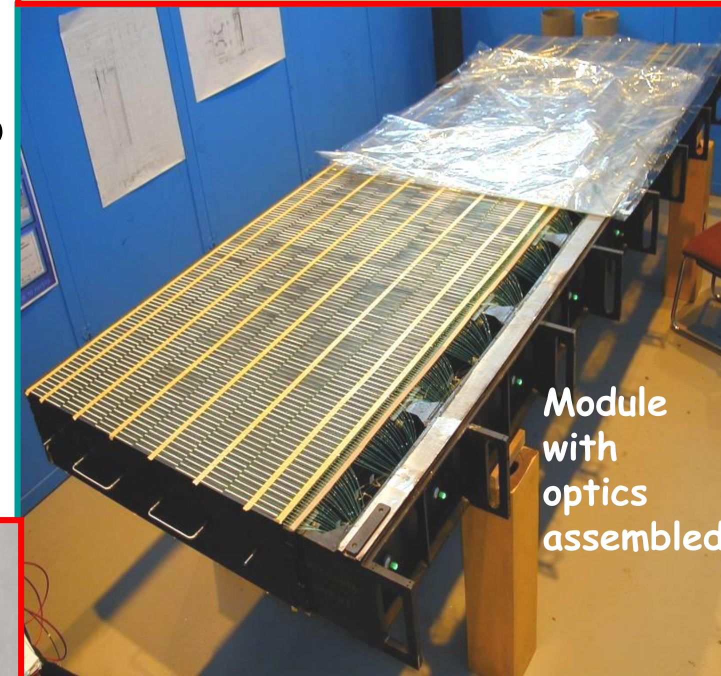

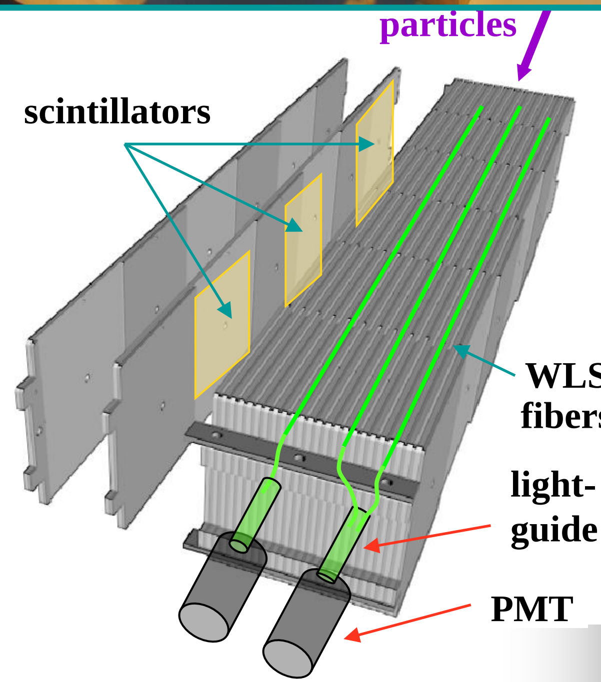

A pulse shape study on 30 GeV electron beam for 6 different layers in depth of the HCAL: 25 ns pulse shaping

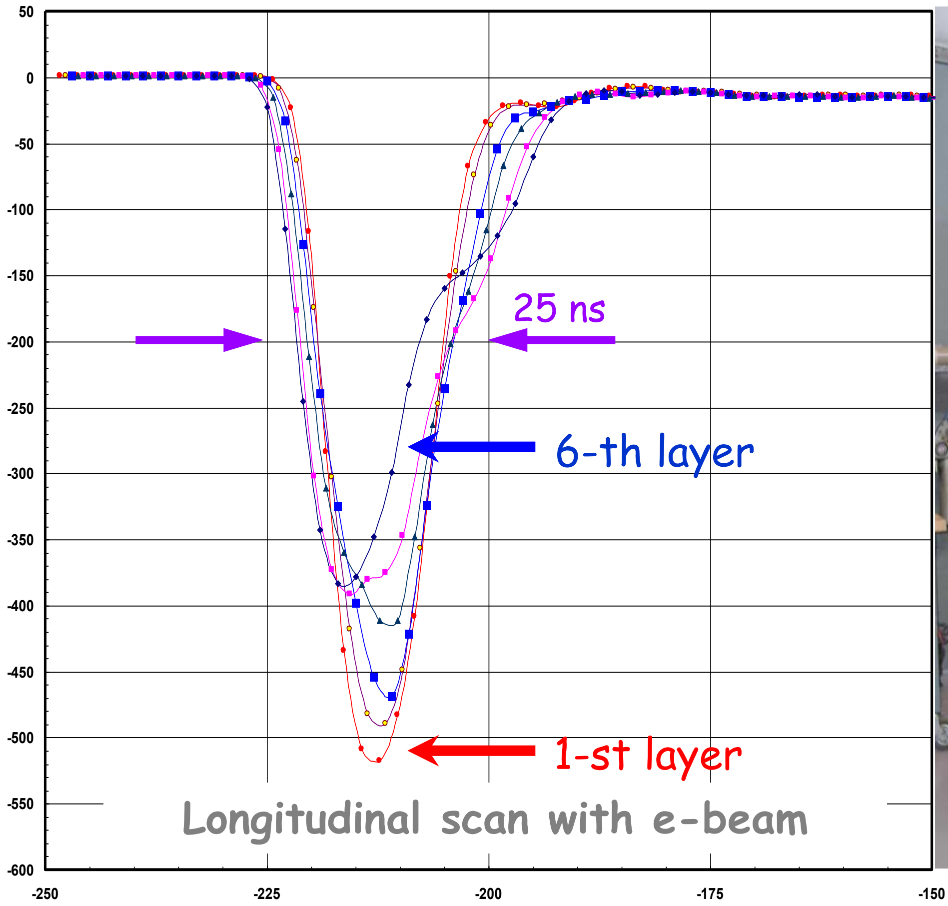

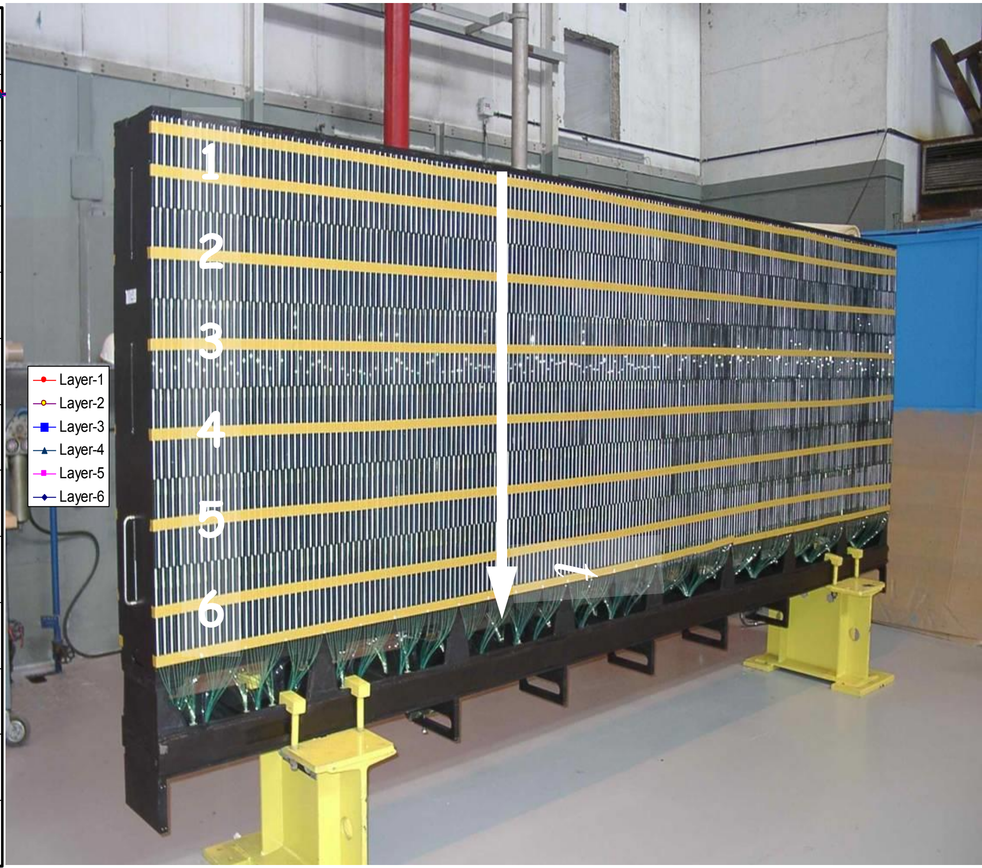

Signal variations due to detector depth and mirrors at fiber ends

Electromagnetic calorimeter

- Shashlik technology, 6016 detector cells/R-O channels, grouped in 3312 modules

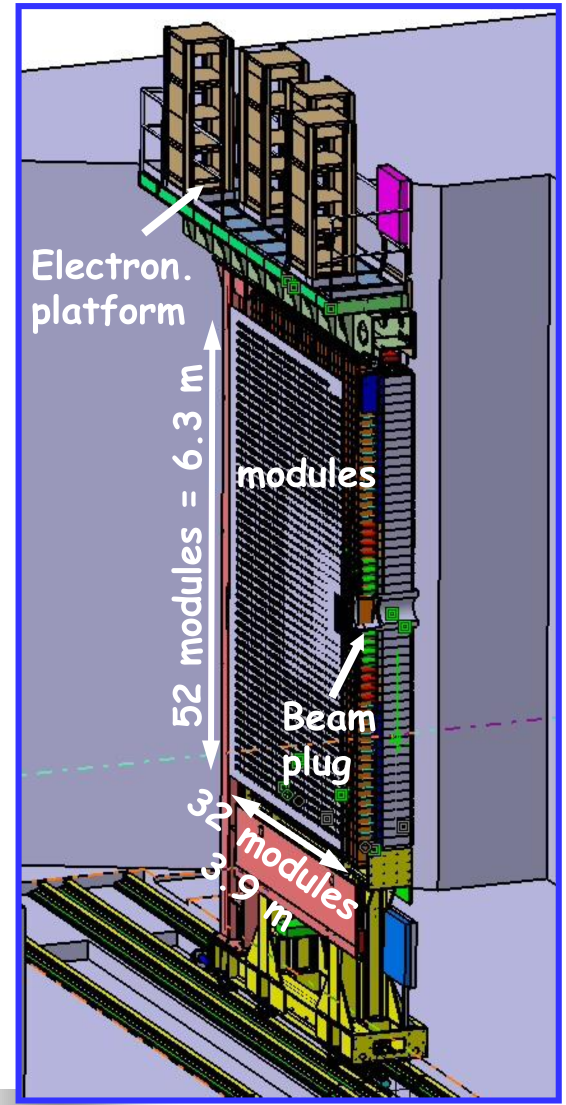

	Inner section	Middle section	Outer section
Inner size, $x \times y$, cm^2	65×48	194×145	388×242
Outer size, $x \times y$, cm^2	194×145	388×242	776×630
Cell size, cm^2	4.04×4.04	6.06×6.06	12.12×12.12
# of modules	176	448	2688
# of channels	1536	1792	2688
# of cells per module	9	4	1
# of fibers per module	144	144	64
Fiber density, cm^{-2}	0.98	0.98	0.44

- Shashlik means skewered meat and was originally made of lamb. The skewers are either threaded with meat only, or with alternating pieces of meat, fat, and vegetables, such as bell pepper, onion, mushroom and tomato.

- Shashlik means skewered meat and was originally made of lamb. The skewers are either threaded with meat only, or with alternating pieces of meat, fat, and vegetables, such as bell pepper, onion, mushroom and tomato.
- In LHCb Shashlik skewed are scintillator and lead tiles, TYVEK paper and covers, and the skewers are WLS fibers

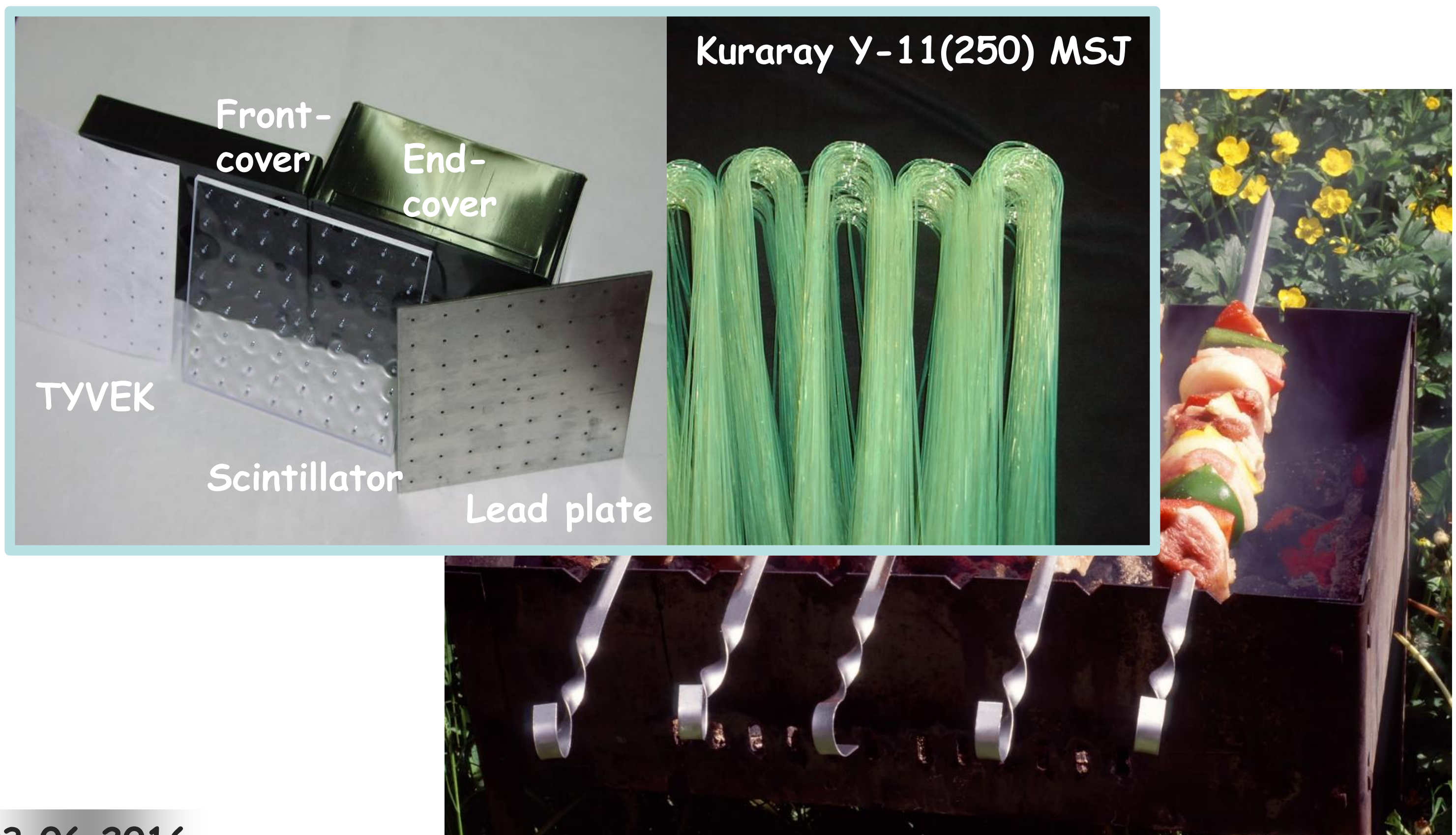

Shashlik technology

- Shashlik means skewered meat and was originally made of lamb. The skewers are either threaded with meat only, or with alternating pieces of meat, fat, and vegetables, such as bell pepper, onion, mushroom and tomato.
- In LHCb Shashlik skewed are scintillator and lead tiles, TYVEK paper and covers, and the skewers are WLS fibers.
- In LHCb Shashlik cannot be eaten and neither smelled, so PMTs are used to extract the signal.

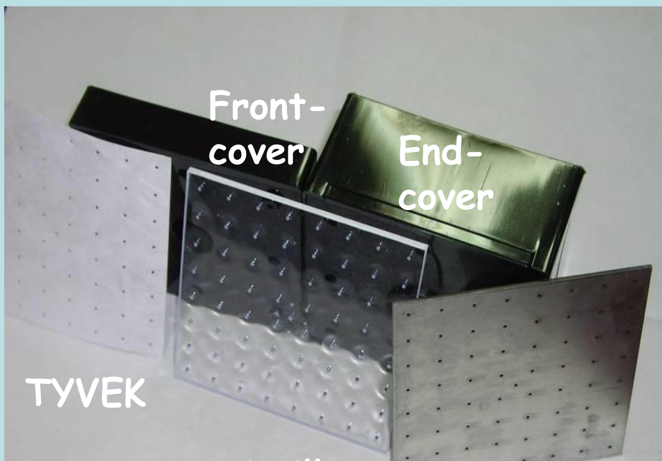

Electromagnetic calorimeter

- ❑ Volume ratio Pb:Sc = 2:4 (mm), 25 X_0 , 1.1 λ depth
- ❑ Light yield: ~3000 ph.e./GeV
- ❑ Granularity varies with the distance from the beam axis
- ❑ Light from scintillator tiles delivered to the readout by WLS fibers

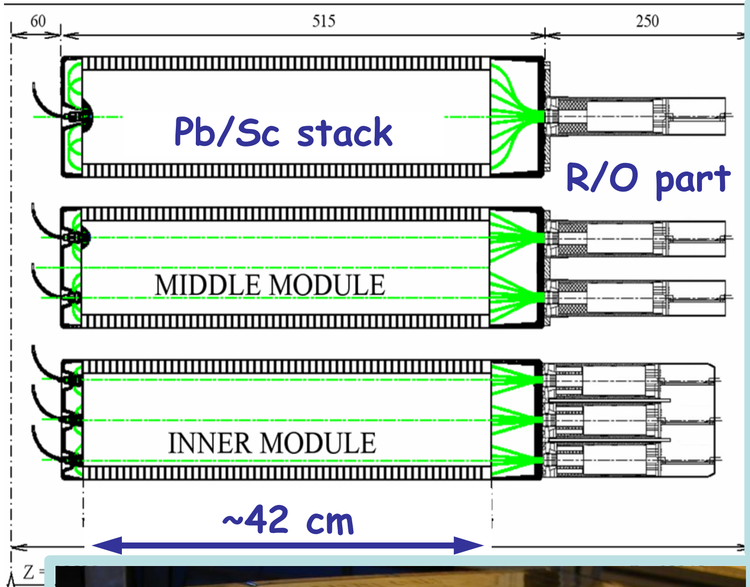

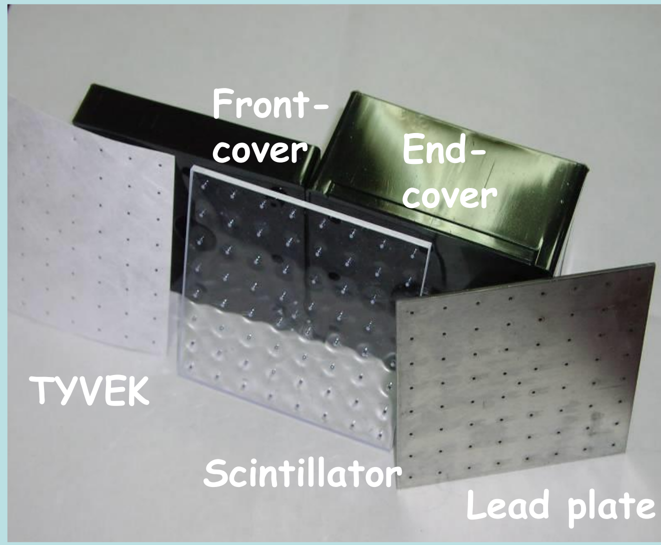

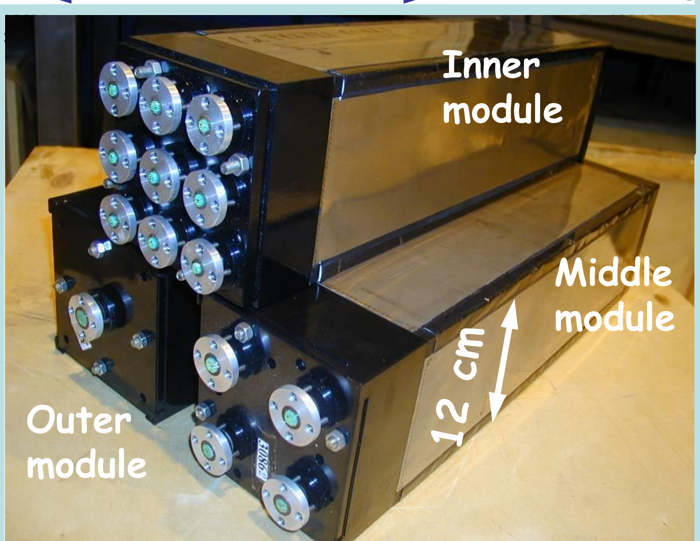

- ❑ Readout: fiber bundle → light mixer → R7899-20 Hamamatsu PMT powered by Cockcroft-Walton base

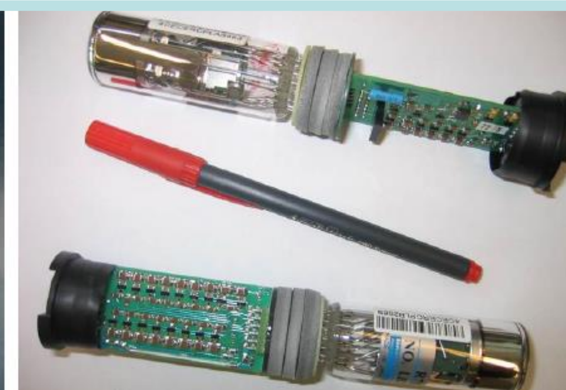

- Tiles are produced with injection moulding technique under high pressure
- Chemical treatment of tile edges, **diffusive light reflection from tile edges** → lateral uniformity!
- In total 450 K tiles produced
- Tile-to-tile spread: r.m.s.<2.5%

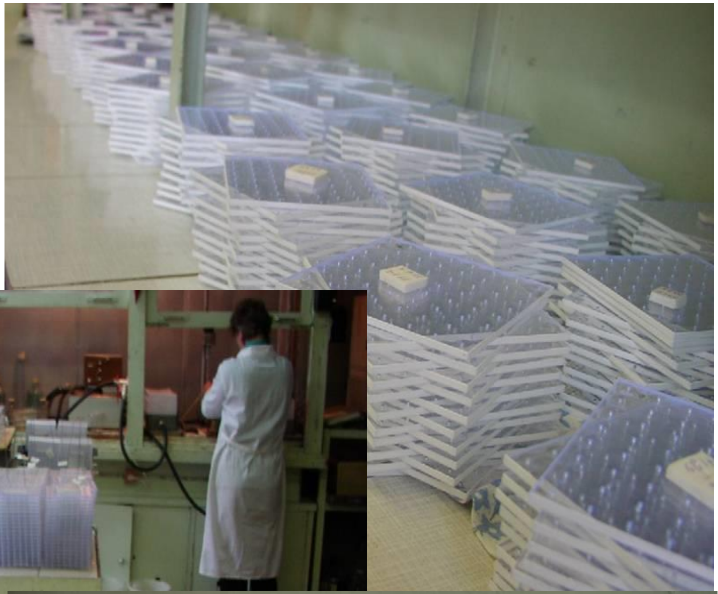

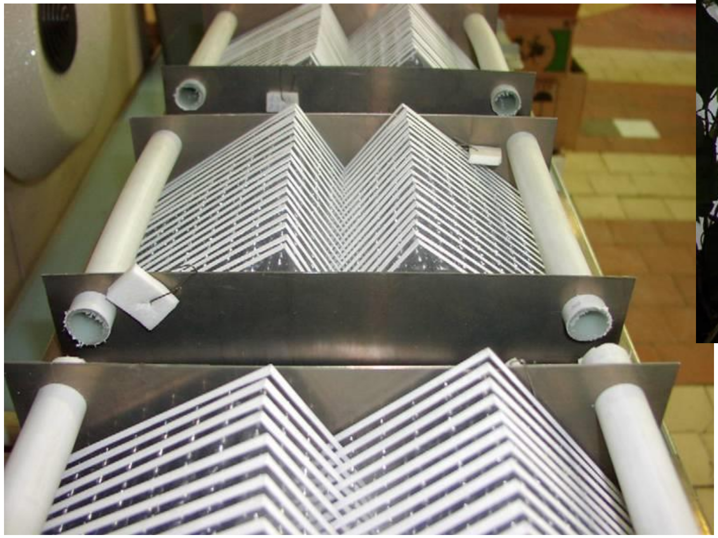

ECAL: production of fiber loops

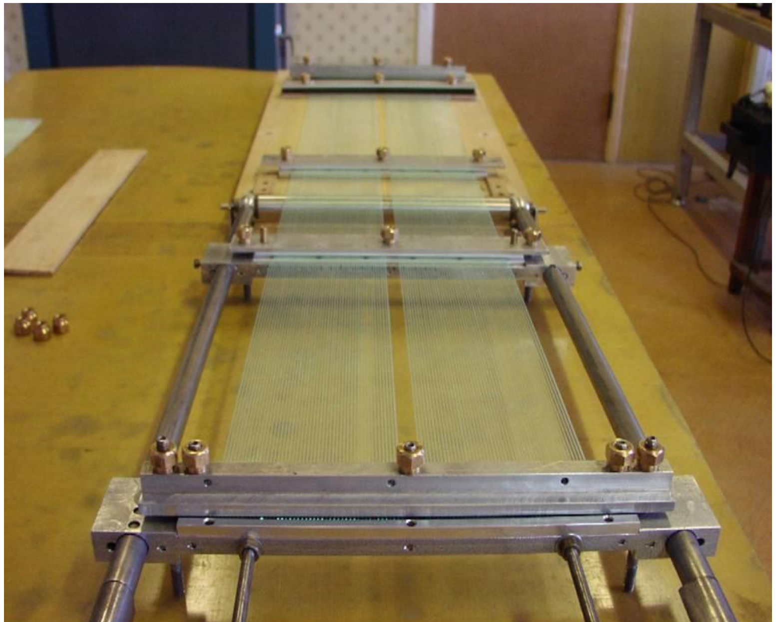

- Fiber bending under the load in a uniformly distributed heating

- They serve handles, and improve cooking efficiency

- They serve handles, and improve cooking efficiency

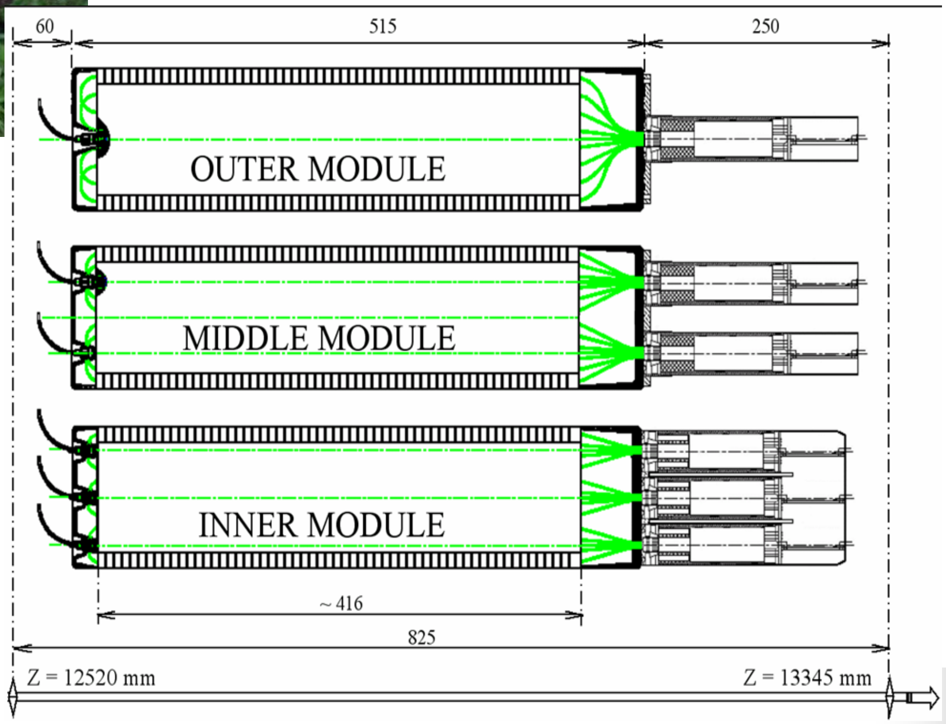

ECAL: fiber loops

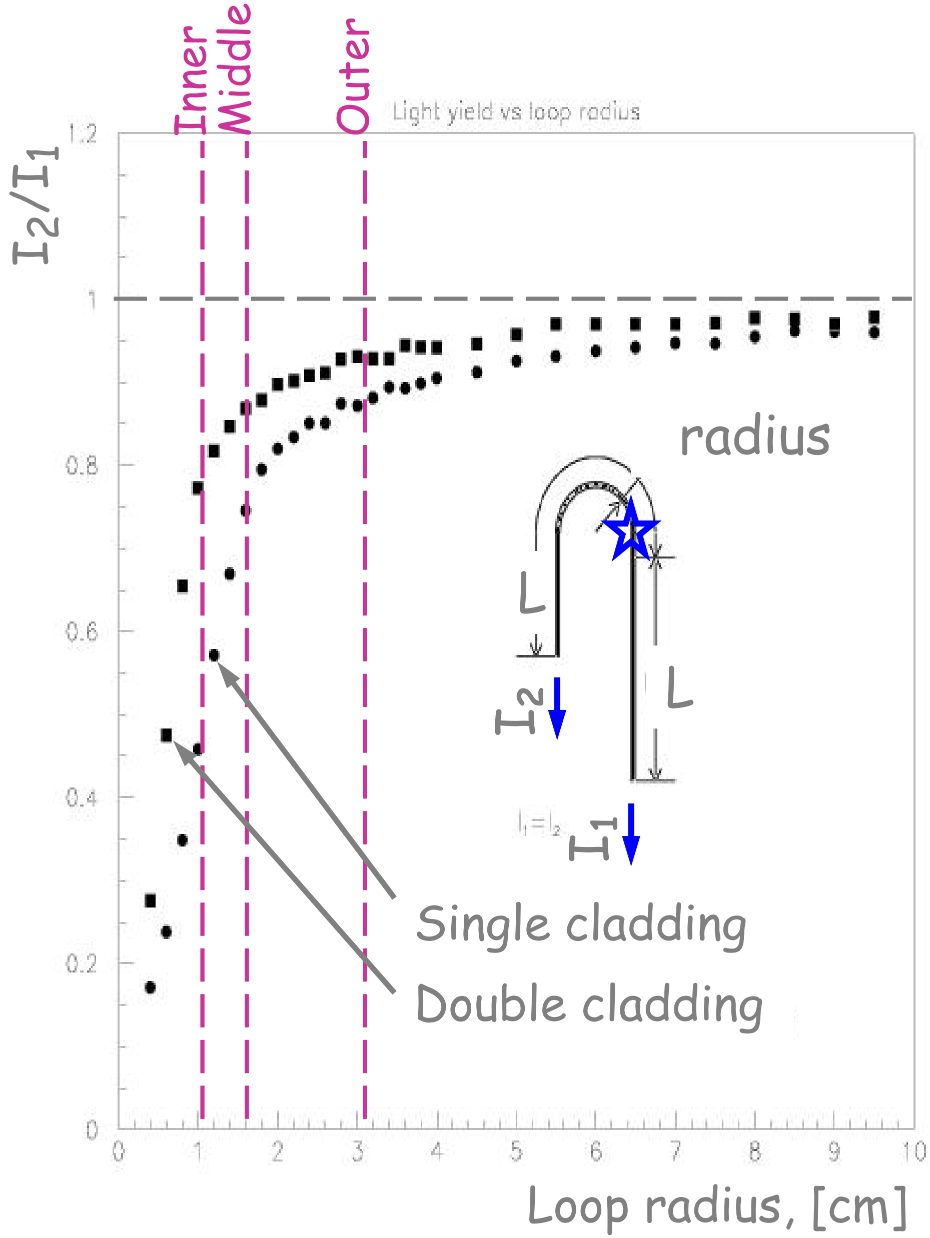

- Fiber bending down to loop radii ~10mm
- In total 140 K loops produced
- Loop-to-loop spread: r.m.s. < 1.6%

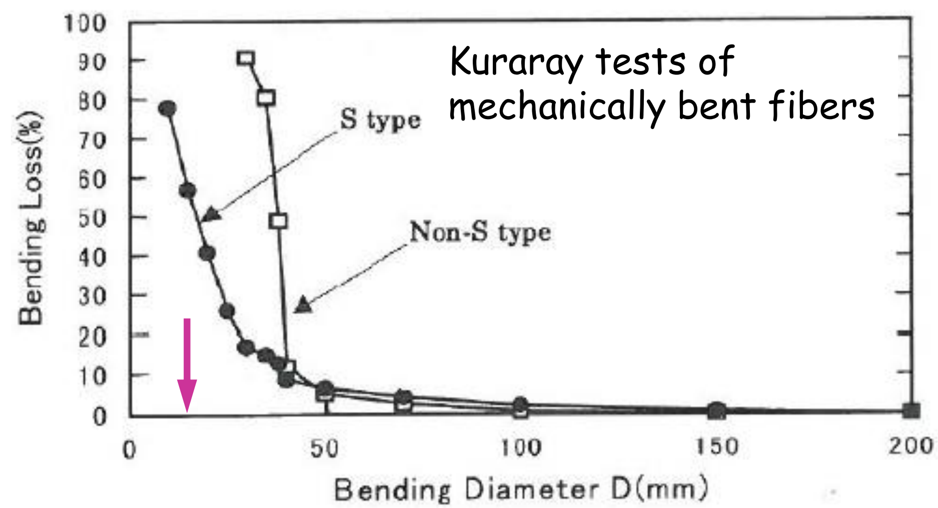

ECAL: module assembly

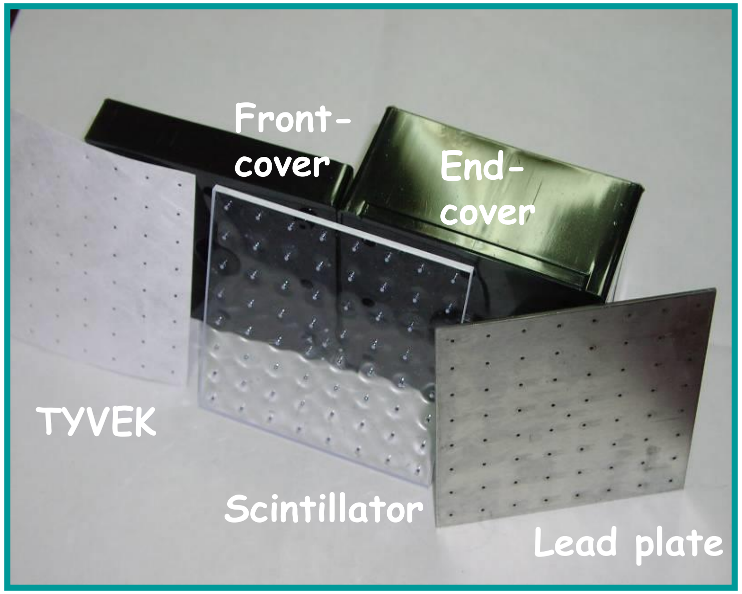

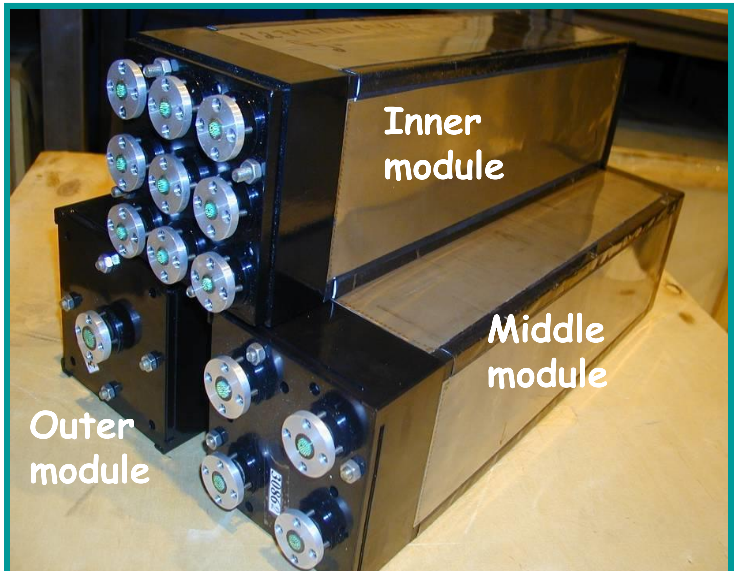

- In total 3.6 K modules produced

- Lateral uniformity of response enters constant term of energy resolution
- **Global uniformity**: light collection efficiency depending on a distance to the tile edge
  - Depends on reflection quality (tile edge treatment !), light attenuation, fiber density, …
- **Local uniformity**: light collection efficiency depending on a distance to fibers
  - Depends on fiber density, reflection quality, mirror/diffusive reflection, light attenuation, …
  - Fiber density is also constrained by a good uniformity region on the PMT photocathode

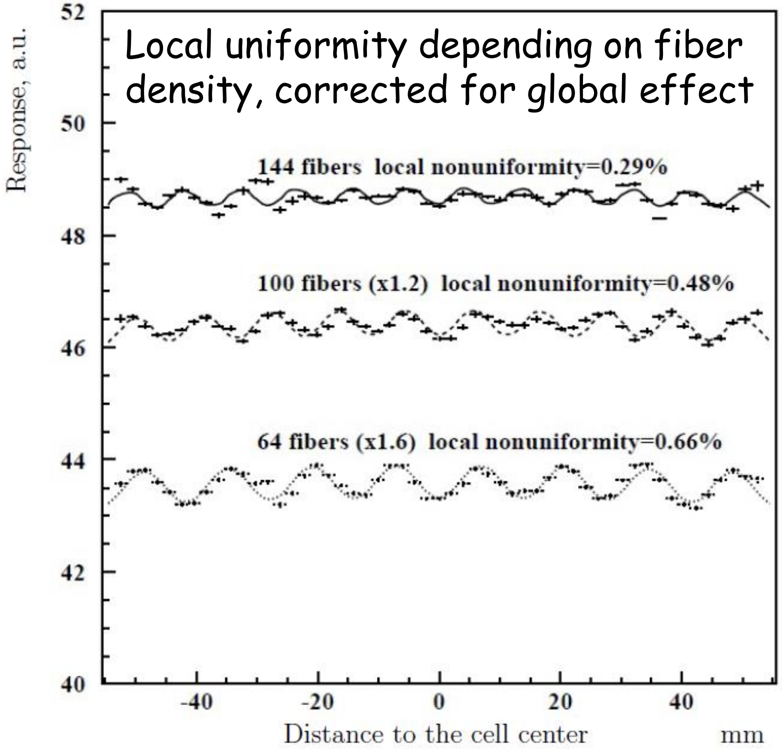

- Uniformity parametrization

$$f(x) = a \times \left[1 - A_{global} \cdot \left(\frac{x - x_0}{l_0/2}\right)^2\right] \times \left[1 - A_{local} \cdot \cos\left\{\frac{2\pi}{d} \cdot (x - x_0)\right\}\right]$$

ECAL: lateral uniformity of response

Energy resolution, Design: $\frac{10\%}{\sqrt{E}} \oplus 1\%$ Measured: $\frac{(9.4\pm0.2)\%}{\sqrt{E}} \oplus (0.83 \pm 0.02)\% \oplus ((145 \pm 13)\ \text{MeV})/E$

Lateral uniformity of response:

Lateral scan of ECAL module with 50 GeV e^- beam

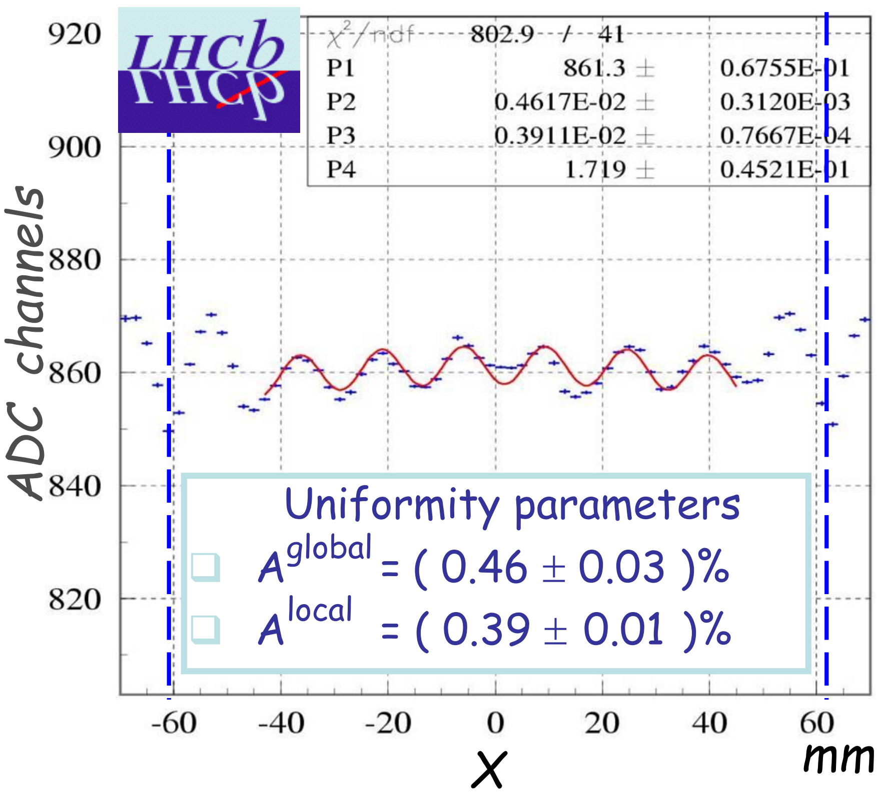

Transverse scan with 80 GeV electrons

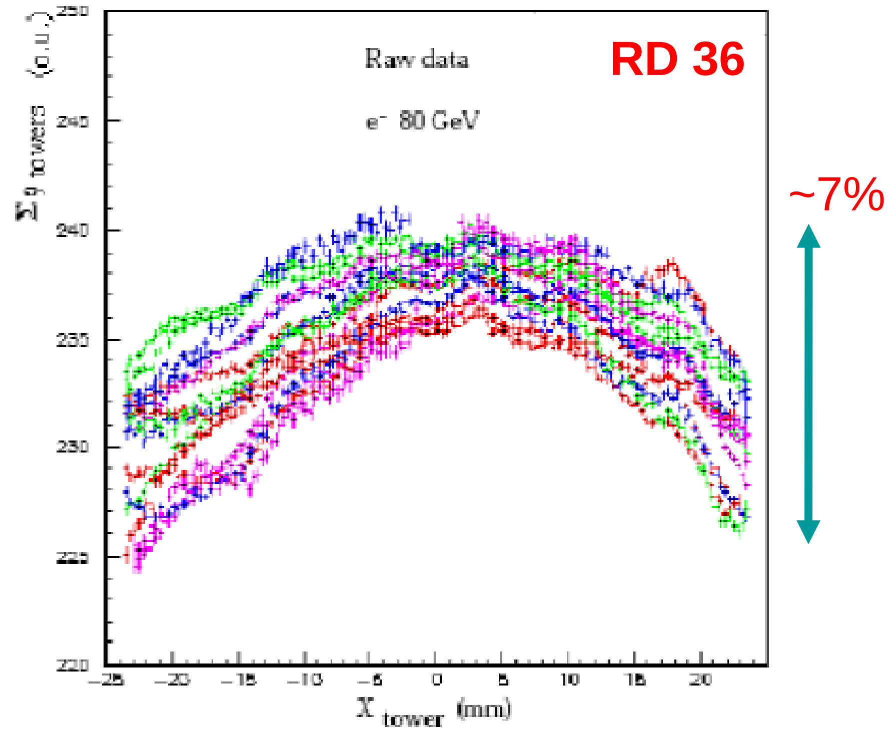

Spread over the module (Max.-to-Min.):

- ±1.3% for e-beam parallel to module axis
- ±0.6% for e-beam at 200 mrad

Energy resolution: constant term

Contribution from the lateral non-uniformity

Errors quoted are the errors of the fit !

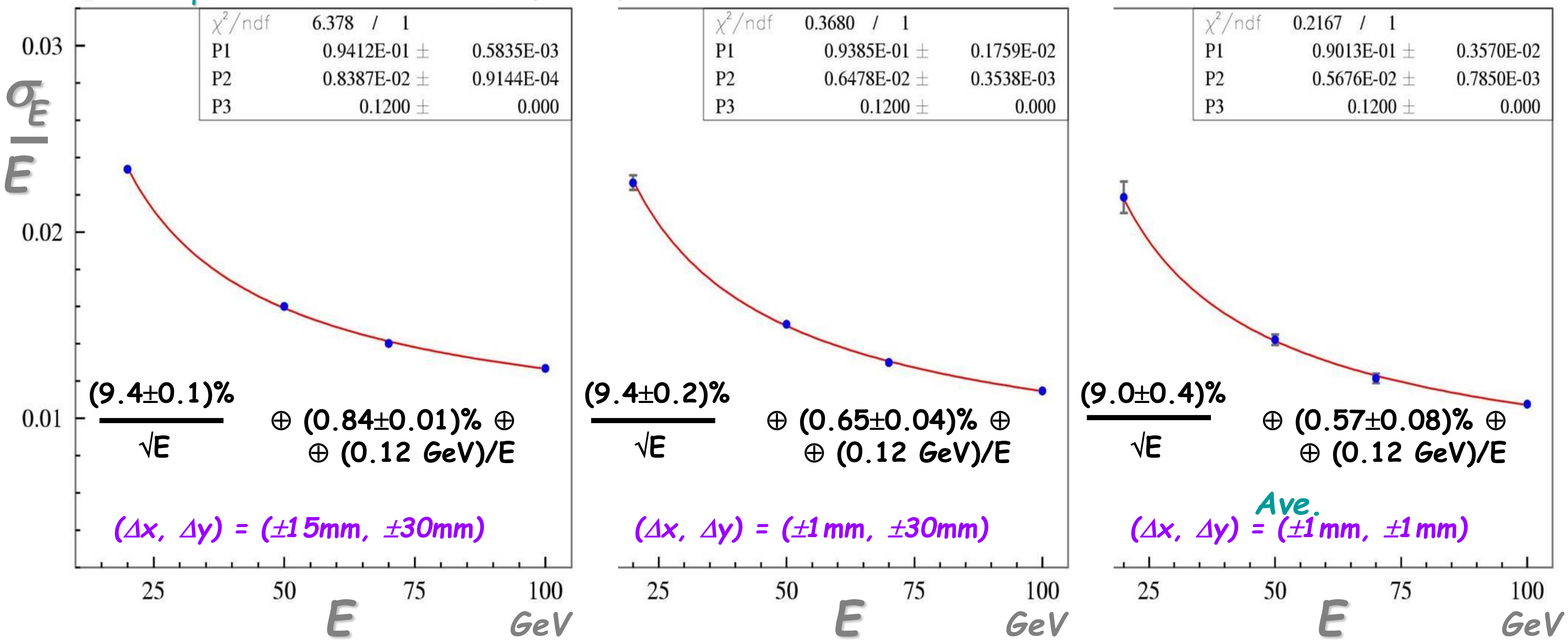

For // tracks, ~half of the constant term value comes from lateral non-uniformity of response

ECAL: cells calibration

- All ECAL cells pre-calibrated with cosmic particles

	Number of cells	Number of bad cells (out of 3σ)	Spread of MIP signal positions	Spread with measurement error (3%) subtracted
Inner	1935	12	8.0%	7.4%
Middle	1798	2	5.3%	4.4%
Outer	2790	4	6.7%	6.0%

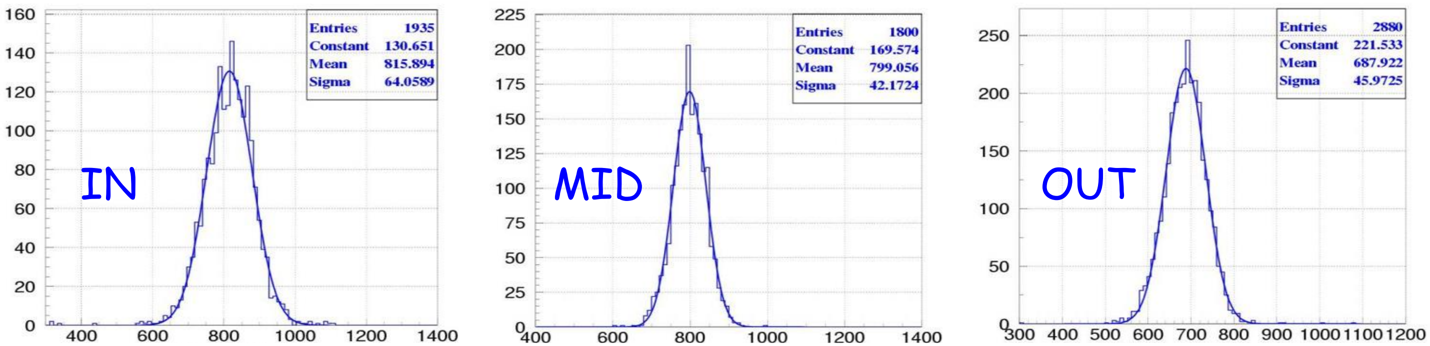

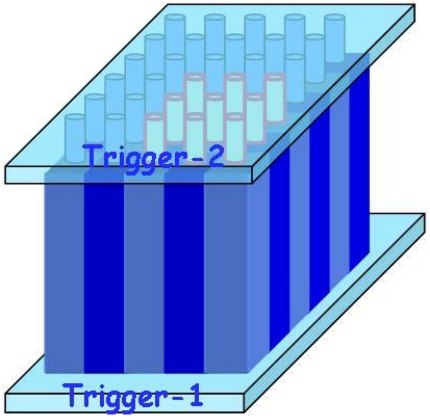

MIP position, ADC channels

- Pre-calibration with cosmic rays, including readout → ~10%
- Gain dependence adjustment (LED pulses) → ~6%
- Resolved π° - iterative procedure to match the mass and minimize width of the peak → ~1%
- E/p of isolated (ECAL) positively identified (RICH) electrons
- Monitoring gain variations with ~11 kHz LED pulses (e.g. corrects rate effect)

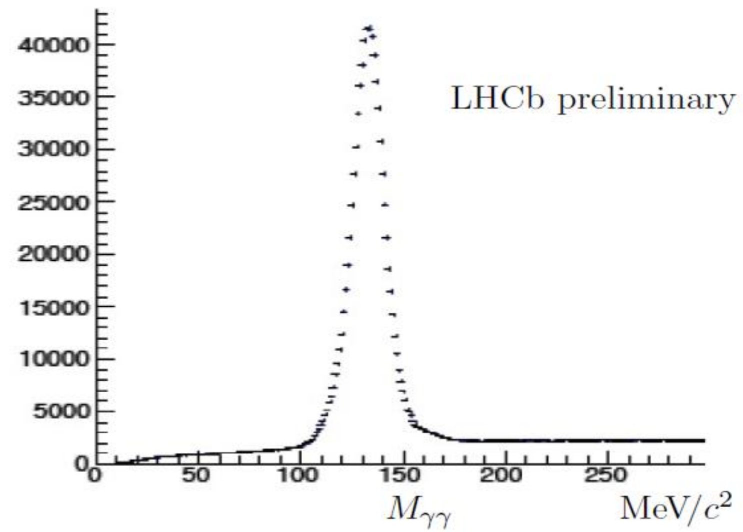

Radiation resistance tests of components for ECAL

Expected dose rate at shower maximum of closest cell: 0.03 rad/s
(x 1.7 from later simulations)

Potential radiation-induced **damage** of

- Scintillator tile: brightness, transparency, edge reflection quality
- WLS fibers: brightness, transparency, loop quality

(structure distortion, active radicals, radiolysis gaseous products, …)

Reduced **prediction power** because of

- tricky comparison between different tests
- difficult to project test results to real experiment operation
- different irradiation conditions: particle types, dose rate, annealing conditions, geometry of irradiation, exactitude of raw material (track up to producer & production batch), …
- annealing effect depends on many things, including dose accumulation rate

Systematic **irradiation tests** of scintillator tiles and few types of WLS fibers, including loops, using different type/rate/geometry/… of irradiation

Remaining **uncertainties**: BASF-165 and fiber loops radiation resistance tested up to 2.5 Mrad; actual dose vs. simulated; different dose rate; realistic decomposition of irradiating particles

- Tiles: PSM-115
- Irradiation: Co60 (VNIIFTRE)
- Total dose: 2 Mrad
- Dose rate: ~10 rad/s

tiles 4 x 4 cm

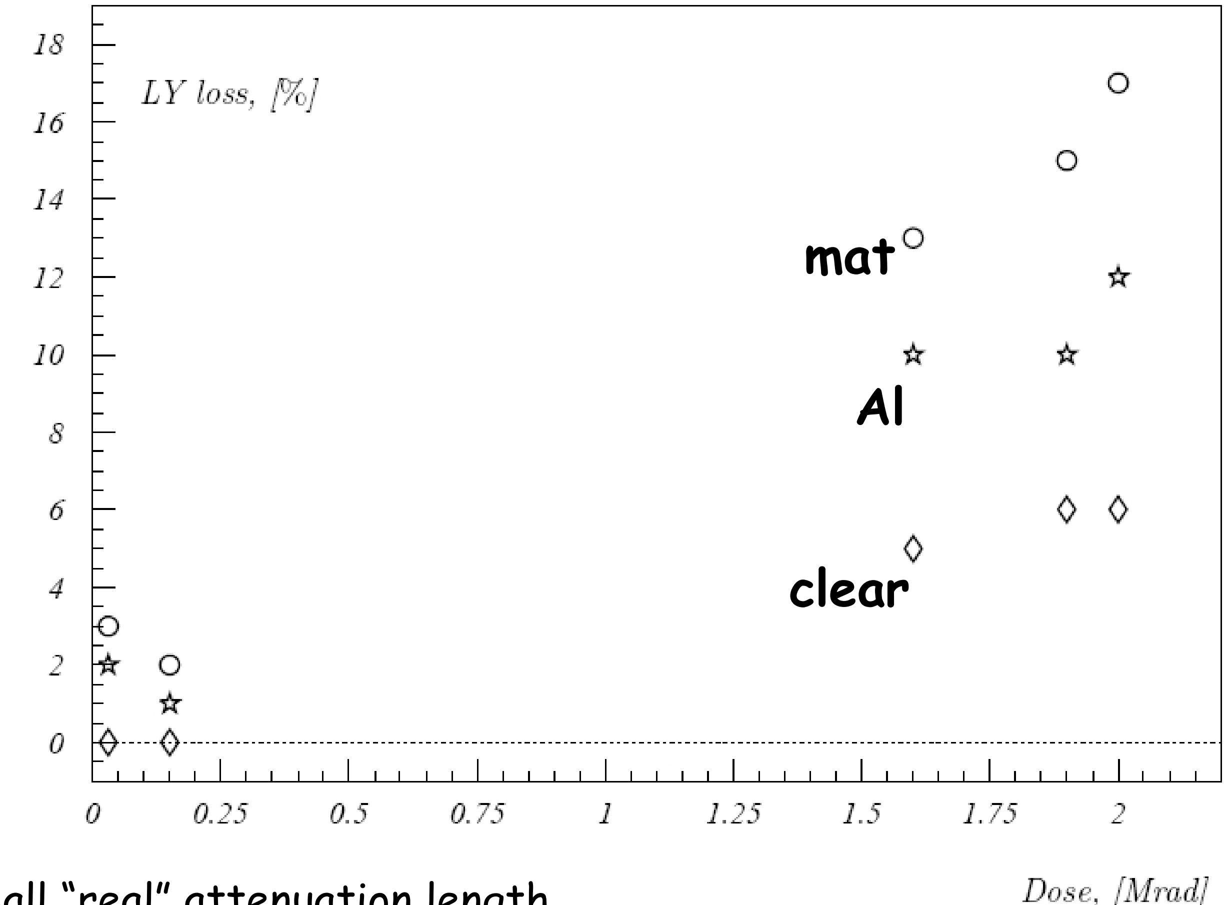

➔ Advantageous to have small “real” attenuation length,
i.e. big fiber density & poor edge reflection

➔ Mat tiles, though yielding better lateral uniformity, degrade faster

Example: irradiation of WLS fibers with protons

ECAL: direct light ~50 cm
+ light passing via the loop

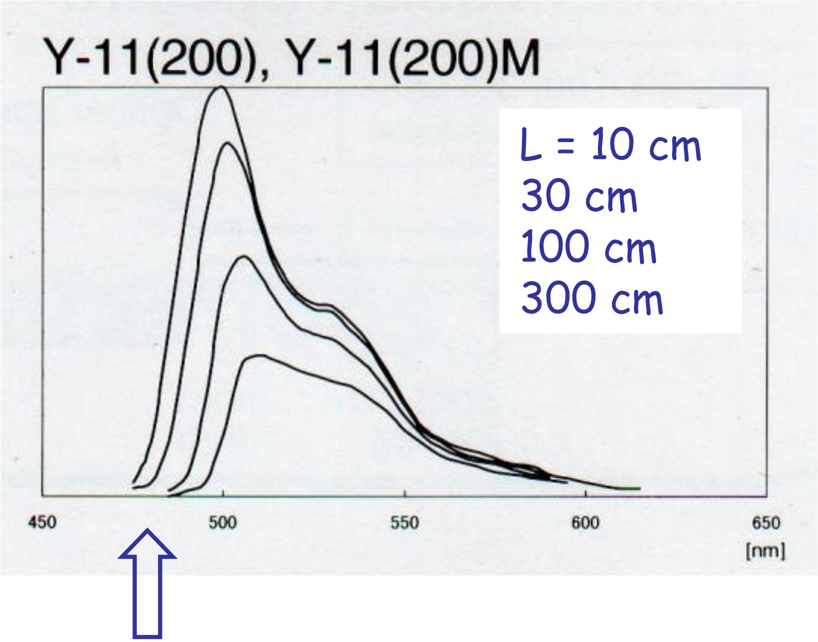

Small λ light dies first under irradiation
➔ longer fibers are "more" radiation resistant

- Fibers: Y11(250)MSJ
- Irradiation: 1.8 GeV **proton beam** (ITEP)
- Total dose: 500, **1000 krad**, rate **~28 rad/s**
- Light attenuation fit: **LY = B e** $^{-x/T}$, where x – distance from tile to the PM.

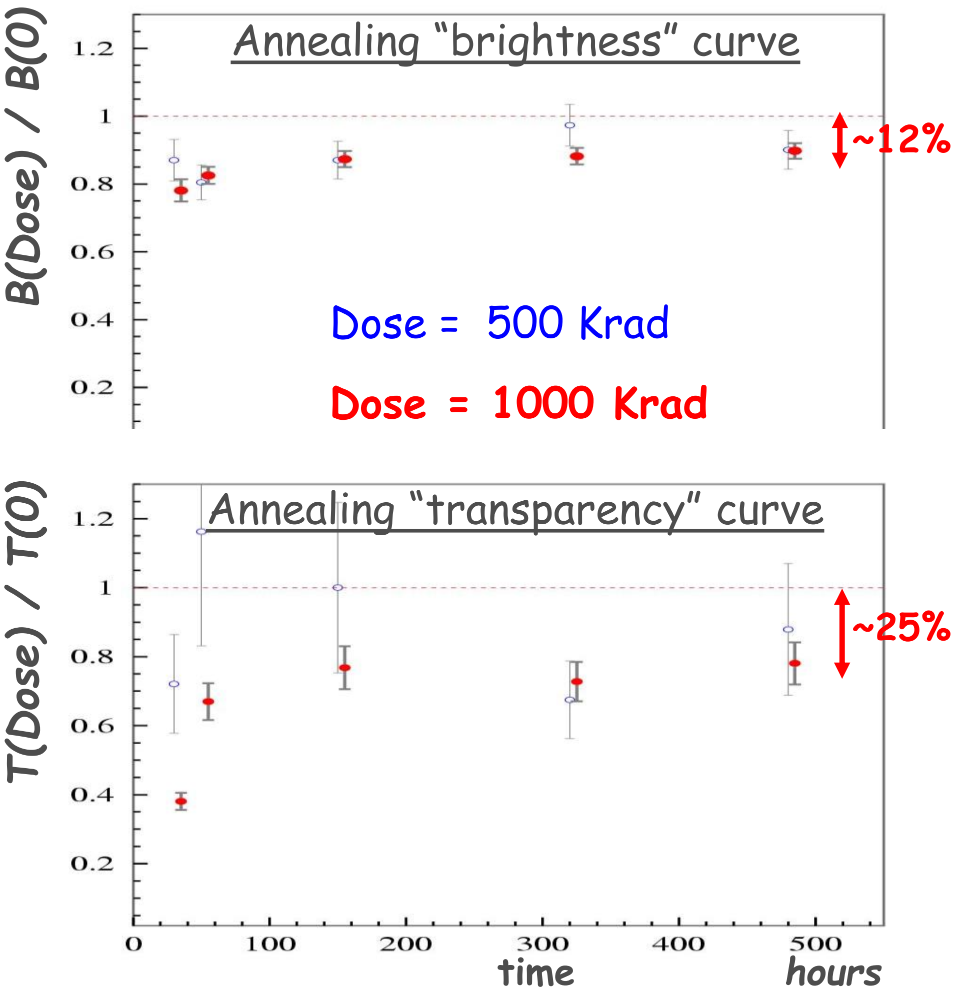

- Irradiation particles: 500 MeV e-beam (LIL)
- Total dose (@ shower max.): 5 Mrad
- Dose rate: 10 rad/s

- Artificial stack: 20 x (1.5mm Pb + 20mm Sc) + fibers (no loops), clear edge

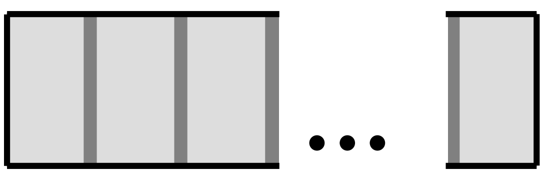

c.f. LHCb stack:
66 x (2mm Pb + 4mm Sc)
+ fiber loops

→ **Longitudinal scan with Sr90 source of irradiated Sc + reference fibers**

PSM-115 + 2.5% p-terphenyl + 0.01% POPOP

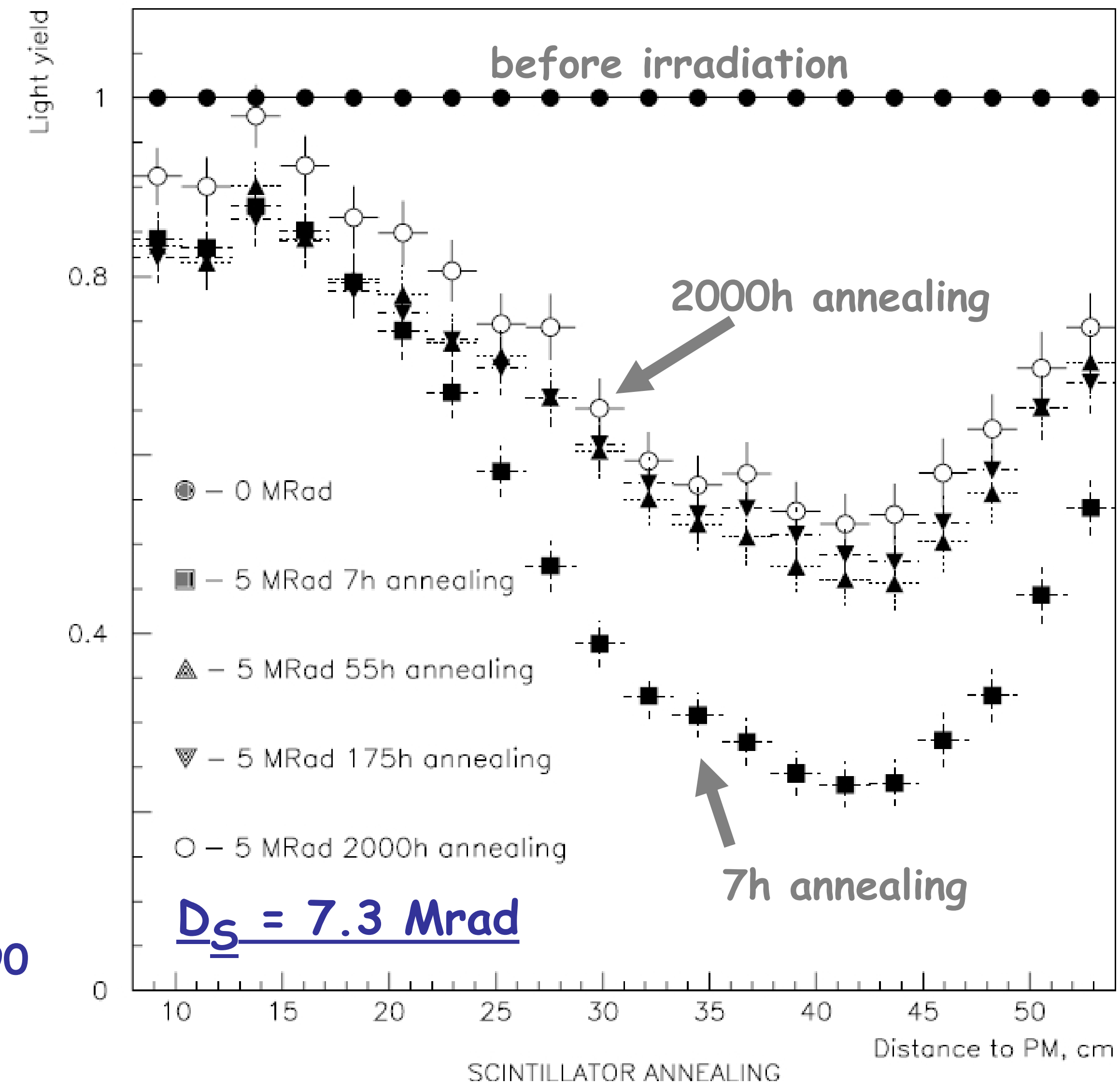

→ Sc LY: $$B_{Sci} = B^0_{Sci} \cdot e^{-\frac{D}{D_S}}$$

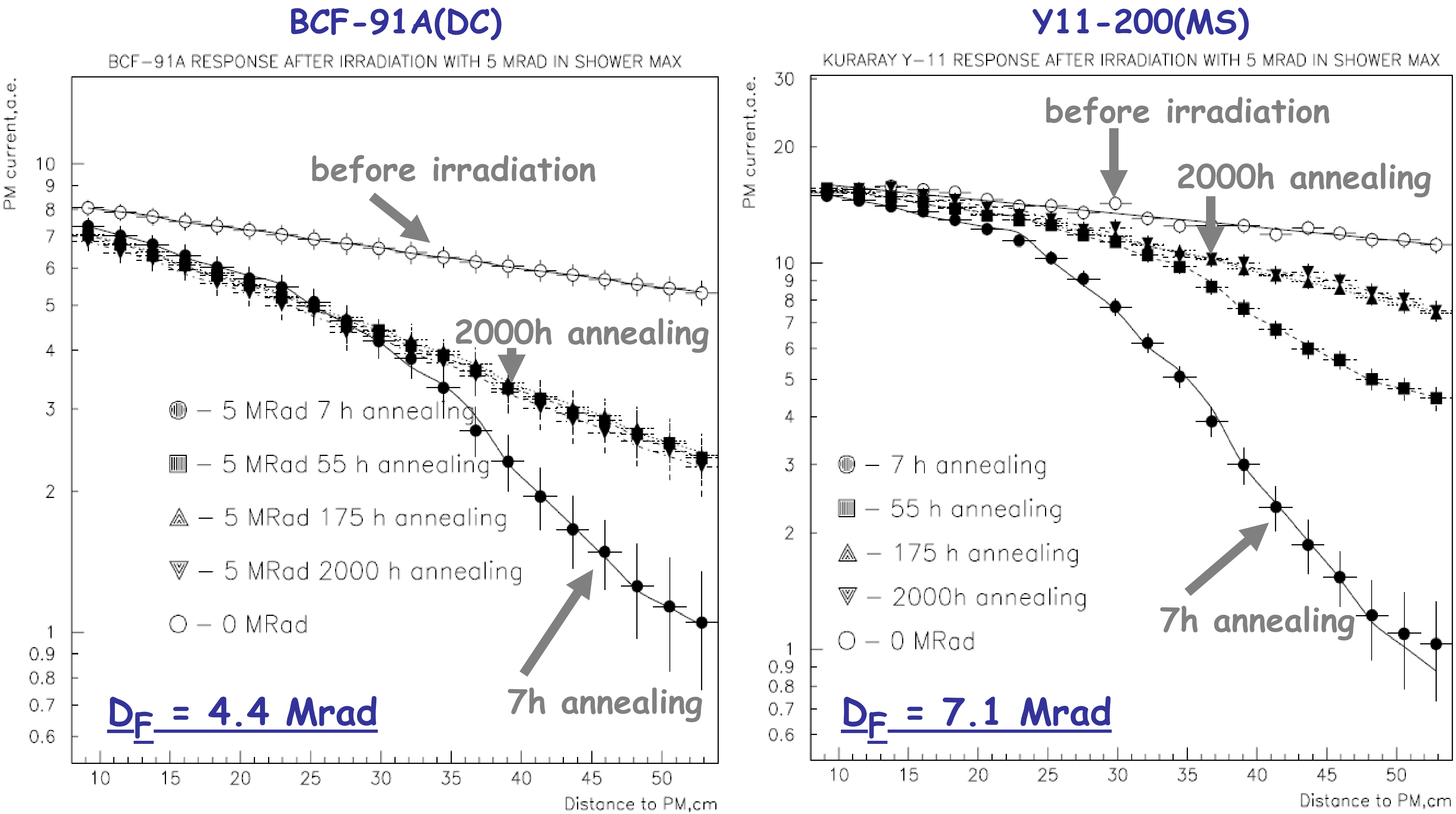

→ Longitudinal scan with Sr90 source of reference Sc + irradiated fibers

→ Attenuation length: $\lambda_{Fib} = \lambda^0_{Fib} \cdot e^{-\frac{D}{D_F}}$

Results from irradiation at LIL: projection to 20 fb^{-1}

→ From measured components degradation + expected dose profile (EM type damage only)

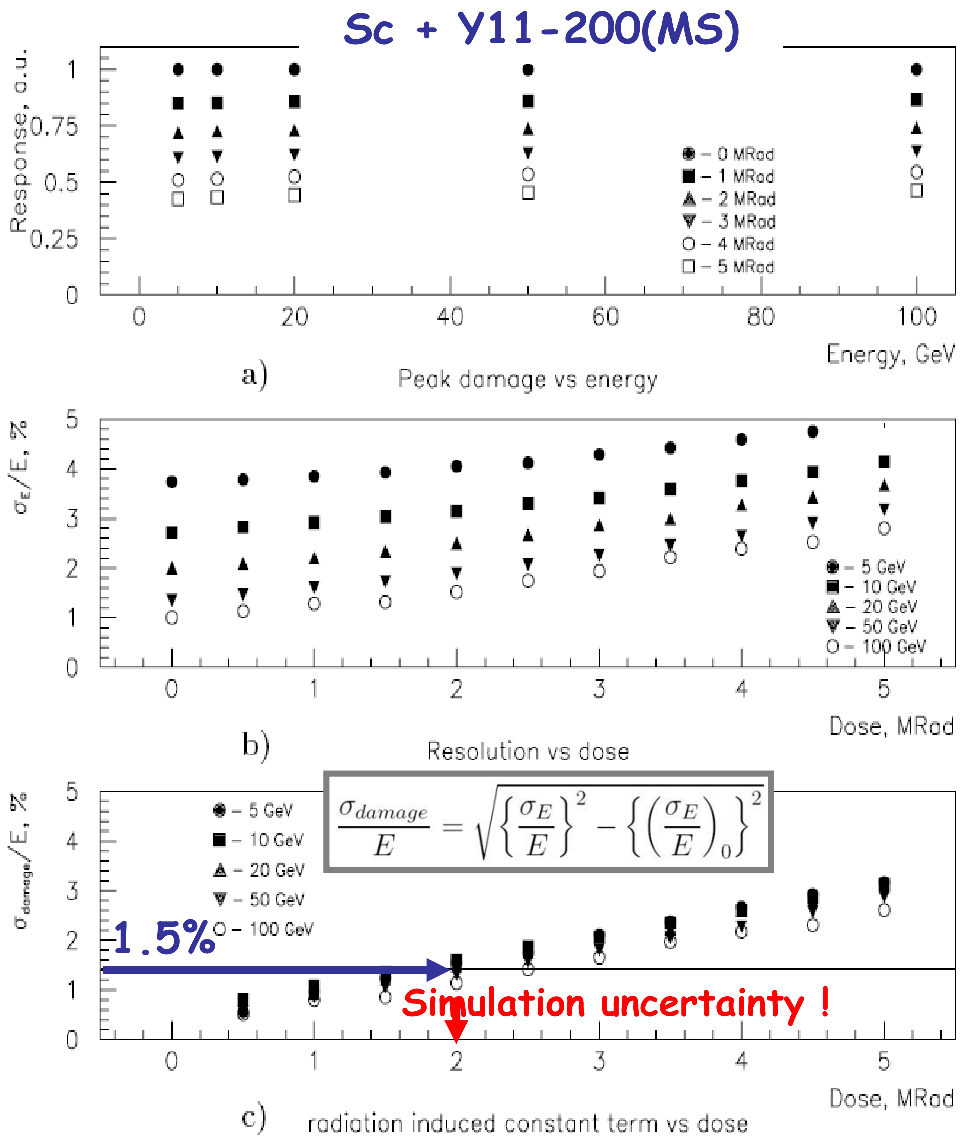

❑ Measure dose map over calorimeter surface ➔ sets of passive monitors installed: Alanine + TLD + pin-diode in common housing

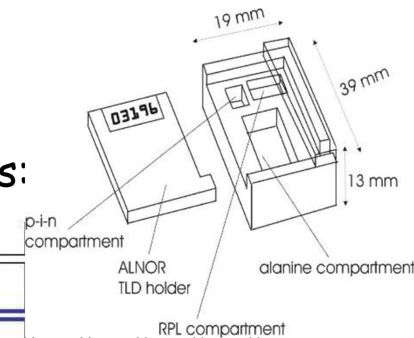

❑ Replaceable innermost modules:

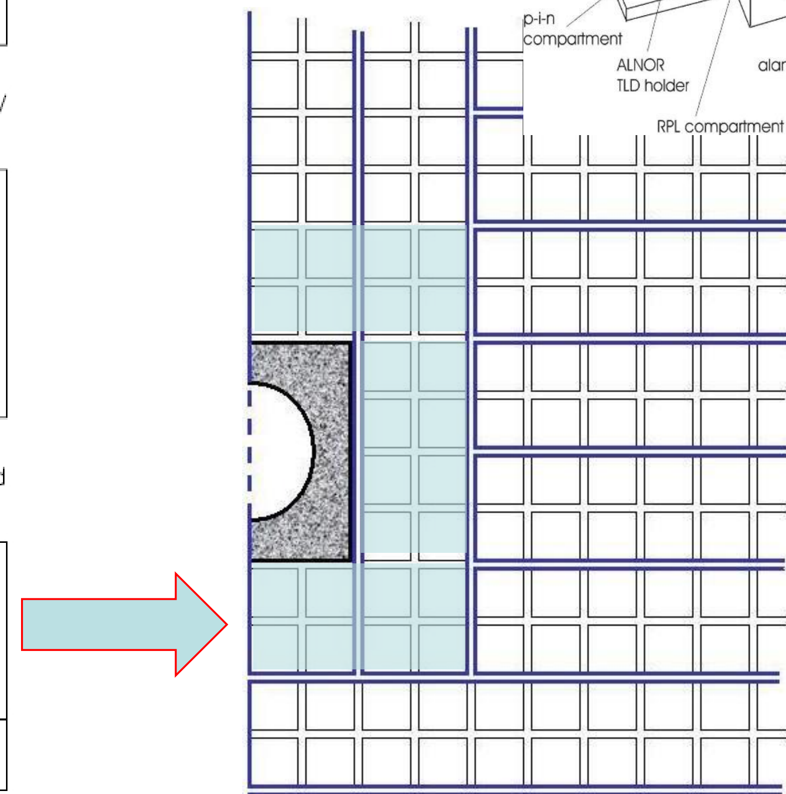

❑ More dedicated irradiation tests, including realistic particle decomposition upstream LHCb

From Yuri Guz

- Irradiation of an Outer ECAL module at CERN PS with 24 GeV protons: 2 runs to ~10^{13} p/cm^2 (~2 Mrad @ shower max) each time, total of 4 Mrad.

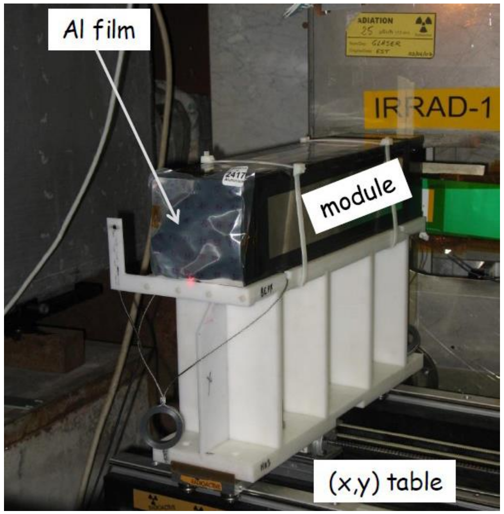

- Measure degradation:
- **Beam tests with e$^-$** at SPS;
- Longitudinal **scan with ^{137}Cs source**

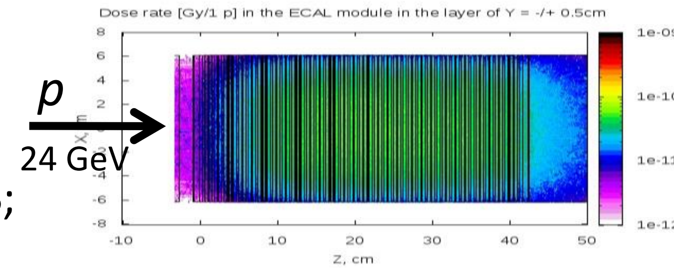

Cs scan results

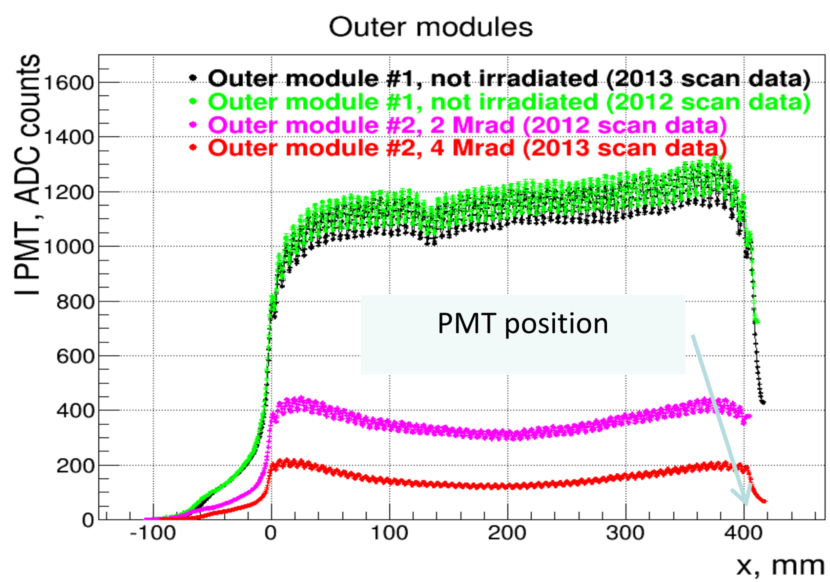

- The module performance is satisfactory with 2 Mrad; not any more with 4 Mrad (upgrade). Expected to be better for Inner modules: higher fiber density. Therefore the ECAL modules should remain operational till ~20 fb^{-1} at least.

- Two Inner type modules were placed in the LHC tunnel at the opposite side from the LHCb interaction point. Equipped with dosimeters.

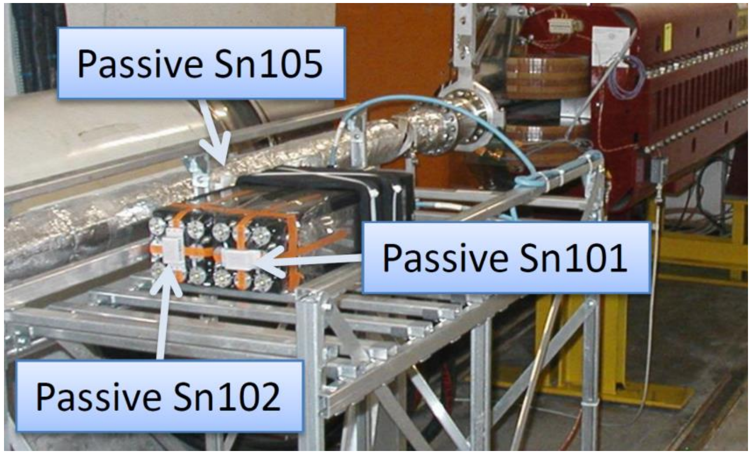

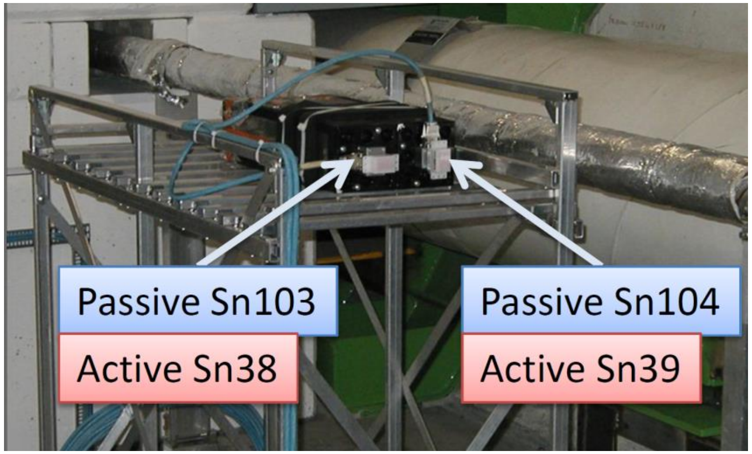

- Readout of dosimeters performed at 1.2 fb^{-1} (~300 krad for cells near beam pipe) and at 3.4 fb^{-1} (~1 Mrad)

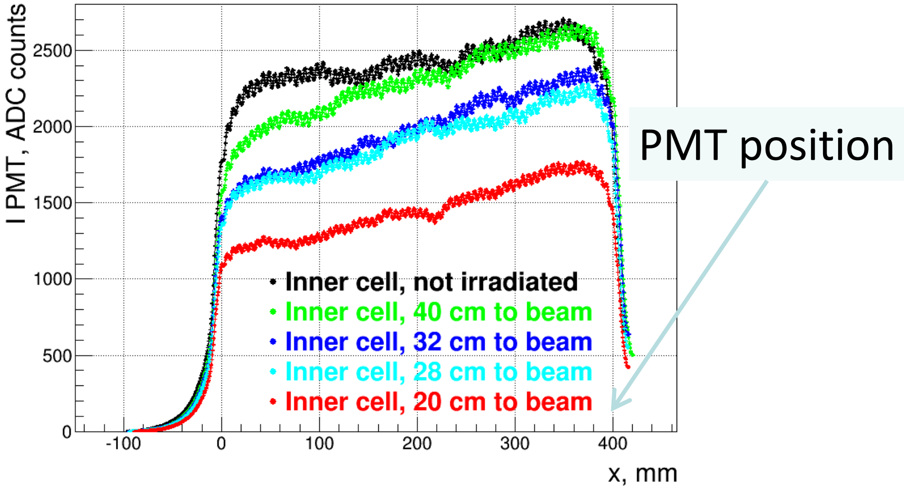

- A (moderate) degradation in the light yield is seen after ~1 Mrad at the ^{137}Cs source scan.

Examples of related physics studies

JHEP 04 (2015) 064

$\sqrt{s}$ = 7 TeV, $\int L dt \sim 1\ fb^{-1}$
$\sqrt{s}$ = 8 TeV, $\int L dt \sim 2\ fb^{-1}$

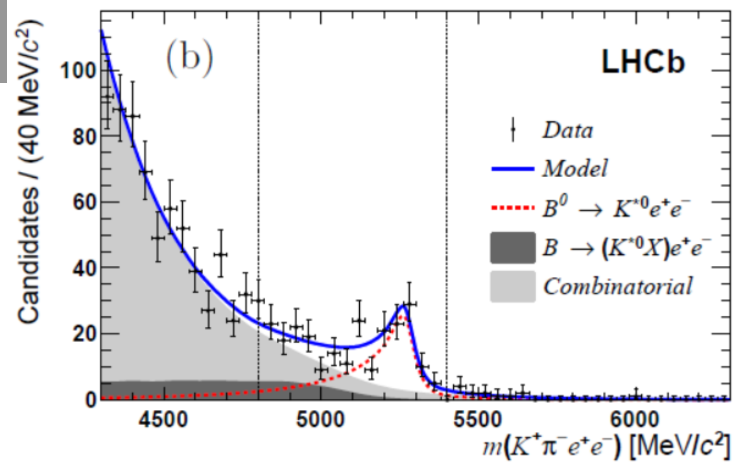

- ❑ Angular analysis of the $B^0 \to K^{*0} e^+ e^-$, decay in the low-q^2 region
- ❑ The e^+e^- mass in [0.002,1.120] GeV^2
- ❑ Observables through angular distributions :

$$\frac{1}{\mathrm{d}(\Gamma+\bar{\Gamma})/\mathrm{d}q^2}\frac{\mathrm{d}^4(\Gamma+\bar{\Gamma})}{\mathrm{d}q^2\,\mathrm{d}\cos\theta_\ell\,\mathrm{d}\cos\theta_K\,\mathrm{d}\tilde{\phi}} = \frac{9}{16\pi}\Bigg[\frac{3}{4}(1-F_\mathrm{L})\sin^2\theta_K + F_\mathrm{L}\cos^2\theta_K + \left(\frac{1}{4}(1-F_\mathrm{L})\sin^2\theta_K - F_\mathrm{L}\cos^2\theta_K\right)\cos 2\theta_\ell + \frac{1}{2}(1-F_\mathrm{L})A_\mathrm{T}^{(2)}\sin^2\theta_K\sin^2\theta_\ell\cos 2\tilde{\phi} + (1-F_\mathrm{L})A_\mathrm{T}^{\mathrm{Re}}\sin^2\theta_K\cos\theta_\ell + \frac{1}{2}(1-F_\mathrm{L})A_\mathrm{T}^{\mathrm{Im}}\sin^2\theta_K\sin^2\theta_\ell\sin 2\tilde{\phi}\Bigg].$$

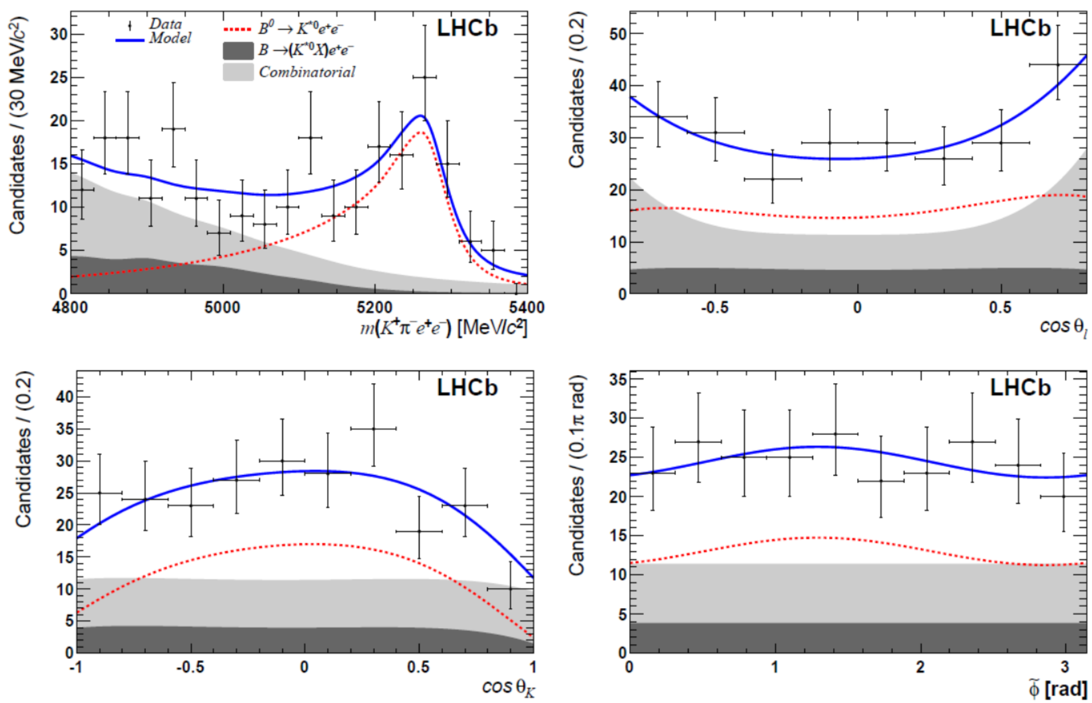

$$F_\mathrm{L} = 0.16 \pm 0.06 \pm 0.03$$
$$A_\mathrm{T}^{(2)} = -0.23 \pm 0.23 \pm 0.05$$
$$A_\mathrm{T}^{\mathrm{Im}} = +0.14 \pm 0.22 \pm 0.05$$
$$A_\mathrm{T}^{\mathrm{Re}} = +0.10 \pm 0.18 \pm 0.05$$

- ❑ In this q^2 region relation between $A_T^{(2)}$ and A_T^{Im} and C_7 and C_7' precise to 5%.

Examples of related physics studies

EPJ C74 (2014) 3092

$\sqrt{s}$ = 7 TeV, $\int L dt \sim 1\ fb^{-1}$

$\sqrt{s}$ = 8 TeV, $\int L dt \sim 2\ fb^{-1}$

- ❑ Production of χ_b and observation of the decay $\chi_b(3P) \to \Upsilon(3S)\,\gamma$

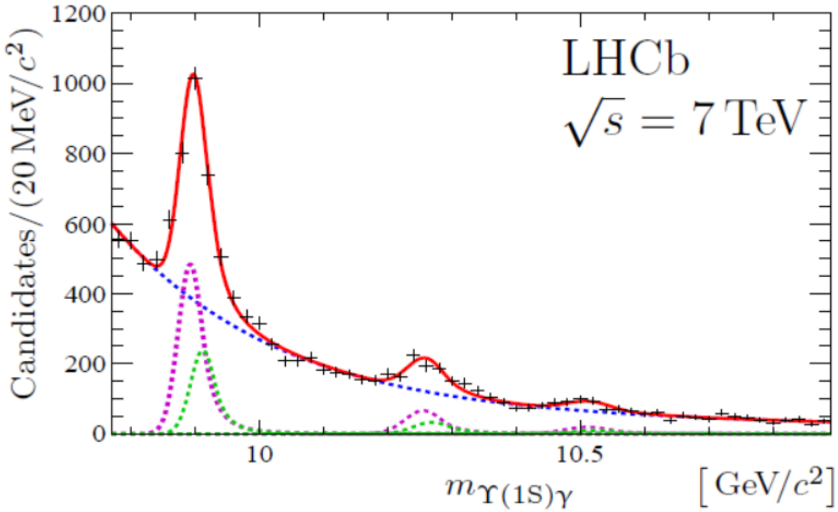

- ❑ Measure fractions of Υ mesons originating from χ_b radiative decays
- ❑ Precise measurement of the $\chi_{b1}(3P)$ mass

$$m_{\chi_{b1}(3P)} = 10\,511.3 \pm 1.7 \pm 2.5\,\mathrm{MeV}/c^2$$

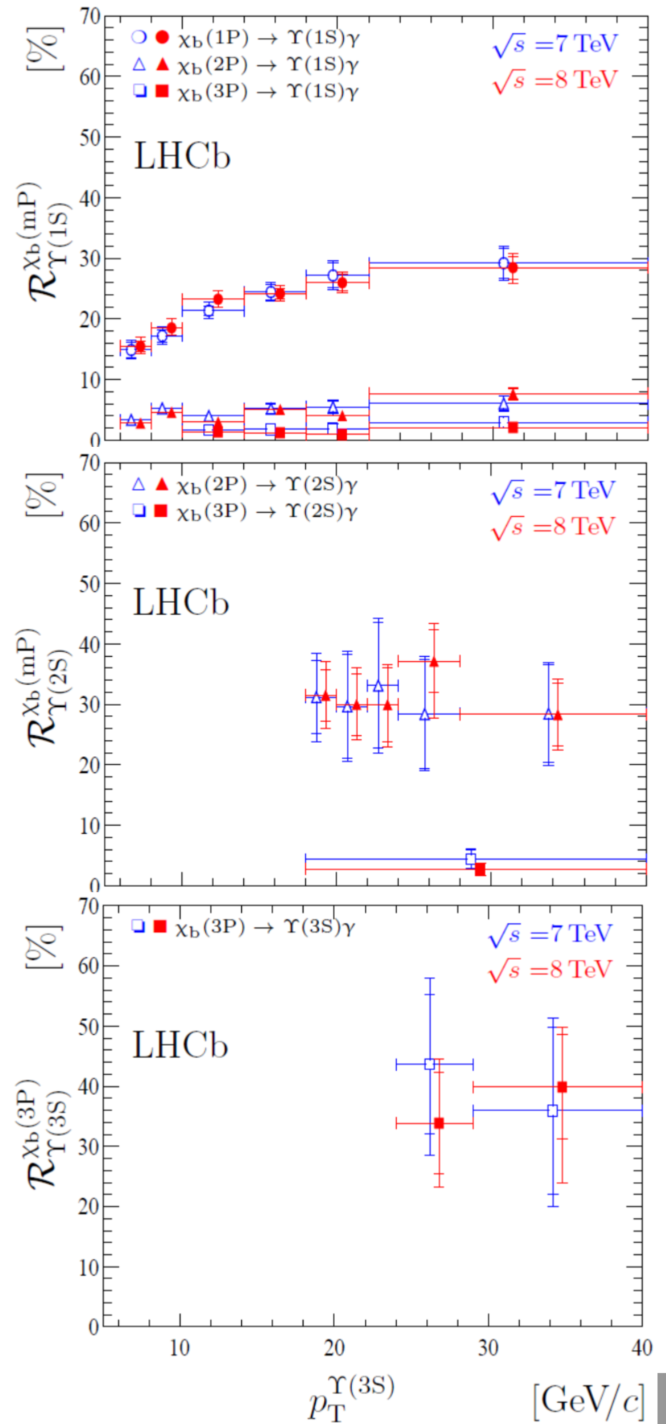

Examples of related physics studies

Nucl. Phys. B867 (2013) 1 $\sqrt{s}$ = 7 TeV, $\int Ldt \sim 1\ fb^{-1}$

- Ratio of BR($B^0 \to K^{*0}\gamma$) / BR($B^0_s \to \phi\gamma$) and direct CP asymmetry in $B^0 \to K^{*0}\gamma$

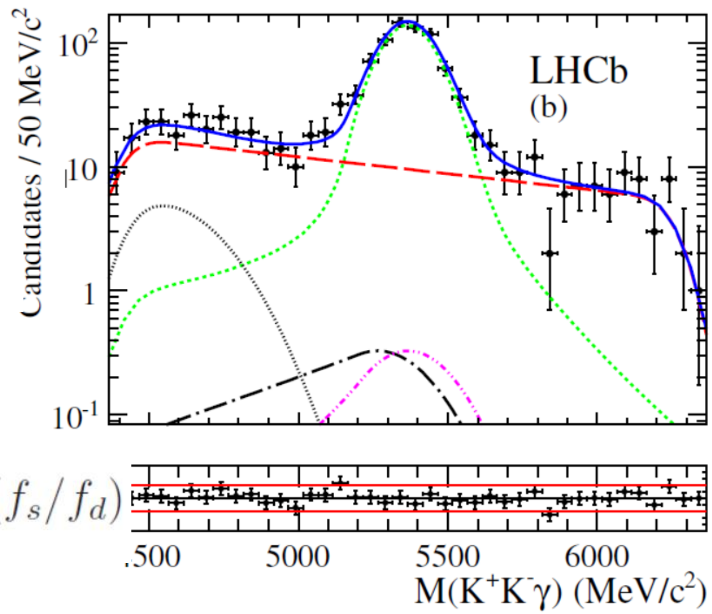

$$\frac{\mathcal{B}(B^0 \to K^{*0}\gamma)}{\mathcal{B}(B^0_s \to \phi\gamma)} = 1.23 \pm 0.06\,(\text{stat.}) \pm 0.04\,(\text{syst.}) \pm 0.10\,(f_s/f_d)$$

$$\mathcal{B}(B^0_s \to \phi\gamma) = (3.5 \pm 0.4) \times 10^{-5}$$

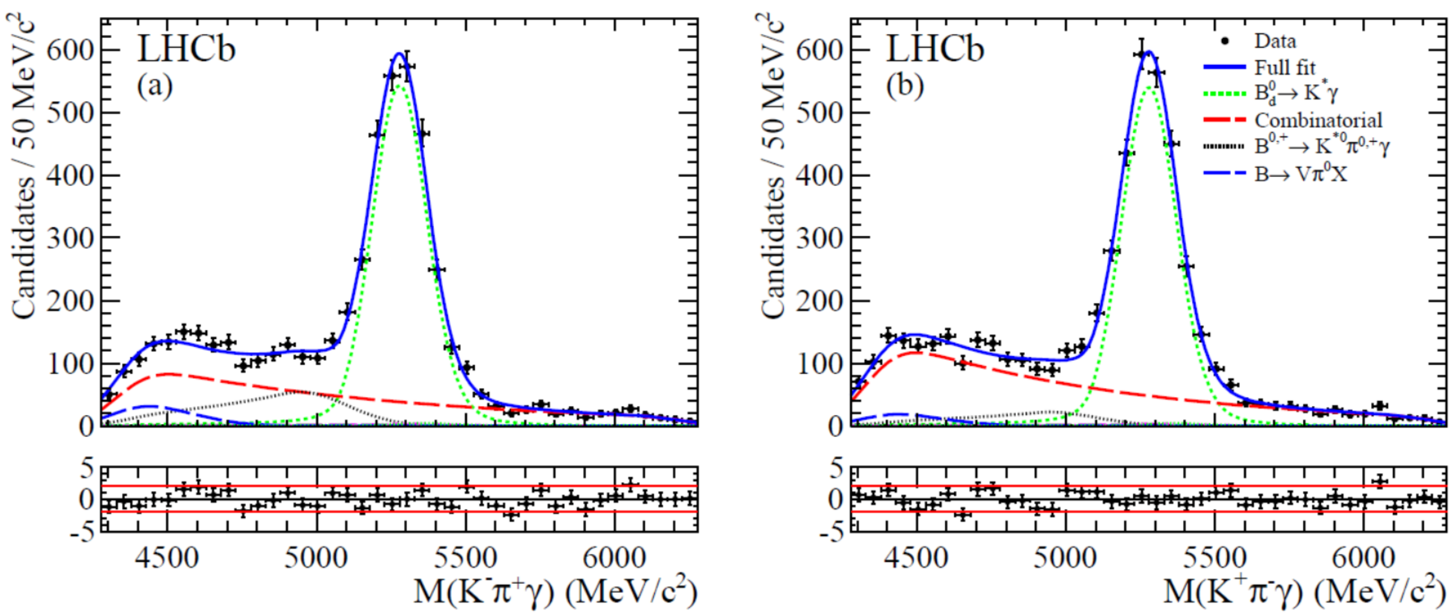

$$\mathcal{A}_{CP}(B^0 \to K^{*0}\gamma) = (0.8 \pm 1.7\,(\text{stat.}) \pm 0.9\,(\text{syst.}))\%$$

Examples of related physics studies

PRL 112 (2014) 161801

$\sqrt{s}$ = 7 TeV, $\int L dt$ ~ 1 fb^{-1}

$\sqrt{s}$ = 8 TeV, $\int L dt$ ~ 2 fb^{-1}

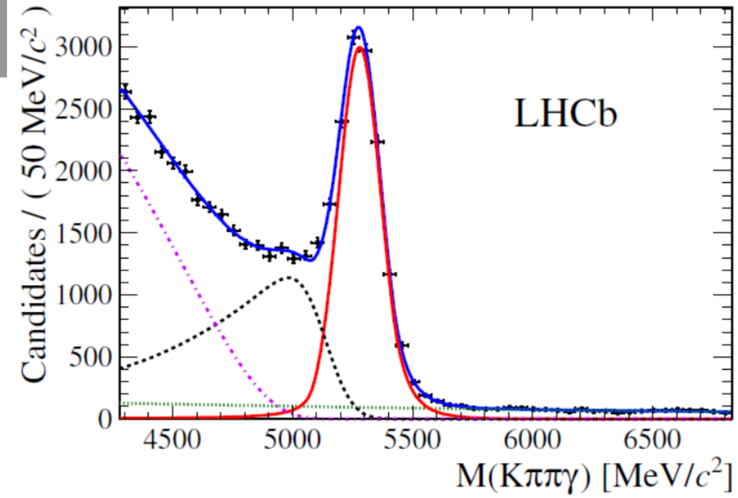

- Photon polarization in b → sγ transitions
- FCNC $B^+ \to K^+\pi^-\pi^+\gamma$, $K^+\pi^-\pi^+$ mass in [1.1,1.9] GeV

$$f(\cos\hat{\theta}; c_0=0.5, c_1, c_2, c_3, c_4) = \sum_{i=0}^{4} c_i L_i(\cos\hat{\theta})$$

$$\mathcal{A}_{\rm ud} = c_1 - \frac{c_3}{4}$$

	[1.1, 1.3]	[1.3, 1.4]	[1.4, 1.6]	[1.6, 1.9]
c_1	6.3±1.7	5.4±2.0	4.3±1.9	−4.6±1.8
c_2	31.6±2.2	27.0±2.6	43.1±2.3	28.0±2.3
c_3	−2.1±2.6	2.0±3.1	−5.2±2.8	−0.6±2.7
c_4	3.0±3.0	6.8±3.6	8.1±3.1	−6.2±3.2
$\mathcal{A}_{\rm ud}$	6.9±1.7	4.9±2.0	5.6±1.8	−4.5±1.9

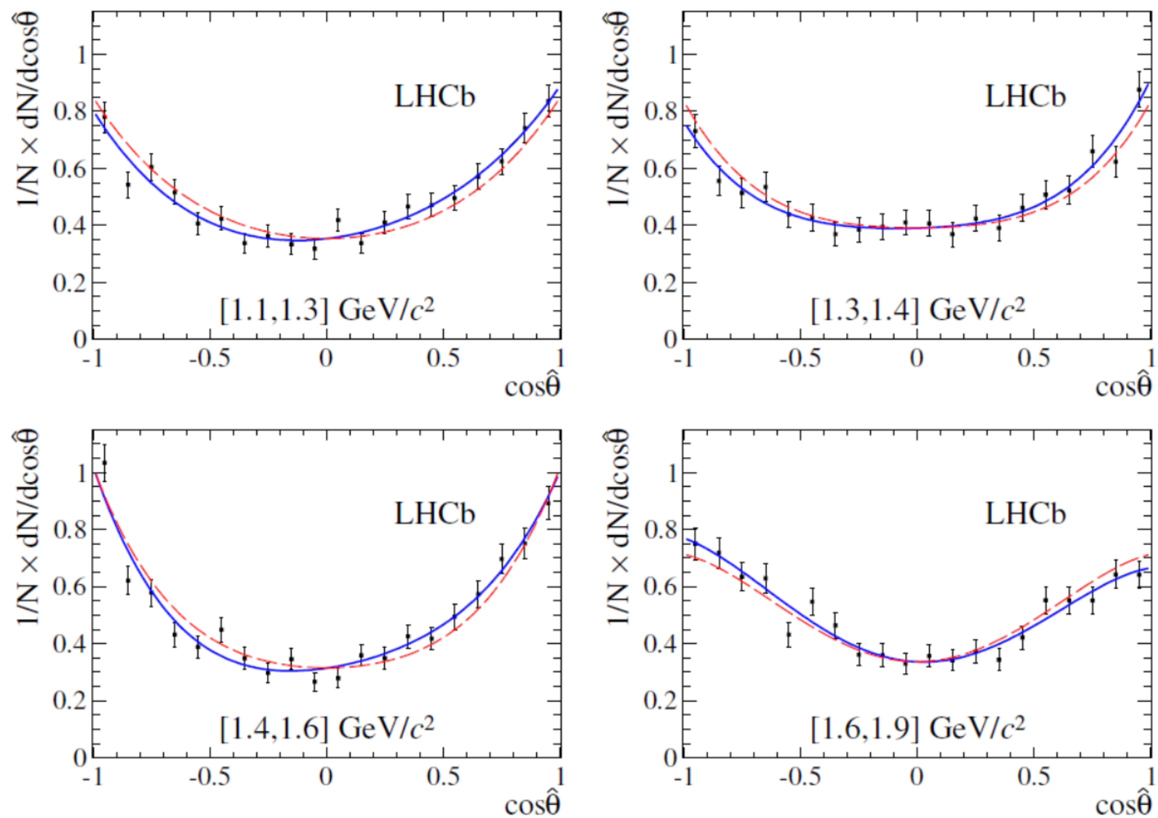

- First observation of a parity-violating photon polarization different from zero at >5σ in b → sγ transitions

PRL 115 (2015) 051801

$\sqrt{s}$ = 7 TeV, ∫Ldt ~ 1 fb^{-1}
$\sqrt{s}$ = 8 TeV, ∫Ldt ~ 2 fb^{-1}

- First observation of charmless $B^0_s \to \eta'\eta'$ decay, pure CP eigenstate
- Reconstruct η′ via decay to $\pi^+\pi^-\gamma$

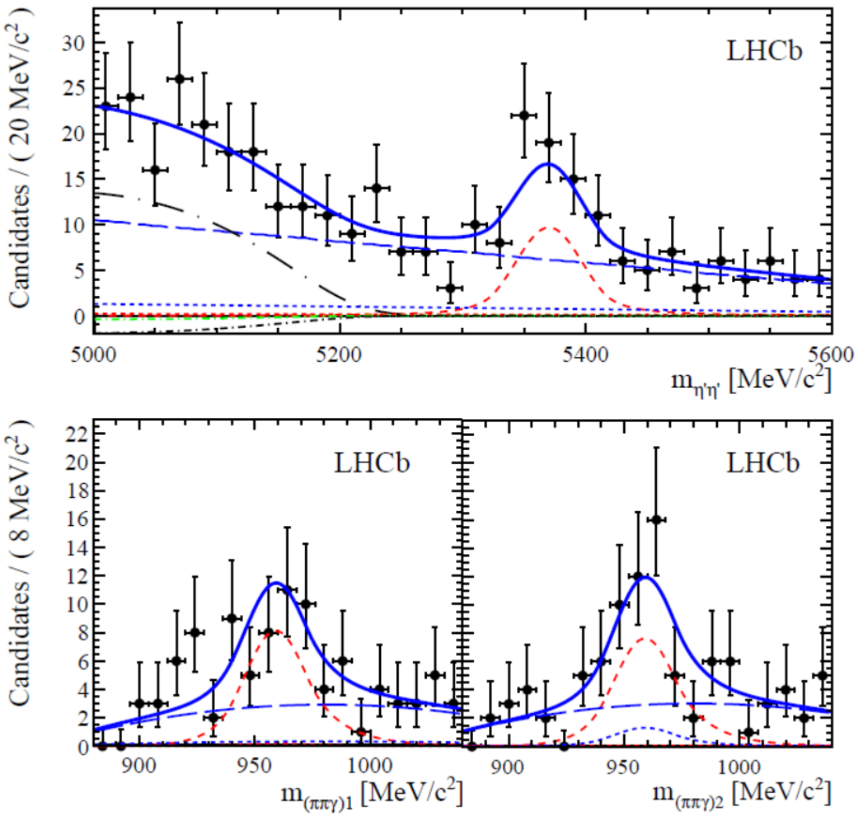

- First observation of $B^0_s \to \eta'\eta'$ with significance at >6σ

$$\frac{\mathcal{B}(B^0_s \to \eta'\eta')}{\mathcal{B}(B^{\pm} \to \eta' K^{\pm})} = 0.47 \pm 0.09\,(\mathrm{stat}) \pm 0.04\,(\mathrm{syst})$$

$$\mathcal{B}(B^0_s \to \eta'\eta') = [3.31 \pm 0.64\,(\mathrm{stat}) \pm 0.28\,(\mathrm{syst}) \pm 0.12\,(\mathrm{norm})] \times 10^{-5}$$

PRD 91 (2015) 112014

$\sqrt{s}$ = 7 TeV, $\int L dt \sim 1\ fb^{-1}$
$\sqrt{s}$ = 8 TeV, $\int L dt \sim 2\ fb^{-1}$

- CP violation in $B^{\mp} \rightarrow Dh^{\mp}$ ($h=K,\pi$) using $D \rightarrow K^{\mp}\pi^{\pm}\pi^{-}$, $D \rightarrow \pi^{+}\pi^{-}\pi^{0}$, and $D \rightarrow K^{+} K^{-} \pi^{0}$
- First observations are obtained of the suppressed ADS decay $B^{\mp} \rightarrow [\pi^{\mp}K^{\pm}\pi^{0}]_D\ \pi^{\mp}$ and the quasi-GLW decay $B^{\mp} \rightarrow [K^{+} K^{-} \pi^{0}]_D\ \pi^{\mp}$

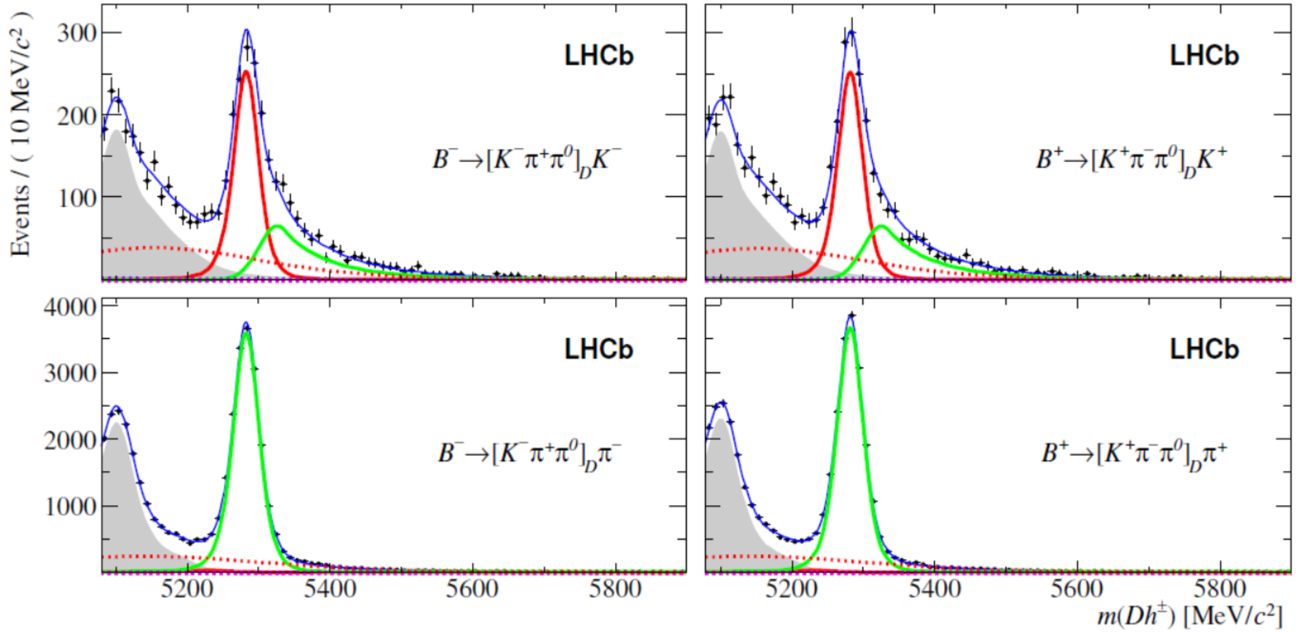

- Constraints on r_B, δ_B, and γ from measured observables

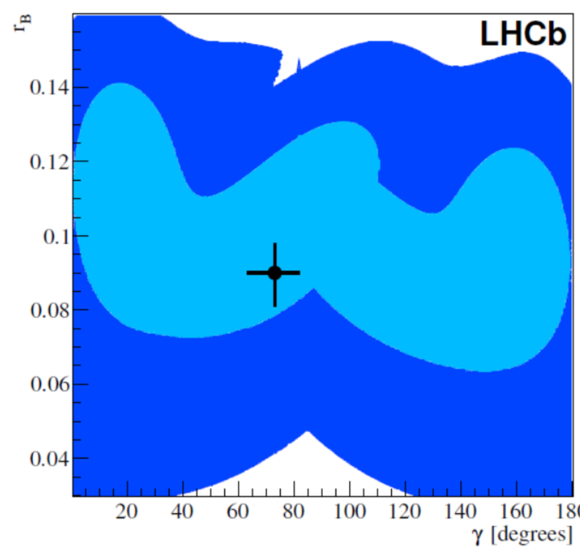

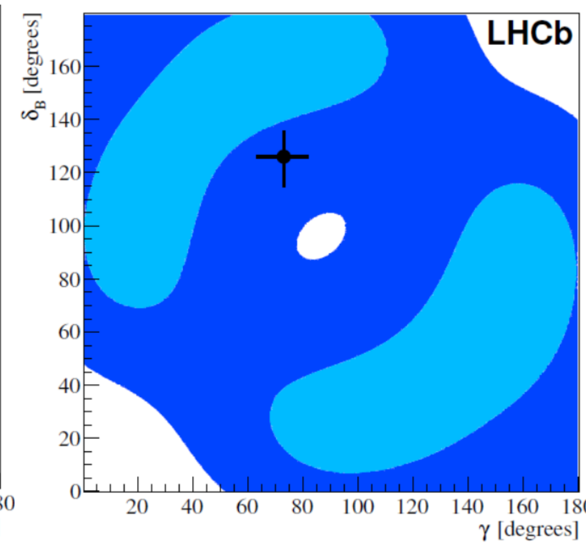

- By 2017, LHCb is expected to take 5-7 fb^{-1} of data @13 TeV.
- Next step: collect >50 fb^{-1} → probe NP effects at % level.
- This requires operation at higher luminosities:

  $(1\text{-}2)\cdot 10^{33}$ @$\sqrt{s}$ = 14 TeV

➔ *UPGRADE*

LHCb Upgrade LoI: CERN-LHCC-2011-001
LHCb Upgrade Framework TDR: CERN-LHCC-2012-007

Type	Observable	Current precision	LHCb 2018	**Upgrade** ($50\,fb^{-1}$)	Theory uncertainty
B_s^0 mixing	$2\beta_s$ ($B_s^0 \to J/\psi\ \phi$)	0.10 [9]	0.025	0.008	~ 0.003
	$2\beta_s$ ($B_s^0 \to J/\psi\ f_0(980)$)	0.17 [10]	0.045	0.014	~ 0.01
	$A_{fs}(B_s^0)$	6.4×10^{-3} [18]	0.6×10^{-3}	0.2×10^{-3}	0.03×10^{-3}
Gluonic penguin	$2\beta_s^{eff}(B_s^0 \to \phi\phi)$	–	0.17	0.03	0.02
	$2\beta_s^{eff}(B_s^0 \to K^{*0}\bar{K}^{*0})$	–	0.13	0.02	< 0.02
	$2\beta^{eff}(B^0 \to \phi K_S^0)$	0.17 [18]	0.30	0.05	0.02
Right-handed currents	$2\beta_s^{eff}(B_s^0 \to \phi\gamma)$	–	0.09	0.02	< 0.01
	$\tau^{eff}(B_s^0 \to \phi\gamma)/\tau_{B_s^0}$	–	5 %	1 %	0.2 %
Electroweak penguin	$S_3(B^0 \to K^{*0}\mu^+\mu^-; 1 < q^2 < 6\,GeV^2/c^4)$	0.08 [14]	0.025	0.008	0.02
	$s_0\ A_{FB}(B^0 \to K^{*0}\mu^+\mu^-)$	25 % [14]	6 %	2 %	7 %
	$A_I(K\mu^+\mu^-; 1 < q^2 < 6\,GeV^2/c^4)$	0.25 [15]	0.08	0.025	~ 0.02
	$\mathcal{B}(B^+ \to \pi^+\mu^+\mu^-)/\mathcal{B}(B^+ \to K^+\mu^+\mu^-)$	25 % [16]	8 %	2.5 %	~ 10 %
Higgs penguin	$\mathcal{B}(B_s^0 \to \mu^+\mu^-)$	1.5×10^{-9} [2]	0.5×10^{-9}	0.15×10^{-9}	0.3×10^{-9}
	$\mathcal{B}(B^0 \to \mu^+\mu^-)/\mathcal{B}(B_s^0 \to \mu^+\mu^-)$	–	~ 100 %	~ 35 %	~ 5 %
Unitarity triangle angles	γ ($B \to D^{(*)}K^{(*)}$)	~ 10–$12°$ [19, 20]	4°	0.9°	negligible
	γ ($B_s^0 \to D_s K$)	–	11°	2.0°	negligible
	β ($B^0 \to J/\psi\ K_S^0$)	0.8° [18]	0.6°	0.2°	negligible
Charm CP violation	A_Γ	2.3×10^{-3} [18]	0.40×10^{-3}	0.07×10^{-3}	–
	ΔA_{CP}	2.1×10^{-3} [5]	0.65×10^{-3}	0.12×10^{-3}	–

Year	Energy	Int. Lumi.
2010	7 TeV	37 pb^{-1}
2011	2.76TeV	71 pb^{-1}
2011	7 TeV	1.0 fb^{-1}
2012	8 TeV	2.2 fb^{-1}
2013	LHC splice repair	
2014		
2015	13 TeV 25 ns bunch crossing	>5 fb^{-1}
2016		
2017		
2018	LHCb upgrade	
2019	5-10 fb^{-1}/year	
2020		
2021		
2022	LHC lumi upgrade	
2023		
2024		

b/c decays with photons in final state (*e.g.* $B_s \to \varphi\gamma$).

- 1 MHz L0 limit with the present trigger
- **For hadronic final states, no gain from increasing the luminosity.** Hadron trigger selects b-events, but not particular final state. Increasing the p_T threshold for hadrons, after certain limit, does not improve the selection purity.

Solution

- **Fully software trigger to select desired final states.**
- Enlarge CPU farm to process the whole 40 MHz input.
- L0-like LLT (with 1-40 MHz output) to follow gradual growth of the HLT farm.
- **FEE should work at 40 MHz → to rebuild for most subdetectors.**

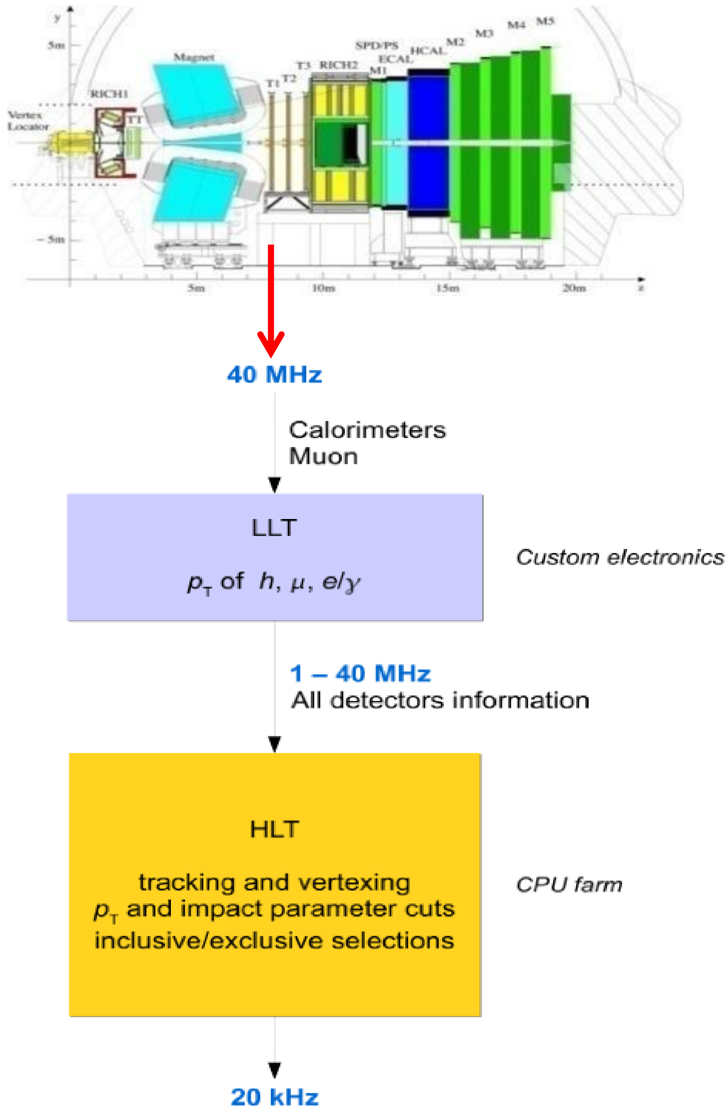

Current: latency-buffer in FE, and zero-suppress after L0 trigger

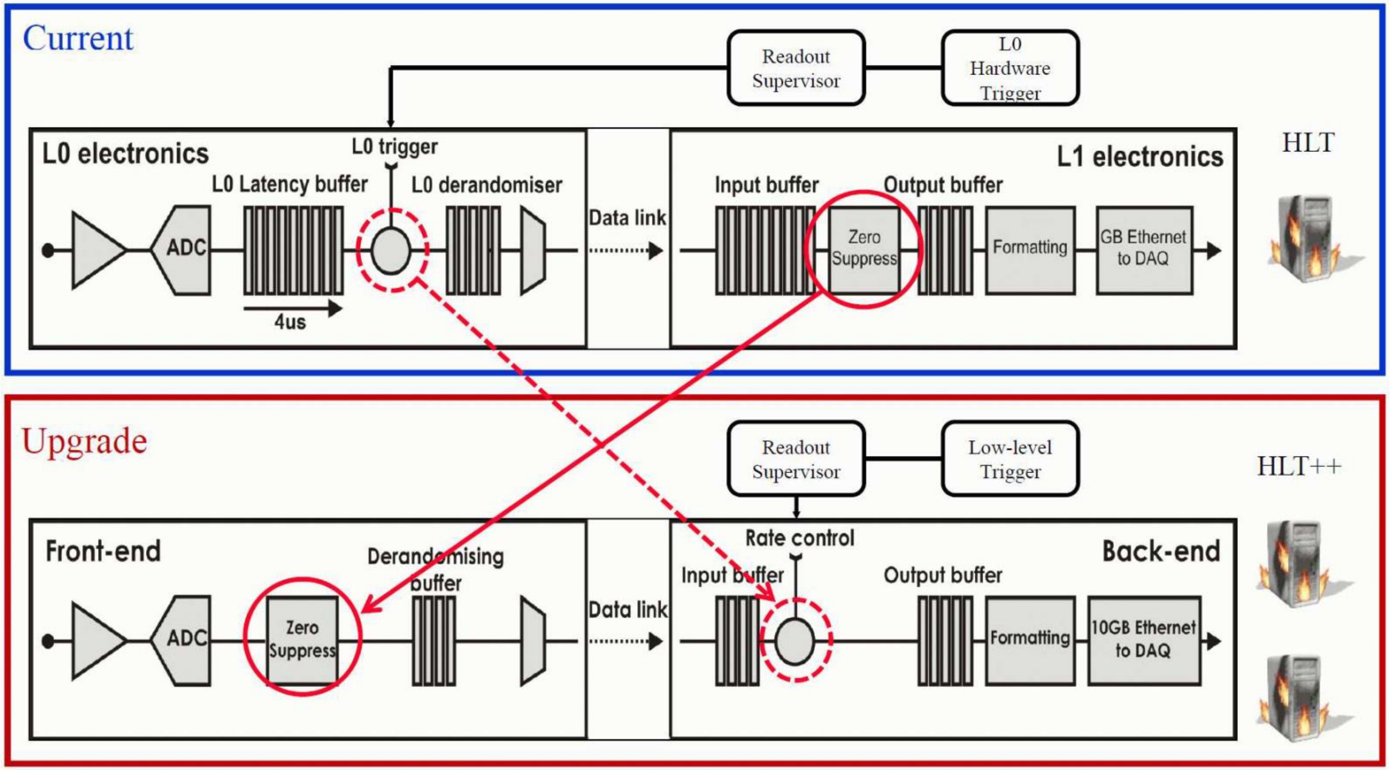

Upgrade: zero-suppress in FE, no trigger decision to FE, LLT in back-end.

- **VELO**: replace the whole detector (rad. damage). New readout chips. Choice between strip and pixel options.
- Other tracking detectors: **OT** central part: scintillating fibers.
- **RICH**: replace HPDs by MAPMTs, as HPDs include RO electronics. Remove aerogel in RICH1 (material budget).
- Additional PID detector between RICH2 and calorimeters: Time of Internally Reflected Cherenkov Light (**TORCH**). Quartz plate radiator, 10-15 ps resolution.

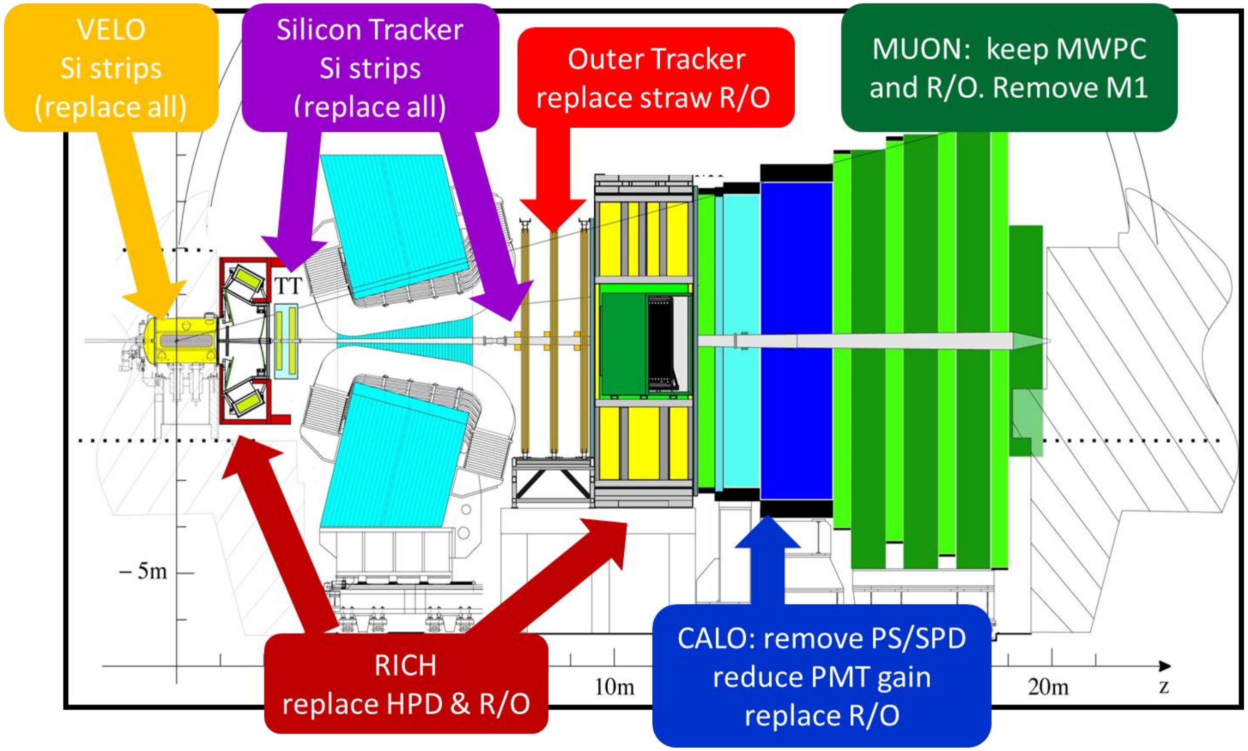

- **CALO**: reduce PMT gains. Remove PS/SPD. Rebuild FEE. Possibly replace few modules in the central area.
- **MUON**: present FEE operational at 40 MHz. Remove the M1 station before calorimeters.

Calorimeter upgrade, radiation resistance

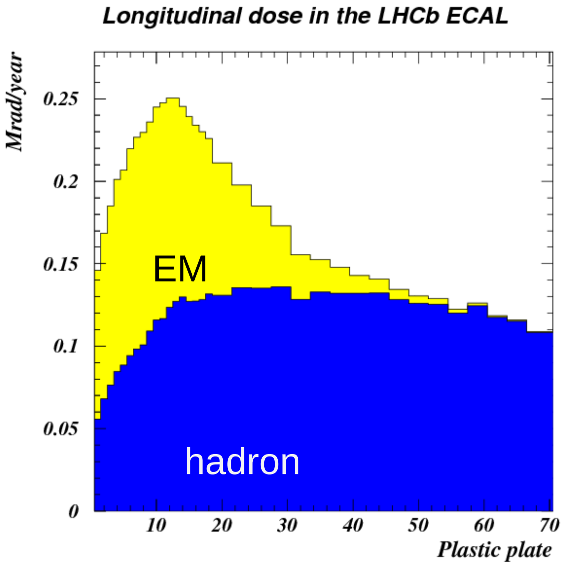

doses per 2 fb^{-1} at $\sqrt{s}$=14 TeV (x25 for 50 fb^{-1})

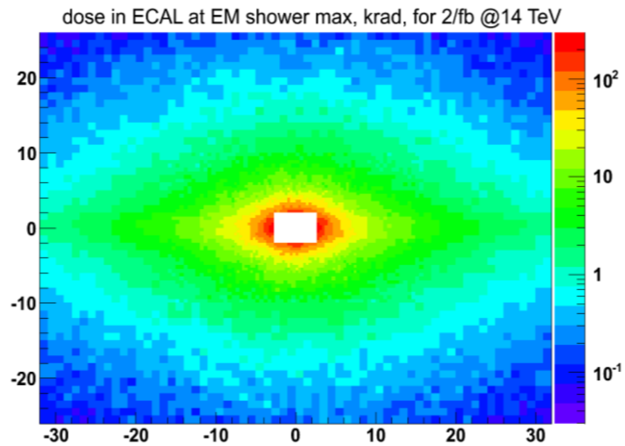

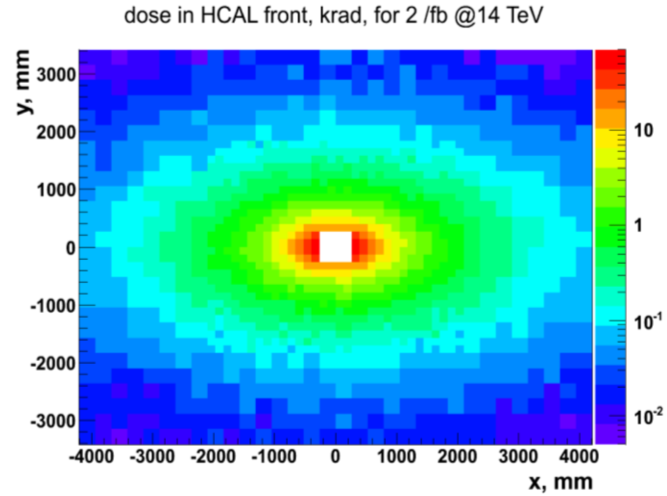

Radiation resistance issues:

- ECAL modules: scintillator and fibers
- ECAL light readout elements: light guides, PMTs (entrance window), CW boards
- HCAL modules: scintillator and fibers
- Not an issue for the HCAL light readout elements (smaller dose behind HCAL)

Can be replaced:

- ECAL/HCAL PMTs, CW bases and light guides
- CW bases operational to 1.5-2 Mrad; ~500 CW bases to be replaced while taking 50 fb^{-1}
- 48 central ECAL modules

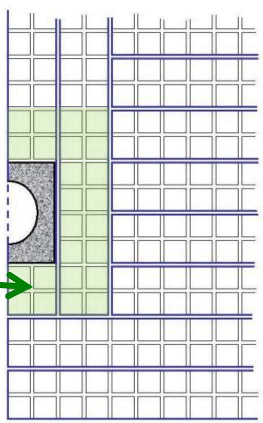

Difficult to replace:

- WLS fibers of ECAL modules
- Other ECAL modules
- HCAL modules, plastic and fibers

- Light yield degradation of front row in each **HCAL** cell, 2011+2012 (3.4 fb^{-1}).

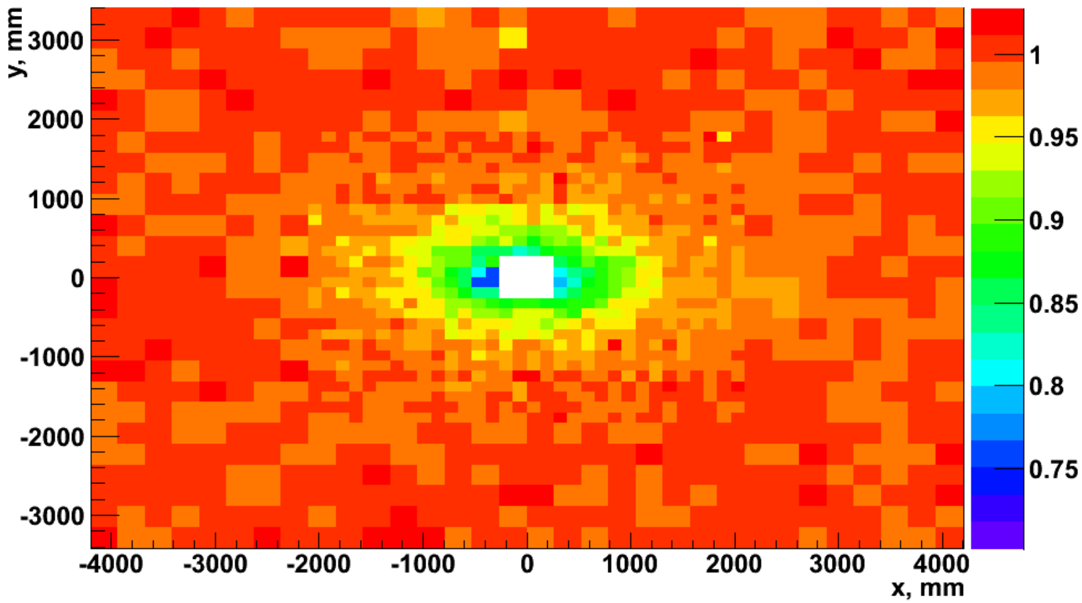

Year	Energy	Int. Lumi.
2010	7 TeV	37 pb^{-1}
2011	2.76TeV	71 pb^{-1}
2011	7 TeV	1.0 fb^{-1}
2012	8 TeV	2.2 fb^{-1}
2013	LHC splice repair	
2014		
2015	13 TeV 25 ns bunch crossing	>5 fb^{-1}
2016		
2017		
2018	LHCb upgrade	
2019	5-10 fb^{-1}/year	
2020		
2021		
2022	LHC lumi upgrade	
2023		
2024		

- Can be compensated by calibration (PMT gain).
- The HCAL might not be used to provide the trigger on high-pT hadron. Loss of very central cells not critical.
- It will be still usable for Muon ID in the Outer region (does not suffer much from radiation).
- Performance of **ECAL** central modules is expected to remain satisfactory to 20-30 fb^{-1}.
- Considering replacement of central modules in 2022-2023.
- **Impact on physics**: pile-up, PID.

Evolution in the History of Paintings of the Virgin

from Robin Urton

How else cooking recipe of Shashlik can be improved ?

New Shashlik geometries

- **Towers** adapted to barrel geometry – ALICE EMCAL
- **Longitudinal segmentation** (was proposed for Linear Collider), both solutions studied with the test beam
    - Either two (or more) readouts using vacuum photodiodes inserted between adjacent modules
    - Or two (or more) scintillator types with different decay times
- Finer **shower sampling**
    - Att.: decreasing Pb thickness only, increases cell depth, while decreasing proportionally Pb and Sc thickness reduces light collection efficiency
    - Sampling fraction of 0.275 mm / 1.5 mm for KOPIO (16 Xo) and PANDA (20 Xo) and sampling term of ~3%/√E

How else cooking recipe of Shashlik can be improved ?

- Further improvement of the **lateral uniformity**
  - Local uniformity:
    - Improve (diffusive vs. mirror !) reflection from tile edges
    - Implement spiral fibers – R&D at IHEP-Protvino
      - About 2% lateral uniformity was demonstrated
      - However, improvement is a function of shower depth, and fiber length is increased
    - Reduce light collection around fibers → masks
      - Holes in TYVEK and use lead as poorly reflecting surface
        - Tested by E. Tarkovsky in 2002, A_{local} = ~0.38% → ~0.18%
      - Ultimately paint TYVEK according to desired suppression
  - Global uniformity: better control of mat thickness and overlap
  - Offline (or online) iterative corrections
- Improvement of **radiation resistance**

- LHCb calorimeter is operational since the beginning of physics data taking
- Calorimeter is delivering trigger and measurement of neutral particles
- HEP calorimeters start to compete with classical calorimeters definition in Google search